Stockholm University

Attraction and Rejection

On the love–hate relationship between stars and black holes

Emanuel Gafton

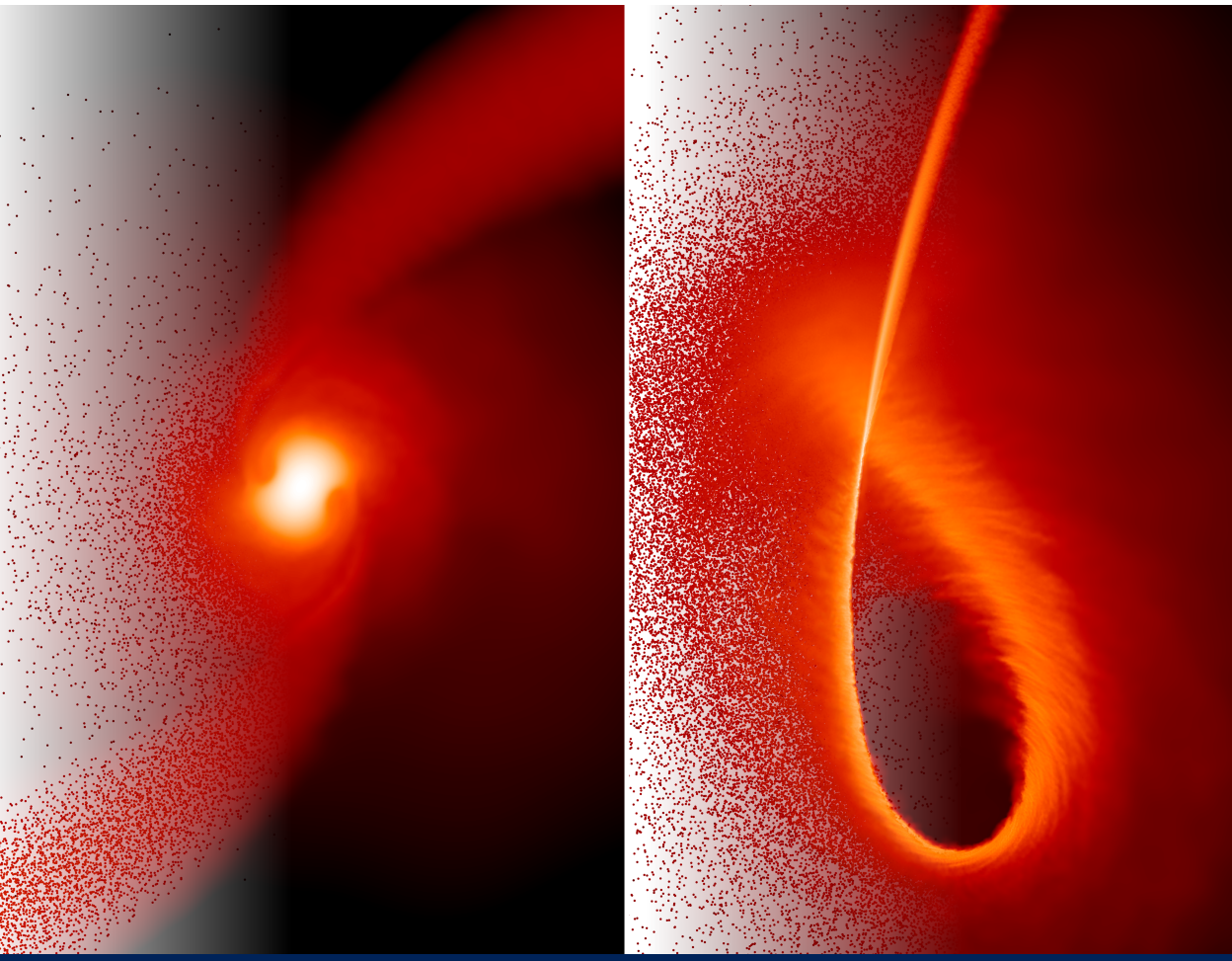

Doctoral Thesis in Astronomy at Stockholm University, Sweden 2019

Attraction and Rejection

On the love–hate relationship between stars and black holes

Emanuel Gafton

Academic dissertation for the Degree of Doctor of Philosophy in Astronomy at Stockholm University to be publicly defended on Wednesday 18 September 2019 at 10.00 in sal FA31, AlbaNova universitetscentrum, Roslagstullsbacken 21.

Abstract

Solitary stars wandering too close to the supermassive black hole at the centre of their galaxy may become tidally disrupted, if the tidal forces due to the black hole overcome the self-gravity holding the star together. Depending on the strength of the encounter, the star may be partially disrupted, resulting in a surviving stellar core and two tidal arms, or may be completely disrupted, resulting in a long and thin tidal stream expected to fall back and circularize into an accretion disc (the two cases are illustrated on the cover of this thesis).

While some aspects of a tidal disruption can be described analytically with reasonable accuracy, such an event is the highly non-linear outcome of the interplay between the stellar hydrodynamics and self-gravity, tidal accelerations from the black hole, radiation, potentially magnetic fields and, in extreme cases, nuclear reactions. In the vicinity of the black hole, general relativistic effects become important in determining both the fate of the star and the subsequent evolution of the debris stream.

In this thesis we present a new approach for studying the relativistic regime of tidal disruptions. It combines an exact relativistic description of the hydrodynamical evolution of a test fluid in a fixed curved spacetime with a Newtonian treatment of the fluid's self-gravity. The method, though trivial to incorporate into existing Newtonian codes, yields very accurate results at minimal additional computational expense.

Equipped with this new tool, we set out to systematically explore the parameter space of tidal disruptions, focusing on the effects of the impact parameter (describing the strength of the disruption) and of the black hole spin on the morphology and energetics of the resulting debris stream. We also study the effects of general relativity on partial disruptions, in order to determine the range of impact parameters at which partial disruptions occur for various black hole masses, and the effects of general relativity on the velocity kick imparted to the surviving core. Finally, we simulate the first part of a tidal disruption with our code and then use the resulting debris distribution as input for a grid-based, general relativistic magnetohydrodynamics code, with which we follow the formation and evolution of the resulting accretion disc.

Stockholm 2019
http://urn.kb.se/resolve?urn=urn:nbn:se:su:diva-167197

ISBN 978-91-7797-582-3
ISBN 978-91-7797-583-0

Department of Astronomy

Stockholm University, 106 91 Stockholm

ATTRACTION AND REJECTION

Emanuel Gafton

Stockholm
University

Attraction and Rejection

On the love–hate relationship between stars and black holes

Emanuel Gafton

ISBN print 978-91-7797-582-3
ISBN PDF 978-91-7797-583-0

Cover image: Snapshots from two simulations of tidal disruptions of solar-type stars by a supermassive black hole. Both images are a blend between the underlying SPH particle distribution (coloured by density) and the density plot as computed using kernel-weighted interpolation. *(Left panel)* Weak encounter, resulting in a partial tidal disruption with a surviving stellar core. *(Right panel)* Deep encounter in Kerr spacetime, resulting in a completely disrupted star; the debris stream is exhibiting significant periapsis shift, due to which the head of the stream is colliding with its tail.
The figure was produced by the author, using data from our own simulations.

Printed in Sweden by Universitetsservice US-AB, Stockholm 2019

Contents

Summaries

Summa

Solivagae stellae, quae ad valde magnum cavum nigrum in centro galaxiae suarum proxime concurrunt, dirumpantur si vires aestuosae debitae cavo nigro viribus internas gravitates quas stellam nexam sustinent superent. Debili concursione stella in futurum stellare cor caudasque duas aestuosas partialiter dirumpitur vel forti concursione stella integra in longum subtilemque fluxum dirumpitur. Hunc redire et circularem fieri exspectatur. Utrique casus fronte huius libri illustrati sunt.

Etsi aliquae quaestiones methodis analyticis recte fere tractarentur, talis diruptio nonlinearis cumulatarum actionum exitus est: stellaris hydrodynamica gravitasque interna, acceleratio aestuosa debita cavo nigro, radiatio forteque campus magneticus et, in extremis, reactiones nucleares. In proximitate cavi nigri relativitas generalis tam fato stellae quam sequente evolutione fluxus stellaris insignis fit.

In hoc libro novam methodum studii diruptionum aestuosarum cum relativitate generali praebemus. Ea descriptionem exactam evolutionis hydrodynamicae fluidi in fixo curvoque spatiotempore cum newtoniensem descriptionem stellaris gravitatis internae combinat. Haec methodus etsi facile includi in codicibus newtoniensibus existentibus, tamen rectos fructus cum minimis additis computis producit.

Hoc novo instrumento parati, ad ordinata studia spatii parametrorum diruptionum aestuosarum, praesertim ad explorationem effectus parametri impacti (describentis vim diruptionis) rotationisque cavi nigri super morphologia energiaque fluxus stellaris proficiscimur. Studemus etiam effectus relativitatis generalis in partialibus diruptionibus, ut definiamus intervallum parametrorum impacti ubi partiales diruptiones occurrunt cum diversis ponderibus cavorum nigrorum, itemque effectus in velocitate collisionis impertiti futuro stellari cordi. Tandem primam partem diruptionis aestuosae simulamus cum codice nostro postque consequentem distributionem stellaris materiae ut initus alterius codicis relativitatis generalis, magnetohydrodynamicae utimur, quo formationem evolutionemque consequentis accretionis disci exsequimur.

Abstract

Solitary stars wandering too close to the supermassive black hole at the centre of their galaxy may become tidally disrupted, if the tidal forces due to the black hole overcome the self-gravity holding the star together. Depending on the strength of the encounter, the star may be partially disrupted, resulting in a surviving stellar core and two tidal arms, or may be completely disrupted, resulting in a long and thin tidal stream expected to fall back and circularize into an accretion disc (the two cases are illustrated on the cover of this thesis).

While some aspects of a tidal disruption can be described analytically with reasonable accuracy, such an event is the highly non-linear outcome of the interplay between the stellar hydrodynamics and self-gravity, tidal accelerations from the black hole, radiation, potentially magnetic fields and, in extreme cases, nuclear reactions. In the vicinity of the black hole, general relativistic effects become important in determining both the fate of the star and the subsequent evolution of the debris stream.

In this thesis we present a new approach for studying the relativistic regime of tidal disruptions. It combines an exact relativistic description of the hydrodynamical evolution of a test fluid in a fixed curved spacetime with a Newtonian treatment of the fluid's self-gravity. The method, though trivial to incorporate into existing Newtonian codes, yields very accurate results at minimal additional computational expense.

Equipped with this new tool, we set out to systematically explore the parameter space of tidal disruptions, focusing on the effects of the impact parameter (describing the strength of the disruption) and of the black hole spin on the morphology and energetics of the resulting debris stream. We also study the effects of general relativity on partial disruptions, in order to determine the range of impact parameters at which partial disruptions occur for various black hole masses, and the effects of general relativity on the velocity kick imparted to the surviving core. Finally, we simulate the first part of a tidal disruption with our code and then use the resulting debris distribution as input for a grid-based, general relativistic magnetohydrodynamics code, with which we follow the formation and evolution of the resulting accretion disc.

Sammanfattning

En ensam stjärna som råkar komma för nära det supermassiva svarta hålet i centrum av sin galax riskerar att slitas sönder. Detta händer om och när tidvattenkrafterna från det svarta hålet blir starkare än stjärnans egen gravitation. I vissa fall blir stjärnan endast ofullständigt söndersliten så att dess kärna överlever medan resten av stjärnmaterien dras ut i två långa armar. I de fall stjärnan blir fullständigt söndersliten blir

dess spillror till en lång ström av gas som faller in i en cirkulär bana och bildar en ackretionsskiva kring det svarta hålet. (De två fallen illustreras på omslagsbilden av denna avhandling.)

Vissa aspekter av dessa våldsamma fenomen kan beskrivas någorlunda med analytiska metoder. Men tidvattenssönderslitningen av en stjärna är en mycket komplicerad process med ett ickelinjärt samspel mellan stjärnans hydrodynamik och självgravitation, tidvattenaccelerationen från det svarta hålet, elektromagnetisk strålning, magnetfält och – i extrema fall – kärnreaktioner. Dessutom blir allmänrelativistiska effekter viktiga i närheten av det svarta hålet och avgörande för stjärnans öde samt den utvecklingen av den resulterande gasströmmen.

I denna avhandling presenteras ett nytt sätt att studera den relativistiska domänen av tidvattenssönderslitningar. Metoden kombinerar en exakt relativistisk beskrivning av den hydrodynamiska utvecklingen av ett test-fluidum i en rumtid med fix krökning medan fluidumets självgravitation behandlas enligt newtonsk mekanik. Metoden, som är trivial att inkorporera i existerande newtonska datorkoder, ger mycket precisa resultat med ett minimum av extra beräkningskostnad.

Med hjälp av det nya verktyget utforskas parameterrymden för tidvattenssönderslitningar av stjärnor på ett systematiskt sätt. Fokus ligger på effekterna på den resulterande strömmen av spillror av impakt-parametern (som avgör förloppets styrka) liksom av det svarta hålets rotation. Allmänrelativistiska effekter vid ofullständiga sönderslitningar studeras också, med målet att fastställa det intervall av impaktparametrar vid vilka sådana inträffar för olika massor på det svarta hålet. Slutligen används koden till att simulera den första fasen av en tidvattenssönderslitning. Den resulterande fördelningen av stjärnspillrorna används sedan som indata till en allmänrelativistisk magnetohydrodynamisk datorkod med vilken vi följer bildningen och utvecklingen av en ackretionsskiva.

Zusammenfassung

Einsame Sterne, die zu nah an einem riesigen Schwarzen Loch in der Mitte ihrer Galaxie wandern, können gezeitenhaft zerstört werden, falls die Gezeitenkräfte des Schwarzen Lochs stärker sind, als die Selbstgravitation, die den Stern zusammenhält. Abhängig von der Stärke der Begegnung, der Stern kann entweder nur teilweise zerstört werden, ein stellarer Kern und zwei Gezeitenarme hinterlassend; oder kann vollständig zerstört werden, in ein langer, schmaler gezeitenhaftiger Strom erfolgend, von dem man den Rückfall und Zirkularisation in einer Akkretionsscheibe erwartet (beide Fälle sind auf das Deckblatt dieser These bebildert).

Während einige Erscheinungen einer gezeitenhaftigen Zerstörung analytisch mit angemessener Genauigkeit beschreibt werden können, so ein Ereignis ist das höchste nichtlineare Ergebnis eines Zusammenspiels zwischen stellarer Hydrodynamik und Selbstgravitation, gezeitenhaftiger Beschleunigung vom Schwarzen Loch her, Strah-

lung, möglicherweise Magnetfelder und, in äußerste Fälle, Kernreaktionen. In der Umgebung des Schwarzen Lochs, allgemeine relativistische Effekte werden wesentlich in der Bestimmung sowohl des Schicksals des Sterns als auch die darauffolgende Entwicklung des Trümmerstroms.

In dieser Behauptung tragen wir einen neuen Ansatz für das Studium des relativistischen Regimes von Gezeitenstörung vor. Es verbindet eine genaue relativistische Beschreibung einer hydrodynamischen Entwicklung einer Testflüssigkeit in einer fest gewölbten Raumzeit mit einer Newtonschen Behandlung der Selbstgravitation der Flüssigkeit. Die Methode, obwohl gezeitenhaft um in bestehende Newtonsche Kode einzubauen, liefert sehr genaue Ergebnisse bei minimalem zusätzlichen Rechenwand.

Mit diesem neuen Instrument ausgerüstet, machen wir uns auf den Weg um den Parameterraum der Gezeitenstörungen systematisch zu erforschen, indem wir uns auf die Auswirkungen des Durchdringungsfaktor (die Stärke der Störungen beschreibend) und der Drehung des Schwarzen Lochs auf der Morphologie und Energetik des entstehenden Trümmerstroms richten. Wir studieren gleichfalls die Effekte allgemeiner Relativität gegenüber partieller Störungen, um die Spannweite der Durchdringungsfaktoren, bei welchen die partiellen Störungen verschiedener Schwarzen Loch-massen vorkommen, zu bestimmen, und die Effekte allgemeiner Relativität gegenüber dem Geschwindigkeitsschlags das auf dem durchhaltenden Kern übertragen wurde. Schließlich, täuschen wir den ersten Teil einer Gezeitenstörung mit unserer Kode vor und als nächstes gebrauchen wir die entstehende Trümmerverteilung als Beitrag für einer gitterbasierten allgemeiner relativistischen Magnetohydrodynamikkode, mit welcher wir die Entstehung und Entwicklung der erfolgenden Akkretionsscheibe beobachten.

Rezumat

Stelele solitare rătăcind prea aproape de supermasiva gaură neagră din centrul galaxiei lor pot ajunge a fi sfîșiate diferențial, dacă forțele de atracție diferențială datorate găurii negre le copleșesc pe cele gravitaționale interne ale stelei. În funcție de energia implicată în această întîlnire, steaua poate fi parțial sfîșiată, ajungînd la starea de un miez stelar cu două brațe, ori poate fi complet sfîșiată, rezultînd o șuviță lungă și subțire care probabil va cădea în cîmpul gravitațional al găurii negre și se va pierde în vîrtejul unui disc de acreție (cele două situații sînt ilustrate pe coperta acestei teze).

În vreme ce unele aspecte ale sfîșierii diferențiale pot fi descrise analitic cu acuratețe rezonabilă, un astfel de eveniment este rezultatul cît se poate de nelinear al interacțiunii dintre: forțele hidrodinamice și gravitaționale interne ale stelei, accelerațiile diferențiale exercitate de gaura neagră, radiație, potențial cîmpuri magnetice și – în cazuri extreme – reacții nucleare. În vecinătatea găurii negre, efectele relativității generale devin importante pentru determinarea deopotrivă a destinului stelei și a

evoluției ulterioare a brîului de rămășițe stelare.

În teza de față prezentăm o nouă abordare, în vederea studierii regimului relativist al sfîșierilor diferențiale. Ea combină o descriere relativistă exactă a evoluției hidrodinamice a fluidului, într-un spațiu-timp fix curbat, cu o perspectivă newtoniană asupra gravitației interne a fluidului. Deși lesne de integrat în coduri sursă newtoniene existente, metoda oferă rezultate foarte acurate, cu minime eforturi computaționale suplimentare.

Echipați cu acest nou instrument, ne-am propus să explorăm sistematic spațiul parametric al sfîșierilor diferențiale, concentrîndu-ne asupra efectelor factorului de impact (care descrie forța sfîșierii) și a rotației găurii negre asupra morfologiei și a energiei brîului de rămășițe stelare. Totodată, am mai studiat efectele relativității generale asupra sfîșierilor parțiale, spre a determina atît intervalul factorilor de impact unde apar sfîșieri parțiale în cazul diferitelor mase ale găurii negre, cît și efectele relativității generale asupra vitezei transmise miezului supraviețuitor. În sfîrșit, am simulat prima parte a sfîșierii diferențiale pe baza metodei noastre și apoi am introdus distribuția rămășițelor rezultate într-un alt cod eulerian, magnetohidrodinamic și general relativist, cu care apoi am urmărit formarea și evoluția discului de acreție rezultat.

Resumen

Cuando una estrella solitaria se acerca demasiado a un agujero negro supermasivo situado en el centro de la galaxia, puede sufrir un evento de disrupción de marea, siempre que la fuerza de marea del agujero negro supere la fuerza de gravedad intrínseca de la estrella, que la mantiene unida. Dependiendo de la violencia de esta interacción, la estrella puede quedar parcialmente destrozada, con un núcleo estelar sobreviente rodeado de dos brazos, o completamente destrozada, sin núcleo sobreviviente, pero con una estructura cuasi tubular larga y delgada, que volverá a aproximarse al agujero negro y formará un disco de acreción. (Los dos casos están ilustrados en el diseño de la tapa de este libro).

Aunque algunas cuestiones sobre las disrupciones de marea pueden ser tratadas con métodos analíticos, estos eventos son el resultado no lineal de la interacción entre la hidrodinámica y la gravitación internas de la estrella, la aceleración de marea debido al agujero negro, la radiación, puede incluir los campos magneticos, y – en casos extremos – las reacciones nucleares. Cerca del agujero negro los efectos de la relatividad general cobran importancia a la hora de determinar tanto el destino de la estrella como la evolución posterior del fluido estelar.

En esta tesis presentamos un nuevo método para estudiar el régimen relativístico de las disrupciones de marea, combinando una descripción relativística exacta de la evolución hidrodinámica del fluido estelar en un espacio-tiempo fijo, pero curvo, con una descripción newtoniana de la gravitación interna del fluido. Nuestro mé-

todo, aunque trivialmente incorporable en cualquier código newtoniano existente, produce resultados muy precisos a cambio de un aumento del coste computacional esencialmente despreciable.

Equipados con esta nueva herramienta, procedemos a explorar sistemáticamente el espacio de parámetros de las disrupciones de marea, concentrándonos en la influencia del parámetro de impacto (que describe la magnitud de la disrupción) y de la rotación del agujero negro sobre la morfología y la distribución energética del fluido estelar resultante. También estudiamos los efectos de la relatividad general sobre las disrupciones parciales, para determinar el intervalo de parámetros de impacto que producen una disrupción parcial dependiendo de la masa del agujero negro, y los efectos de la relatividad general sobre el aumento de velocidad transferido al núcleo estelar sobreviviente. Finalmente, después de simular la primera parte de una disrupción con nuestro código, usamos la distribución de fluido resultante como condición inicial para un código euleriano, relativístico y magnetohidrodinámico, con el fin de estudiar la formación y evolución del disco de acreción resultante.

List of papers

The following papers, given in inverse chronological order and referred to in the text by their Roman numerals, are included in this thesis.

Paper I: **Tidal disruptions by rotating black holes: effects of spin and impact parameter**
Gafton, E. & Rosswog, S.
MNRAS, **487**, 4790–4808 (2019), arXiv: 1903.09147.

Paper II: **Tidal disruptions by rotating black holes: relativistic hydrodynamics with Newtonian codes**
Tejeda, E., **Gafton, E.**, Rosswog, S. & Miller, J.
MNRAS, **469**, 4483–4503 (2017), arXiv: 1701.00303.

Paper III: **Magnetohydrodynamical simulations of a tidal disruption in general relativity**
Sądowski, A., Tejeda, E., **Gafton, E.**, Rosswog, S. & Abarca, D.
MNRAS, **458**, 4250–4268 (2016), arXiv: 1512.04865.

Paper IV: **Relativistic effects on tidal disruption kicks of solitary stars**
Gafton, E., Tejeda, E., Guillochon, J., Korobkin, O. & Rosswog, S.
MNRAS, **449**, 771–780 (2015), arXiv: 1502.02039.

Author's contribution

My contribution to the papers included in this thesis can be summarized as follows:

Paper I: I came up with the idea for this paper, ran all the simulations, devised and ran the postprocessing operations, created all the figures, wrote the entire first draft (including the appendices) and about $\sim$ 98% of the final text of the paper.

Paper II: I wrote most of the first draft of the paper (Sections 1, 3.2, 4, 5, 6). I set up, ran and analysed all the SPH simulations, and created most of the figures (Figures 1, 3, 4, 5, 6, 7, 8, 9, 10, 11, 12, 13). The idea for this method was already foreshadowed in the appendices of Paper IV (for the Schwarzschild case), though it was E. Tejeda (the first author) who derived the mathematical equations for the Kerr case.

Paper III: I set up and ran the SPH simulations for this paper, participated in their conversion to grid data and in the analysis of the results; I also contributed with corrections to the first draft of the paper.

Paper IV: The idea for this paper was suggested by the third author, J. Guillochon. I set up and ran all the simulations, devised and ran the postprocessing operations, created most of the figures (Figures 1, 2, 3, 4, 5, 6, 7, 9), wrote the first draft (excluding the appendices) and about $\sim$ 80% of the final text of the paper.

Contribution from the licentiate

This thesis builds upon the author's licentiate thesis (defended on December 18, 2015). The literature review and the analytical description of tidal disruptions have been updated and included in this thesis (as Chapters 1 and 2). Of the papers included in this thesis, only Paper IV was part of the licentiate.

By chapters, the contribution from the licentiate thesis is as follows:

Chapter 1: This chapter was included in the licentiate; for this thesis it has been reviewed and updated, and around 10% of the text and references are new.

Chapter 2: The theoretical derivations were included in the licentiate, and have been updated; where typos or mistakes were found, they have been corrected; around 20% of the text is new, as various subsections have been added to introduce quantities that were not discussed in the licentiate; some figures have been changed and some new figures have been added (resulting from the work on Paper I).

Chapter 3: The description of how SPH is used to simulate TDEs was present in the licentiate, but this chapter has been heavily edited. Around 80% of the material in Sec. 3.1 is new, and a significant part of the text in the licentiate thesis has been left out. On the other hand, Sec. 3.2 was not part of the licentiate thesis. It is based on the theoretical presentation from Paper II, although it is written in a more detailed style.

Chapter 4: This chapter summarizes the results from all our papers, and in particular of Paper I. It contains a few items discussed in the last chapter of the licentiate, related to partial disruptions, but most of it (around 95%) is new material.

Publications not included in this thesis

The following co-authored publications are not included in this thesis.

1. **A metallicity study of 1987A-like supernova host galaxies**
   Taddia, F., Sollerman, J., Razza, A. **Gafton, E.**, [5 authors], *A&A*, **558**, A143 (2013), arXiv: 1308.5545.

2. **MODA: a new algorithm to compute optical depths in multi-dimensional hydrodynamic simulations**
   Perego, A., **Gafton, E.**, Cabezón, R., Rosswog, S. & Liebendörfer, M., *A&A*, **568**, A11 (2014), arXiv: 1403.1297.

3. **The high-redshift gamma-ray burst GRB140515A. A comprehensive X-ray and optical study**
   Melandri, A., Bernardini, M.G., D'Avanzo, P., Sanchez-Ramirez, R., [9 authors], **Gafton, E.**, [11 authors], *A&A*, **581**, A86 (2015), arXiv: 1506.03079.

4. **Primary black hole spin in OJ 287 as determined by the General Relativity centenary flare**
   Valtonen, M. J., Zola, S., Ciprini, S., Gopakumar, A., [83 authors], **Gafton, E.**, [3 authors], *ApJL*, **819**, L37 (2016), arXiv: 1603.04171.

5. **A Search for QPOs in the Blazar OJ287: Preliminary Results from the 2015/2016 Observing Campaign**
   Zola, S., Valtonen, M., Bhatta, G., [89 authors], **Gafton, E.**, [2 authors], *Galaxies*, **4**, 41 (2016).

6. **The WEAVE observatory control system**
   Picó, S., Abrams, D.C., Benn, C., [9 authors], **Gafton, E.**, [7 authors], *Proceedings of the SPIE*, **10704**, 107042A (2018).

7. **Stochastic Modeling of Multiwavelength Variability of the Classical BL Lac Object OJ 287 on Timescales Ranging from Decades to Hours**

Goyal, A., Stawarz, Ł., Zola, S., [43 authors], **Gafton, E.**, [66 authors], *ApJ*, **863**, A175 (2018), arXiv: 1709.04457.

8. **Authenticating the Presence of a Relativistic Massive Black Hole Binary in OJ 287 Using Its General Relativity Centenary Flare: Improved Orbital Parameters**
Dey, L., Valtonen, M.J., Gopakumar, A., [36 authors], **Gafton, E.**, [64 authors], *ApJ*, **866**, A11 (2018), arXiv: 1808.09309.

2013

- ATel #5087, *NOT spectroscopic classifications of optical transients*

2014

- GCN #16253, *GRB 140512A: Optical observations from the 2.5 m NOT*
- GCN #16278, *GRB 140515A: Optical observations from the 2.5 m NOT*
- GCN #16290, *GRB 150416A: NOT optical observations*
- GCN #16310, *GRB 140512A: Redshift from NOT*

2016

- GCN #19136, *GRB 160303A: Optical observations from the NOT*
- GCN #19152, *GRB 160303A: Continued optical monitoring from NOT*
- GCN #19834, *GRB 160821B: NOT optical afterglow candidate*
- GCN #20146, *GRB 161108A: NOT candidate afterglow*
- GCN #20150, *GRB 161108A: NOT redshift*
- GCN #20258, *GRB 161214A: NOT observations of the afterglow*
- ATel #8802, *Optical Photometry of the flaring gamma-ray blazar AO 0235+164*
- ATel #9734, *Spectroscopic Classification of ASASSN-16na with the Nordic Optical Telescope*
- ATel #9741, *Detection of a very red source at the position of SWIFT J1753.5-0127*
- ATel #9744, *Spectroscopic observations of AT2016hvu and PNV J00424181+4113433 with the Nordic Optical Telescope*
- ATel #9834, *Spectroscopic observation of the supernova SN2016ios/Gaia16byj by NUTS (NOT Un-biased Transient Survey)*
- ATel #9836, *Spectroscopic observation of SN 2016ieq and SN 2016isg by NUTS (NOT Un-biased Transient Survey)*

2017

- ATel #10694, *Spectroscopic classification of SN 2017frc by NUTS (NOT Unbiased Transient Survey)*
- ATel #10698, *Spectroscopic observation of SN2017gkk by NUTS (NOT Unbiased Transient Survey)*

List of figures

sharp dropoff in the flaring rate at $m_{\rm bh} \sim 10^8\,M_\odot$, which confirms that – complementary to AGNs, which are biased towards the larger SMBHs – TDEs are biased towards lower-mass SMBH. The other observation is that MS stars are the most common victims of disruption by SMBHs with $m_{\rm bh} \lesssim 10^8\,M_\odot$, while RG and AGB stars dominate the demographics for larger SMBHs.

This figure reproduces Fig. 14 of MacLeod *et al.* (2012).

Fig. 2.3 on p. 15: Histograms of total mechanical energy $\mathcal{E}$ after disruption, for various parabolic Newtonian encounters with impact parameters β between 0.6 and 1 (*left panel*), and between 2 and 10 (*right panel*). Darker hues correspond to higher values of β. In these simulations, we use $m_\star = M_\odot, r_\star = R_\odot, m_{\rm bh} = 10^6\,M_\odot$. The logarithmic scale on the y axis allows us to easily read off the energy spread $d\mathcal{E}$ from the chart.

This figure was produced by the author, using data from our own simulations.

Fig. 2.4 on p. 15: Width of the $\Delta\mathcal{E}$ interval (scaled by $\mathcal{E}_{\rm ref} = Gq^{1/3}M_\odot/R_\odot$) that contains 98% of the particles, plotted against the impact parameter β. We observe that $\Delta\mathcal{E}$ does not follow a simple power law. For comparison, we overplot the $\Delta\mathcal{E} \sim k\beta^2$ power law given by Eq. (2.17) (dashed black line), and the $\Delta\mathcal{E} \sim k\beta^0$ law given by Eq. (2.18) (horizontal dotted line). Empirically, we find $k \approx 2.05$ for our $\gamma = 5/3$ non-rotating polytrope.

The data behind these plots came from our own simulations; the figure was published as Fig. 12 in Paper II.

Fig. 2.5 on p. 25: The return rate of the debris exhibits a characteristic "outburst-like" evolution, consisting of a fast rise (of the order of days) and a slow decay (of the order of years). If the circularization time scale is much shorter than the fallback time scale – and this question, far from being answered, is currently being pursued by a number of groups –, the light curve will exhibit a very similar behaviour. This plot shows the $\dot{M}$ curves for TDEs with $0.55 \leq \beta \leq 11$. While β has an obvious influence on the rise of the $\dot{M}$ curve (in both slope and maximum value), all curves with $\beta \gtrsim 1$ exhibit essentially the same decay governed by a $t^{-5/3}$ power law (oblique, gray dotted lines).

This figure was produced by the author, using data from our own simulations, and is essentially a simplified version of the Newtonian panel of Fig. 8 in Paper I.

Fig. 2.6 on p. 29: Two representations of the loss cone: a) A star with a given orbital trajectory lies within the loss cone if the angle ϑ between the position and the velocity vectors falls within the range of the critical $\vartheta_{\rm lc}$; b) In the space spanned

by the energy and angular momentum, the loss cone contains orbits with angular momenta $L \leq L_{\rm lc}$, given in terms of $\mathcal{R} \equiv L^2/L_{\rm lc}(\mathcal{E})^2$.

This figure reproduces Fig. 1 of Merritt (2013).

Fig. 2.7 on p. 39: Magnitude of relativistic effects as a function of the periapsis distance $r_{\rm p}$ expressed in gravitational radii $r_{\rm g} = Gm_{\rm bh}/c^2$, as computed using Eqs. (2.84), (2.85) and (2.87), assuming an orbit with $e = 0.98$. Decreasing the eccentricity slightly increases the magnitude of the angular precessions (since it reduces the apocentre distance, which appears in the denominator), but most TDEs will have $e \approx 1$. Changing the black hole spin has a very small effect on the Lense–Thirring precession, as evidenced by the small difference between the green lines. We observe that all effects decrease by more than two orders of magnitude within 100 $r_{\rm g}$, and that the third order effects (here, Lense–Thirring precession) is about two orders of magnitude weaker than the second-order effects (apsidal precession and gravitational redshift).

This figure was produced by the author, based on Eqs. (2.84), (2.85) and (2.87).

Fig. 3.1 on p. 48: Spatial distribution of the tidal debris shortly after the first periapsis passage (red particles), and at the beginning of the second periapsis passage (green particles), in a parabolic ($e = 1$; *left panel*) and an elliptical ($e = 0.8$; *right panel*) encounter. The figure reveals the virtually one-dimensional nature of the stream as it returns to the SMBH and starts the circularization process. The effect is much more pronounced in parabolic encounters, while in elliptical encounters the width of the stream can often be resolved satisfactorily. If not carefully handled, the head of the debris stream (consisting of single particles returning to periapsis one by one) may cause serious problems to the simulation, as discussed in the main text.

This figure was produced by the author, using data from our own simulations.

Fig. 4.1 on p. 60: Morphological types of debris stream seen in our simulations. The colour coding denotes self-bound (yellow), bound (red), unbound (blue) and plunging (green) particles, with the colour intensity being related to the logarithm of the density. Types E, F and G are only seen in relativistic simulations. The axes are given in units of GM/c^2 and with the origin in the centre of mass of the debris. The dashed black arrow points in the direction of the black hole, while the solid green arrow points in the direction of motion of the centre of mass.

This figure was produced by the author, using data from our own simulations, and was included as Fig. 3 in Paper I.

Abbreviations and symbols

Abbreviations

AGN	**A**ctive **G**alactic **N**ucleus
AU	**A**stronomical **U**nit
BH	**B**lack **H**ole
GR	**G**eneral **R**elativity
HVS	**H**yper-**V**elocity **S**tar
IMBH	**I**ntermediate-**M**ass **B**lack **H**ole
MHD	**M**agneto**h**ydro**d**ynamics
MS	**M**ain-**S**equence
NS	**N**eutron **S**tar
QSO	**Q**uasi-**S**tellar **O**bject
SMBH	**S**uper-**M**assive **B**lack **H**ole
SPH	**S**moothed **P**article **H**ydrodynamics
TDE	**T**idal **D**isruption **E**vent
TVS	**T**urbo-**V**elocity **S**tar
WD	**W**hite **D**warf
XRB	**X**-**R**ay **B**inary System

Symbols

β	impact parameter
$\beta_{\rm d}$	critical impact parameter for disruption
ℓ_z	specific angular momentum along the BH spin axis

γ	polytropic exponent
γ_{ad}	adiabatic exponent
$\mathcal{E}$	specific mechanical energy
$\mathcal{L}$	specific angular momentum
$M_\odot$	mass of Sun
$R_\odot$	radius of Sun
σ	velocity dispersion
a	black hole Kerr parameter
c	speed of light
c_{s}	speed of sound
c_{v}	specific heat at constant volume
G	gravitational constant
J	black hole spin
k_{B}	Boltzmann constant
L_{Edd}	Eddington luminosity
m_{bh}	mass of black hole
m_{p}	mass of proton
$m_\star$	mass of star
n	polytropic constant
r_{a}	apapsis distance
r_{e}	event horizon radius
r_{g}	gravitational radius
r_{h}	black hole radius of influence
r_{p}	periapsis distance
r_{s}	Schwarzschild radius
r_{t}	tidal radius
$r_\star$	radius of star
z	redshift

1

Preliminaries

The world is indeed full of peril,
and in it there are many dark places.
Haldir

Direct observations of the centre of M87 (Event Horizon Telescope Collaboration *et al.*, 2019), as well as dynamical studies of stellar and gas kinematics near the cores of local galaxies such as the Milky Way (Schödel *et al.*, 2003; Ghez *et al.*, 2008), M31 (Kormendy & Bender, 1999; Bender *et al.*, 2005; Garcia *et al.*, 2010) and M32 (van der Marel *et al.*, 1997) provide strong evidence for the existence of supermassive black holes (SMBH). Numerous indirect observations have established that SMBHs span a wide range of masses, from $\sim 10^5\ M_\odot$ (Secrest *et al.*, 2012) to as much as a few $\times 10^{10}\ M_\odot$ (van den Bosch *et al.*, 2012). Recent reviews on the nature, properties and manifestations of our own galaxy's supermassive black hole, Sgr A*, have been published by Genzel *et al.* (2010) and Morris *et al.* (2012). The formation and evolution of these extreme objects are still subject of debate (Volonteri, 2012), but it is generally accepted that gas accretion onto them is the mechanism behind quasars (historically called quasi-stellar objects, and hence frequently abbreviated to QSOs), the most energetic form of active galactic nuclei (AGNs): luminous sources that can outshine the rest of their host galaxy by a few orders of magnitude. The idea of quasars being gas accretion-powered supermassive black holes goes back to Lynden-Bell (1969).

Such highly luminous AGNs are thought to have been a common occurence a few billion years after the Big Bang (during the so-called "quasar era" at redshift $z \sim 3$, see e.g. Kormendy & Richstone, 1995; Richstone *et al.*, 1998), but AGN activity has since subsided, and most nearby galactic nuclei (including our own) are nowadays quiescent, with the SMBHs dim and hence probably starved of fuel (Rees, 1990; Ho, 2008; Schawinski *et al.*, 2010). Their dimness is one of the major unresolved problems in accretion theory, since most of these SMBHs seem to have enough gas around them to sustain a steady AGN (e.g., Menou & Quataert 2001): the occurrence of a radiatively inefficient (advection- or convection-dominated) accretion mode might be the answer to the dimness problem (Narayan, 2002).

It is in any case difficult to probe the existence and determine the properties (mass and spin, no hair) of SMBHs. While for nearby galaxies one can resolve the stellar distribution near the galactic centre and thus conduct dynamical observations (e.g., Ghez *et al.*, 2008), or even monitor tiny variations in the activity of the SMBH (faint, but frequent flares on time scales of days, e.g. Garcia *et al.* 2010; Li *et al.* 2011; Zubovas *et al.* 2012), in more distant galaxies only the $\sim 1\%$ of SMBHs undergoing major accretion episodes can be observed directly. The question then, arises, of what transient events might brighten up these SMBHs, and of how to predict and explain their observational signature.

Tidal disruptions, violent events in which stars are ripped apart into loose gas streams by the extremely steep gravitational potential of a black hole[1] were first proposed as means of fuelling AGNs (Hills, 1975; Sanders, 1984), but Shields & Wheeler (1978) showed that they cannot in fact provide the required steady supply of energy.

> Their reasoning is twofold, though one must first distinguish between two AGN models: (a) black hole steadily accreting gas as it is produced, versus (b) black hole having quiescent periods during which a large amount of gas ($\sim 10^6\ M_\odot$) is stored, followed by brief periods of gas ingestion at high luminosities ($\sim$ the Eddington luminosity, $L_{\rm Edd}$).
> For the first scenario, tidal disruption rates are not high enough to sustain a continuous gas flow, because low angular momentum orbits are quickly depleted of stars (this so-called "loss cone depletion" will be discussed in Sec. 2.4.2), and subsequent relaxation of stars into disruptive orbits is too slow to give adequate QSO luminosity, even when enhanced by some collective process (e.g., inside a stellar cluster). Also, it cannot be neglected that the most luminous quasars have the stellar disruption radius far inside the event horizon (except for the giant stars; see Sec. 2.1.5), which means that tidal disruption of solar-type stars cannot happen there in the first place.
> For the second scenario, such a mass of gas cannot be supported by its own internal pressure, though it can be supported in a disc by angular momentum. Various instabilities can then trigger the phase of rapid accretion and high luminosity. Tidal disruptions can certainly contribute to such an accretion disc, along with general infall of galactic gas, usually triggered by galaxy mergers (e.g., Younger *et al.*, 2009), and gas produced by nearby stellar winds (e.g., Cuadra *et al.*, 2006).

Later on, Frank & Rees (1976) estimated for the first time the rates and probable manifestations of tidal disruptions by massive black holes in globular clusters, and (more like a proof of concept) applied their results to a galactic nucleus with a supermassive black hole. The idea was taken further by Frank (1978), Lidskii & Ozernoi

[1] It is steep in the sense that the potential difference over a relatively short distance (the radius of the star) is large enough to overcome the self-gravity of the star, causing its disruption.

(1979) and Lacy *et al.* (1982), who discussed the fate of the gas liberated by tidal disruptions, but it was Rees (1988) who laid the foundations of the modern theory of tidal disruptions, by describing their evolution, the light curves, the possible radiation-driven outflows, and the fate of the ejected, unbound material.

Gas originating from processes other than tidal disruptions (for instance, the already-mentioned infall of galactic gas and the winds from young stars close to the SMBH) is probably also orbiting these massive black holes, and its accretion would also give rise to flares and allow us to probe the SMBHs. However, the amount and the distribution of gas near galactic centres cannot be easily predicted, and gas accretion episodes can be relatively chaotic: with the exception of the inner ~ 10 pc around Sgr. A*, where the extent of the surounding gas is observationally constrained, very little is known about the properties of the media surrounding the SMBHs of inactive galaxies, and limits can only be placed on their density and pressure structures based on first principles. Also, gas dynamics is governed not just by gravitational forces, but also by pressure and magnetic forces, while stars are "clean gravity probles" (Alexander, 2003). Their structure is well-known from more "peaceful" environments, and their luminosities and spectra act as proxies for their mass and age (that is, of course, if they behave the same in such extreme environments). The stellar distribution in the dense environment around a SMBH is then much better constrained, both theoretically and observationally, and can lead to more accurate predictions concerning the rates and the evolution of tidal disruption events. For instance, in a galaxy like ours, which is believed to harbour a SMBH of $\sim 4 \times 10^6\ M_\odot$ (e.g., Ghez *et al.*, 2008), the expected tidal disruption rates are between $10^{-6}\ \mathrm{yr}^{-1}$ (Syer & Ulmer, 1999; Donley *et al.*, 2002) and $10^{-4}\ \mathrm{yr}^{-1}$ (Magorrian & Tremaine, 1999; Brockamp *et al.*, 2011), with the exact rates depending on the steepness of the galactic nuclear density profile, stellar evolution, etc. (Wang & Merritt, 2004) (conservative, respectively generous estimates might extend these values by an order of magnitude in either direction). The rates would be enhanced by the presence of a massive perturber, such as an intermediate mass black hole (Chen & Liu, 2013) or a cluster of $\sim 10^4$ stellar-mass black holes (Miralda-Escudé & Gould, 2000) co-orbiting the SMBH.

Tidal disruptions can therefore teach us about supermassive black holes in galactic nuclei in several ways, which we will quickly summarize. First, they can reveal the presence and the mass of the central black hole.

> We have already mentioned that individual stellar orbits around Sgr. A* are directly measurable (e.g., Ghez *et al.*, 2008; Gillessen *et al.*, 2009a; Genzel *et al.*, 2010). In external galaxies, direct imaging of individual stars in the galactic nuclei is not possible, but an alternative is available instead. For moderately massive, nearby galaxies in which the SMBH's radius of influence (Eq. 2.7) can be spatially resolved, one can take a long-slit spectrum across the centre of the galaxy, which gives an estimate of the velocity dispersion

σ as a function of radius r. $\sigma(r)$ can then be used to obtain either a crude estimate of the black hole's mass according to $Gm_{\rm bh}/r \approx \sigma^2(r)$, or a more exact value by fitting families of stellar orbits to the surface brightness profile and velocity dispersion data (e.g., Gebhardt *et al.*, 2000). Similar procedures can be developed for observing gas instead of starlight (e.g., Atkinson *et al.*, 2005). For more distant galaxies, SMBH masses can only be measured in a number of fortunate circumstances, such as the presence of an AGN whose brightness variability and emission line broadness allow the estimation of the SMBH mass (e.g., Landt *et al.*, 2013, and references therein), or the presence of water masers, whose orbital motion can be measured very precisely using radio interferometry (e.g., Greene *et al.*, 2010).

In Chapter 2 we will show that most properties of tidal disruptions (such as evolution time scales, peak luminosities and wavelengths) correlate well with the mass of the SMBH. Since tidal disruptions do not depend on the presence of an AGN and are fairly luminous (visible up to a redshift $z \sim 1$ according to Strubbe, 2011), they provide an independent technique for calculating SMBH masses, even in faint and distant galaxies. In fact, Milosavljević *et al.* (2006) argued that the number of tidal disruption-powered sources should increase with redshift because back then SMBHs were smaller, galactic nuclei were denser, and stars were more massive, all these enhancing the tidal disruption rate.

The accretion of gaseous debris from a disrupted star also provides a laboratory for testing accretion theories, which can then be applied to understand more complicated scenarios (such as galaxy mergers).

The ability of an accretion flow to radiate away its energy has major implications on its dynamics (see, e.g., Krolik, 1999; Frank *et al.*, 2002). For sub-Eddington accretion rates, the theory is fairly simple: the disc is geometrically thin because the time scale on which photons are created (thermally or by bremsstrahlung) and diffuse vertically out of the disc is much longer than the time in which gas can spiral inwards within the disc. Radiation therefore provides an efficient cooling mechanism, and the disc is expected to emit as a multicolor blackbody. If the accretion rate surpasses the Eddington limit, however, radiation may no longer cool the disc efficiently. Photons are trapped in the disc, which becomes hot; a part of the photons may be advected with the fluid towards the black hole, while the other part may drive – through sheer radiation pressure – some of the low angular momentum gas in an outflow away from the black hole (e.g., King & Pounds, 2003). The dynamics and observational signatures of super-Eddington accretion flows have been studied theoretically (e.g., Abramowicz *et al.*, 1988) and numerically (e.g., Ohsuga *et al.*, 2005), but they remain unsolved questions in ac-

cretion theory. Intriguingly, since the trapping and advection of photons in super-Eddington flows are expected to saturate the luminosity of SMBHs, such systems have recently been suggested to work as cosmological standard candles (Wang *et al.*, 2013).

There are few chances of observing super-Eddington flows in action, most notably in quasars (e.g., Kollmeier *et al.*, 2006) and, very rarely, in those X-ray binary systems (XRBs) that are in the so-called "very high state" (e.g., Esin *et al.*, 1997). Tidal disruption would provide another such opportunity, since the initial inflow of gas towards the black hole after the star has been disrupted is expected to occur at super-Eddington rates (this will be calculated in a simple way in Sec. 2.3.3). Tidal disruptions could perhaps be easier to interpret than AGNs and XRBs, since they may have a more predictable mass feeding rate and inflowing gas geometry. In addition, the time scales on which tidal disruptions events unfold would allow us to observe a wide range of feeding rates within just months to years.

Tidal disruption rates can also shed a light on the structure and history of galactic nuclei, on scales that cannot be resolved through direct imaging (except perhaps for a handful of local galaxies).

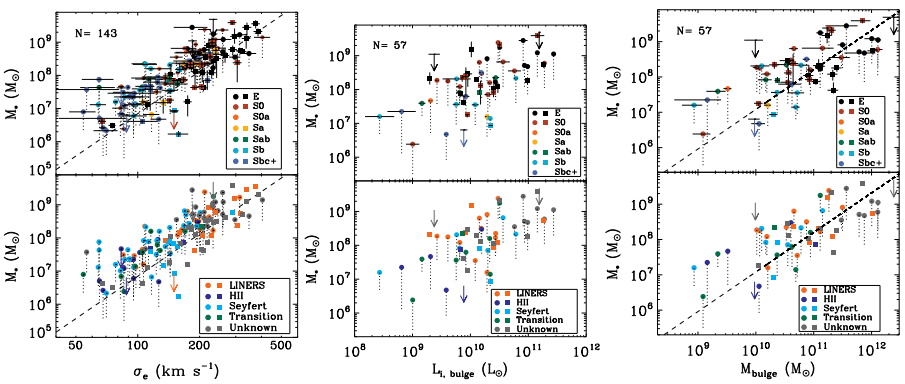

Figure 1.1: The $m_{\rm bh}$–$\sigma_{\rm b}$, $m_{\rm bh}$–$L_{\rm b}$ and $m_{\rm bh}$–$m_{\rm b}$ relations in two sample sets of galaxies (*upper* and *lower panels*). This figure reproduces Figs. 4, 5 and 6 of Beifiori *et al.* (2012).

Observational studies found empirical scaling relations between the mass of the SMBH and properties of its surrounding galactic bulge (see Fig. 1.1), such as stellar velocity dispersion $\sigma_{\rm b}$ ("$m_{\rm bh}$–$\sigma_{\rm b}$" relation; Gebhardt *et al.*, 2000; Ferrarese & Merritt, 2000; Pota *et al.*, 2013), luminosity $L_{\rm b}$ ("$m_{\rm bh}$–$L_{\rm b}$" relation; Kormendy & Richstone, 1995; Faber *et al.*, 1997; Ferrarese & Ford, 2005), bulge mass $m_{\rm b}$ ("$m_{\rm bh}$–$m_{\rm b}$" relation; Magorrian *et al.*, 1998; Häring & Rix, 2004), central light deficit (Hopkins & Hernquist, 2010), and total number of globular clusters (Burkert & Tremaine, 2010). This is a surprising

feature considering that the bulge extends far beyond the gravitational influence of the black hole, and suggests that SMBHs and bulges evolve together (Silk & Rees, 1998; Di Matteo *et al.*, 2005) in a (so-far) poorly-understood process which is nevertheless of central interest to the field of galaxy evolution. The relevance for tidal disruptions is that the density structure of the bulge nucleus determines which processes dominate the funnelling of stars on to disruption orbits, therefore controlling the disruption rate. For example, in spherically symmetric and isotropic nuclei, two-body relaxation is likely the main driver of stars on disruption orbits (e.g., Frank & Rees, 1976). In triaxial or axisymmetric potentials (typical of e.g. bar or spiral discs), chaotic stellar orbits can enhance the disruption rate without requiring gravitational scattering (e.g., Merritt & Poon, 2004), and the same can happen in the vicinity of two merging SMBHs (e.g., Chen *et al.*, 2009). Observation of tidal disruption rates can therefore, at least in principle, put constraints on the structure and history of distant galactic nuclei that cannot be otherwise resolved.

Tidal disruptions also contribute to the growth of seed black holes into full-fledged SMBHs (Zhao *et al.*, 2002; Miralda-Escudé & Kollmeier, 2005; Bromley *et al.*, 2012), with the total mass of stars consumed by one SMBH over the lifetime of its galaxy expected to be as high as $10^6\ M_\odot$, independent of galaxy luminosity (Magorrian & Tremaine, 1999). In the Milky Way, where individual stars and their orbits can be observed directly, tidal disruptions can also be used to probe general relativistic effects close to the black hole. Expected post-Newtonian deviations include orbital periapsis shift, Lense-Thirring precession and gravitational redshift (these will be discussed in Sec. 2.5), and possibly low-frequency gravitational waves, since disruptions of very low-mass main sequence stars are similar in signature to the extreme-mass ratio inspiral scenarios (Frank & Rees, 1976; Wang & Merritt, 2004; Madigan *et al.*, 2011).

Finally, tidal disruption of stellar binary systems that venture too close to the black hole may be able to explain a number of puzzling observations around Sgr. A*. First, they are thought to be the source of high velocity stars ($v \gtrsim 1000$ km s^{-1}) ejected from our galaxy (Sesana *et al.*, 2007), since the classical binary supernova scenario (Blaauw, 1961) can only produce velocities $\lesssim 300$ km s^{-1} for solar-type stars (Antonini *et al.*, 2010). Tidal disruptions may also be the key to the origin of the S-stars, apparently young, main sequence stars in tight eccentric orbits around the SMBH (e.g., Perets & Gualandris, 2010). The observations of the S-stars are of paramount importance for measuring the properties of and understanding the dynamics around Sgr. A* (e.g., Eisenhauer *et al.*, 2005; Gillessen *et al.*, 2009b), and will be reviewed in Sec. 2.4.3.

2

Theoretical aspects

I have had my results for a long time:
but I do not yet know how I am to arrive at them.
Carl Friedrich Gauss

We begin our analysis of tidal disruption events (TDEs) by introducing a number of length scales, time scales, and other physical quantities that govern the evolution of such events.

Equations will often be rescaled to typical quantities that appear in TDEs (e.g., $10^6\,M_\odot$ for SMBH masses, parsecs or gravitational radii for distances, etc.). We note that in the literature physical lengths are sometimes expressed in terms of angular sizes for a distance to the Galactic Centre of $r_0 \approx 8$ kpc, corresponding to 1 arcsec $\approx$ 0.039 pc (e.g., Eisenhauer *et al.*, 2003).

2.1 Length scales

2.1.1 Event horizon

The event horizon can be thought of as a one-way surface that matter and light can only cross going inwards. Since matter plunging into the event horizon becomes causally disconnected from the rest of the universe, the existence of an event horizon directly affects the overall dynamics and energy budget in an accretion system.

For a non-rotating black hole, the event horizon is located at the Schwarzschild radius r_s,

$$\begin{aligned} r_\mathrm{s} &= \frac{2Gm_\mathrm{bh}}{c^2} \\ &\approx 9.6\times10^{-8}\ \mathrm{pc}\left(\frac{m_\mathrm{bh}}{10^6\,M_\odot}\right). \end{aligned} \tag{2.1}$$

For a spinning black hole with spin J and Kerr parameter $a \equiv J/m_\mathrm{bh}c$, the event

horizon r_e is situated at (e.g., Misner *et al.*, 1973, p. 879)

$$\begin{aligned} r_e &= \frac{Gm_{bh}}{c^2} + \sqrt{\left(\frac{Gm_{bh}}{c^2}\right)^2 - a^2}, \\ &= x\frac{Gm_{bh}}{c^2} \end{aligned} \tag{2.2}$$

with $1 \leq x \leq 2$ and $x = 1$ for a maximally spinning ($a = Gm_{bh}/c^2$ or $J = Gm_{bh}{}^2/c$) black hole. In this thesis and in the papers we will normally use the dimensionless spin parameter $a^\star \equiv Jc/Gm_{bh}{}^2$, which ranges from -1 to 1, with the convention that $a^\star > 0$ for prograde orbits and $a^\star < 0$ for retrograde orbits.

2.1.2 Innermost stable circular orbit

Typically referred to as "ISCO", it marks the transition radius within which stable circular motion is no longer possible. For a standard thin accretion disc, this implies the existence of an inner edge from which the fluid falls essentially freely into the BH. The radius of this orbit is a function of the spin parameter of the BH. The formula for it is (see e.g. Frolov & Novikov, 1998):

$$r_{isco} = \frac{Gm_{bh}}{c^2}\left(3 + Z_2 \pm \left[(3 - Z_1)(3 + Z_1 + 2Z_2)\right]^{1/2}\right), \tag{2.3}$$

where

$$Z_1 = 1 + \left(1 - a^{\star 2}\right)^{1/3}\left[(1 + a^\star)^{1/3} + (1 - a^\star)^{1/3}\right] \tag{2.4}$$

$$Z_2 = \left(3a^{\star 2} + Z_1{}^2\right)^{1/2}. \tag{2.5}$$

For a Schwarzschild black hole, therefore, the ISCO is located at $3\,r_s$.

2.1.3 Marginally bound circular orbit

In general relativity there is a critical value for the angular momentum of a test particle below which the resulting centrifugal repulsion is not enough to prevent the trajectory from plunging into the BH's event horizon. This translates into a minimum periapsis distance that a given trajectory can attain. In the case of marginally bound particles (i.e. particles with parabolic-like energies), the corresponding radius is given by (Bardeen, Press & Teukolsky, 1972):

$$r_{mb} = 2m_{bh} - a + 2\sqrt{m_{bh}(m_{bh} - a)}. \tag{2.6}$$

In the context of TDEs, the different ways in which this radius and the tidal radius scale with the BH's mass ($r_{mb} \propto m_{bh}$ and $r_t \propto m_{bh}{}^{1/3}$, respectively) imply that, for a given type of star, there exists a maximum possible value of m_{bh} above which the star will be swallowed whole inside the BH horizon before being tidally disrupted, see Fig. 2.1 below.

2.1.4 Radius of influence

The central black hole's radius of influence r_h defines the region where stellar dynamics is dominated by the gravity of the black hole. Kinematically, this corresponds approximately to the sphere that encloses stellar (plus dark matter) mass (m_st) equal to the mass of the black hole, $m_\mathrm{st}(r < r_\mathrm{h}) \sim m_\mathrm{bh}$, so that the gravitational potential of the SMBH is greater than the combined gravitational potential of the surrounding stars. Measurements around Sgr. A* indicate that $m_\mathrm{st}(r \lesssim 2\ \mathrm{pc}) \simeq m_\mathrm{bh}$ and $m_\mathrm{st}(r \lesssim 4\ \mathrm{pc}) \simeq 2\ m_\mathrm{bh}$ (Schödel *et al.*, 2003), which gives a radius of influence of the order of $r_\mathrm{h} \sim 2$ pc.

Customarily, the radius of influence has been defined by equating the kinetic energy of a star ($\sim m_\star {\sigma_\star}^2$) to its energy in the gravitational potential of the black hole ($\sim Gm_\star m_\mathrm{bh}/r$), while ignoring factors of order unity,

$$\begin{aligned} m_\star {\sigma_\star}^2 &= \frac{Gm_\star m_\mathrm{bh}}{r_\mathrm{h}} \\ r_\mathrm{h} &= \frac{Gm_\mathrm{bh}}{{\sigma_\star}^2}, \\ &\approx 1.72\ \mathrm{pc} \left(\frac{m_\mathrm{bh}}{10^6 M_\odot}\right) \left(\frac{\sigma_\star}{50\ \mathrm{km\ s^{-1}}}\right)^{-2}, \end{aligned} \tag{2.7}$$

where $\sigma_\star$ is the one-dimensional stellar velocity dispersion, ${\sigma_\star}^2 = \langle {v_\star}^2 \rangle$, where the average is over the stellar velocity distribution. While this approximation holds for an isothermal sphere, in which $\langle {v_\star}^2 \rangle$ is independent of position (e.g., Binney & Tremaine, 2008, Sec. 4.3.3), for a non-isothermal density distribution (as in the case of real galactic nuclei), $\sigma_\star$ is in fact a function of radius, and the above expression is not well defined and can only serve as an order-of-magnitude estimate.

Comparing the numerical value of r_h (Eq. 2.7) with the value of r_s (Eq. 2.1), we notice ~ 8 orders of magnitude in difference. Since general relativistic effects only become important on distances of the order of the Schwarzschild radius, most of the stars that move under the influence of the SMBH follow essentially Keplerian orbits.

2.1.5 Tidal radius

Tidal disruption occurs when a star of mass $m_\star$ and radius $r_\star$ approaches a supermassive black hole of mass m_bh on an orbit with periapsis r_p smaller than the tidal radius r_t, defined as the distance at which the gravitational acceleration at the surface of the star ($\sim Gm_\star/{r_\star}^2$) is surpassed by the tidal acceleration ($\sim Gm_\mathrm{bh} r_\star/r^3$), i.e.

$$\frac{Gm_\star}{{r_\star}^2} \lesssim \frac{Gm_\mathrm{bh} r_\star}{r^3} \Rightarrow {r_\mathrm{t}}^3 \simeq \frac{m_\mathrm{bh}}{m_\star} {r_\star}^3, \tag{2.8}$$

which leads directly to the usual definition,

$$r_t = \alpha r_\star \left(\frac{m_{bh}}{m_\star}\right)^{1/3} \tag{2.9}$$

$$= 100\, R_\odot \left(\frac{r_\star}{R_\odot}\right)\left(\frac{m_{bh}}{10^6\, M_\odot}\right)^{1/3}\left(\frac{m_\star}{M_\odot}\right)^{-1/3}\left(\frac{\alpha}{1}\right), \tag{2.10}$$

$$\overset{(2.1)}{\approx} 24.8\, r_s \left(\frac{r_\star}{R_\odot}\right)\left(\frac{m_{bh}}{10^6\, M_\odot}\right)^{-2/3}\left(\frac{m_\star}{M_\odot}\right)^{-1/3}\left(\frac{\alpha}{1}\right). \tag{2.11}$$

The dimensionless coefficient α is of order 1, and depends on the structure of the star. It was found to be ≈ 1.69 for a homogeneous, incompressible body (Luminet & Carter, 1986; Novikov *et al.*, 1992) and ≈ 0.89 for an $n = 3$ polytrope (Sridhar & Tremaine, 1992; Diener *et al.*, 1995). The critical periapsis distance $r_p = r_t$ at which the tidal forces disrupt a star is also called the effective Roche limit. Alternative physical formulations for the tidal disruption criterion are that the star is disrupted when its typical density ($\sim m_\star/{r_\star}^3$) falls bellow the density the SMBH would have had if its mass were spread over the volume ${r_t}^3$ ($\sim m_{bh}/{r_t}^3$), or when the crossing time through the dissipation zone $\left(\sim ({r_t}^3/Gm_{bh})^{1/2}\right)$ falls bellow the star's free fall time $\left(\sim ({r_\star}^3/Gm_\star)^{1/2}\right)$ (e.g., Alexander, 2012). Naturally, both alternative formulations yield the exact same expression for r_t we derived in Eq. (2.8).

The tidal radius gives a measure of whether tidal forces are able to remove mass from the stellar surface, but the final fate of the star depends on whether these forces are strong enough to disrupt the star's densest regions. It is even possible for a core resulting from a seemingly complete disruption to recollapse into a self-bound object (Guillochon & Ramirez-Ruiz, 2013).

We point out the inverse dependence of r_t/r_s on m_{bh} in Eq. (2.11): this implies that if m_{bh} is sufficiently large, r_t can become smaller than r_s (or than r_e in the case of rotating black holes). Since tidal disruption can only occur if r_t lies outside the event horizon (Eq. 2.2), extremely massive black holes tend to "swallow" stars whole, without disrupting them first. Since

$$\frac{r_t}{r_e} \overset{(2.2),(2.9)}{=} \alpha r_\star \left(\frac{m_{bh}}{m_\star}\right)^{1/3}\frac{c^2}{xGm_{bh}}$$

$$\propto x^{-1}{\rho_\star}^{-1/3}{m_{bh}}^{-2/3}, \tag{2.12}$$

it follows that the more compact the star to be disrupted, the less massive the SMBH must be. In other words, for a star with a given $r_\star$ and $m_\star$, there exists a maximal black hole mass m_{bh} which is still able to disrupt the star. This implies that tidal disruption of main-sequence stars is an ineffective mechanism for powering more massive AGNs ($m_{bh} \gtrsim 10^8 M_\odot$), since the tidal gravity of these black holes would be too small to destroy the star before it crosses the event horizon (these SMBHs could still disrupt

giant stars though, see Figs. 2.1 and 2.2). Such an encounter would leave little, if any electromagnetic signature, although some gravitational wave emission could still be detected (Kobayashi *et al.*, 2004). Beloborodov *et al.* (1992) showed that this mass limit can be slightly increased for Kerr black holes, as long as the disrupted star approaches from a favourable direction.

Incidentally, some authors (e.g., Magorrian & Tremaine, 1999) find it useful to distinguish the "consumption" rate (the rate at which stars come within a radius r_t of the BH, even if the periapsis lies inside the event horizon) from the "flaring" rate (the rate of disruption of stars outside the horizon of the BH). This distinction should be taken into account when comparing rates of "disruption" events from various papers.

In an attempt to explain the lack of massive S-stars (see Sec. 2.4.3) very close ($\lesssim$ 10 AU) to the black hole, Li & Loeb (2013) recently suggested that heat deposited by excitation of modes within the star at each periapsis passage (under the cumulative effect of tidal heating by the SMBH and the gravitational interaction of the background stars) can lead to a runaway disruption of the star as far as five times farther than the normal tidal disruption radius. Unfortunately, since this is a secular effect, it probably has negligible consequences on the tidal disruption rates.

Another interesting possibility is related to the Brownian motion of the black hole (see, e.g., Alexander & Livio, 2001). Under the gravitational influence of the dense stellar cluster surrounding it, the SMBH oscillates about the common centre of mass with an amplitude much larger than the tidal radius, on a time scale comparable to the orbital period of the tidally disturbed stars (see Merritt *et al.* 2007 for simulations and a discussion). Stars approaching on disruptive orbits may therefore "just escape" doom.

2.1.6 Impact parameter

The strength of a tidal disruption event can be characterised by the dimensionless parameter (Press & Teukolsky, 1977)

$$\eta = \left(\frac{m_\star}{m_{\rm bh}} \frac{{r_{\rm p}}^3}{{r_\star}^3} \right)^{1/2}, \tag{2.13}$$

where $r_{\rm p}$ is the periapsis distance (see Sec. 2.1.7), although a significant part of the literature on tidal disruption uses the related impact parameter β, defined as

$$\beta = \frac{r_t}{r_{\rm p}} \overset{(2.9),(2.13)}{=} \eta^{-2/3}. \tag{2.14}$$

The outcome of the encounter is encoded in the parameter β. Generally, the star is disrupted when $\beta \gtrsim 1$. For $\beta \sim 1$, the star smoothly disrupts without any strong compression near periapsis, while for $\beta \gg 1$ the compression at periapsis is very

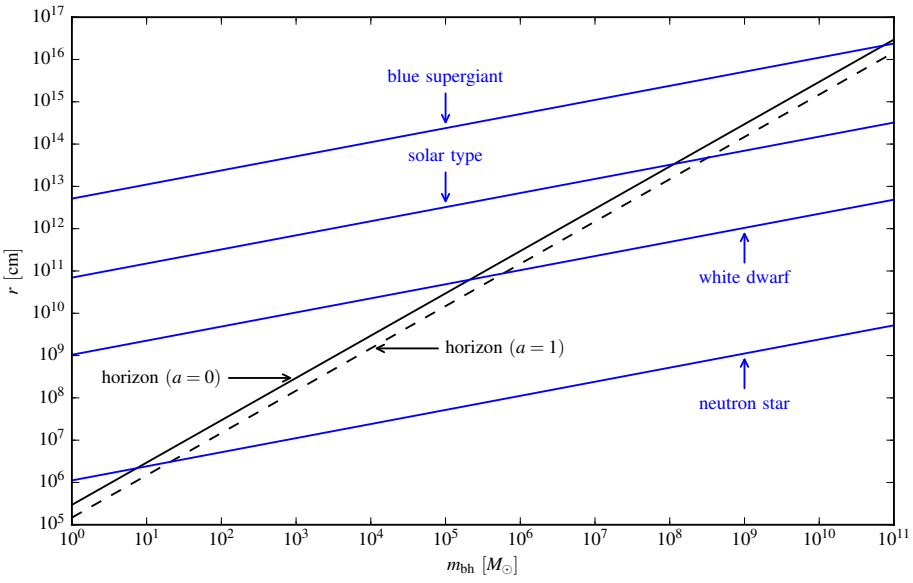

Figure 2.1: Tidal radius $r_{\rm t}$ and event horizon radius $r_{\rm e}$ as a function of black hole mass for various types of stars. Having a steeper dependence on the black hole mass than the tidal radius, see Eqs. (2.2) and (2.9), the event horizon eventually overcomes it, rendering tidal disruption impossible. In this example, the neutron star ($m_\star = 1.4\,M_\odot$, $r_\star = 12.5$ km) can only be disrupted by stellar-mass black holes ($m_{\rm bh} \lesssim 10\,M_\odot$), the white dwarf ($m_\star = 0.6\,M_\odot$, $r_\star = 9000$ km) can only be disrupted by intermediate mass black holes ($m_{\rm bh} \lesssim 10^5\,M_\odot$), the main-sequence star ($m_\star = M_\odot$, $r_\star = R_\odot$) can only be disrupted by supermassive black holes up to $m_{\rm bh} \lesssim 10^8\,M_\odot$, while the blue supergiant ($m_\star = 20\,M_\odot$, $r_\star = 200\,R_\odot$) can be disrupted even by the largest black holes ($m_{\rm bh} \simeq 10^{11}\,M_\odot$).

strong and causes a supersonic "pancaking" of the star into the orbital plane (Carter & Luminet, 1983, 1985).

A related quantity is the critical impact parameter for disruption $\beta_{\rm d}$, defined as the impact parameter necessary for a complete disruption of the star (with no surviving self-bound stellar remnant). It was first calculated by Diener *et al.* (1995) as $\beta_{\rm d} = 1.12$ for $\gamma = 4/3$ polytropes and $\beta_{\rm d} = 0.67$ for $\gamma = 5/3$ polytropes. Later on, Guillochon & Ramirez-Ruiz (2013) found instead the values $\beta_{\rm d} = 1.9$ for $\gamma = 4/3$ polytropes and $\beta_{\rm d} = 0.95$ for $\gamma = 5/3$ (the latter also confirmed in Paper IV and by Mainetti *et al.*, 2017), with the caveat that the exact boundary between survival and destruction for real stars might be different depending on rotation, metallicity and age. Stars that are counter-rotating with respect to the orbital axis, for instance, are much more difficult to disrupt (even when the orbit formally reaches the tidal radius), but such an encounter may give rise to peculiar X-ray transients (Sacchi & Lodato, 2019). The metallicity and age of the star, on the other hand, generate a

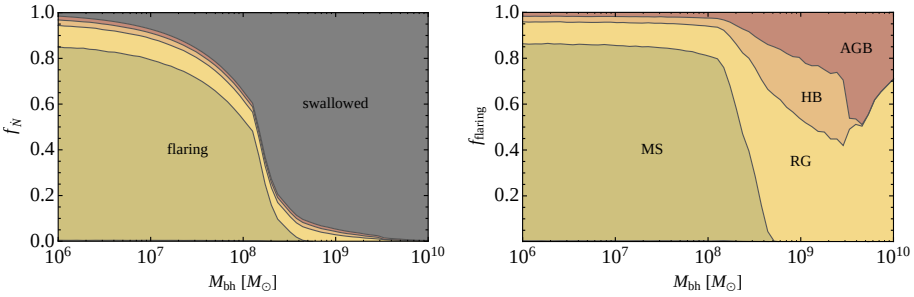

Figure 2.2: Fractional composition of stars scattered into the loss cone (*left panel*) and the demographics of the flaring events (*right panel*). The abbreviations refer to main-sequence stars (MS), red giants (RG), horizontal branch stars (HB), and asymptotic giant branch stars (AGB). The most striking observation is the sharp dropoff in the flaring rate at $m_{\rm bh} \sim 10^8\,M_\odot$, which confirms that – complementary to AGNs, which are biased towards the larger SMBHs – TDEs are biased towards lower-mass SMBH. The other observation is that MS stars are the most common victims of disruption by SMBHs with $m_{\rm bh} \lesssim 10^8\,M_\odot$, while RG and AGB stars dominate the demographics for larger SMBHs. This figure reproduces Fig. 14 of MacLeod *et al.* (2012).

departure from the simple polytropic structure typically assumed in numerical and analytic studies, and may have significant effects not only on the disruption limit, but also on the peak, time to peak, and shape of the mass fallback rate (Law-Smith *et al.*, 2019).

Alexander & Morris (2003) proposed the concept of squeezars, stars with $\beta \gtrsim 1$ that have narrowly escaped disruption but are caught on highly eccentric orbits around the SMBH. These would generate transients with an atypically high luminosity, comparable to their Eddington luminosity, powered by the tidal interactions with the black hole. Their expected life time, limited by mass loss near periapse, can be orders of magnitude larger than that of a normal ($\beta < 1$) tidal disruption event, providing an oportunity to observe the effects of strong tides in stars.

2.1.7 Apsides

The periapsis $r_{\rm p}$ (often called pericentre[2]) is the point at which the star is closest to the black hole, and its ratio to the tidal radius (β, discussed above) is the single most important quantity for determining the outcome of the encounter.

The first periapsis approach, while the star is still self-bound, is crucial because the entire star has virtually the same orbital kinetic energy. This means that the difference

[2] An archaic term for the periapsis of an orbit around a supermassive black hole is *peribarathron* (Young *et al.*, 1977), from the Ancient Greek *βάραθρον*, a supposedly bottomless pit in Athens into which the dead bodies of executed criminals were cast, and from which there was no return. Unfortunately, the term didn't quite catch on.

in specific binding energies of the future debris (at this point still parts of the star) comes entirely from the spread in potential energies with respect to the black hole at r_p.[3] This spread is well approximated via a first-order Taylor expansion of the SMBH potential around the star's centre of mass at periapsis ($r \equiv r_p$),

$$\mathcal{E}(r_p + \delta r) = -\frac{Gm_{bh}}{r_p} + \frac{Gm_{bh}}{{r_p}^2}\delta r + O(\delta r^2). \tag{2.15}$$

The spread in energies $\Delta\mathcal{E}$ between the most bound ($r = r_p - r_\star$) and the least bound ($r = r_p + r_\star$) parts of the star is then given by

$$\begin{aligned}
\Delta\mathcal{E} &= \mathcal{E}\left(r_p + r_\star\right) - \mathcal{E}\left(r_p - r_\star\right) \\
&\overset{(2.15)}{\approx} \left[-\frac{Gm_{bh}}{r_p} + \frac{Gm_{bh}}{{r_p}^2} r_\star\right] - \left[-\frac{Gm_{bh}}{r_p} + \frac{Gm_{bh}}{{r_p}^2}\left(-r_\star\right)\right] \\
&= 2\frac{Gm_{bh}}{r_p}\frac{r_\star}{r_p}, \qquad (2.16) \\
&\overset{(2.9),(2.14)}{\sim} kGq^{1/3}\frac{m_\star}{r_\star}\beta^2, \qquad (2.17)
\end{aligned}$$

where $q \equiv m_{bh}/m_\star$, and k is a constant of order unity related to stellar structure and rotation prior to disruption. Assuming $r_\star \ll r_p$, this spread is much smaller than the specific kinetic energy at periapsis ($\sim Gm_{bh}/r_p$), but much larger than the specific binding energy of the star ($\sim Gm_\star/r_\star$) (e.g., Lacy *et al.*, 1982).

The validity of this widely used expression (Kochanek, 1994; Ulmer, 1999; Strubbe & Quataert, 2009; Kasen & Ramirez-Ruiz, 2010; Lodato & Rossi, 2011) has recently been questioned by Stone *et al.* (2013), based on the argument that by the time the star reaches periapsis, its fluid elements are already moving on almost ballistic trajectories. They propose that a more accurate estimate can be obtained by taking the potential gradient at the moment of tidal disruption, i.e. when the star crosses the tidal sphere and becomes unbound, which would simply replace r_p by r_t in Eq. (2.16). Using Eq. (2.14), the new equation for the energy spread could be rewritten in terms of the impact parameter β as

$$\begin{aligned}
\Delta\mathcal{E} &\overset{(2.16),(2.14)}{\sim} k\frac{Gm_{bh}}{r_t/\beta}\frac{r_\star}{r_t/\beta} \\
&\sim k\beta^n\frac{Gm_{bh}}{r_t}\frac{r_\star}{r_t}, \qquad (2.18)
\end{aligned}$$

with $n = 2$ for the standard picture and $n = 0$ for the revised expression, although detailed analysis of the tidal compression can lead to intermediate or piecewise values

[3] In all fairness, tidal torques also spin-up the star, creating a difference between the kinetic energies of the closest and the farthest parts of the star. This difference, of the order of $\sim Gm_\star/r_\star$, while comparable to the binding energy of the star taken from the orbit, is much smaller than the spread in potential energies.

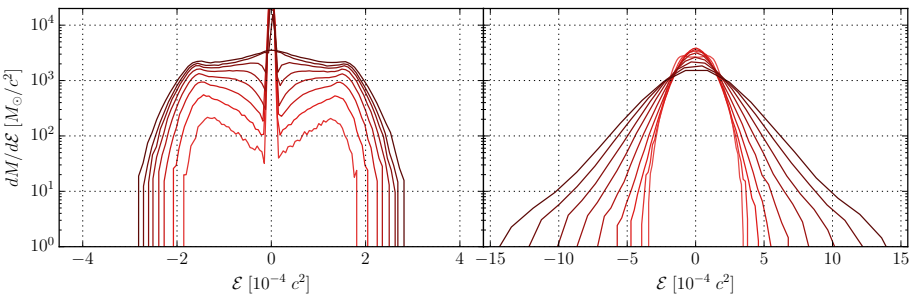

Figure 2.3: Histograms of total mechanical energy $\mathcal{E}$ after disruption, for various parabolic Newtonian encounters with impact parameters β between 0.6 and 1 (*left panel*), and between 2 and 10 (*right panel*). Darker hues correspond to higher values of β. In these simulations, we use $m_\star = M_\odot$, $r_\star = R_\odot$, $m_{\rm bh} = 10^6\, M_\odot$. The logarithmic scale on the y axis allows us to easily read off the energy spread $d\mathcal{E}$ from the chart.

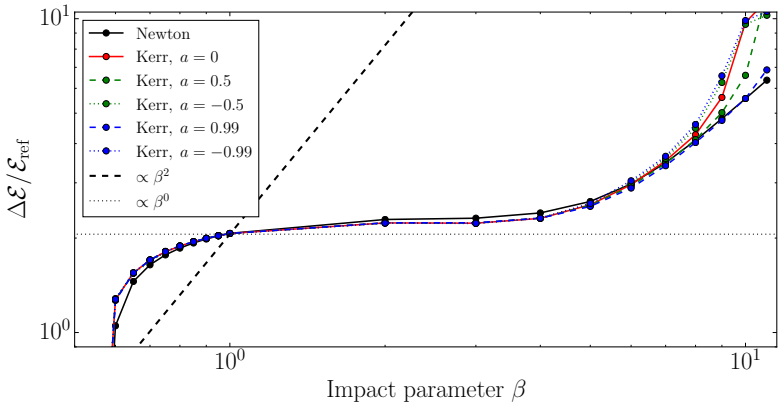

Figure 2.4: Width of the $\Delta\mathcal{E}$ interval (scaled by $\mathcal{E}_{\rm ref} = Gq^{1/3}M_\odot/R_\odot$) that contains 98% of the particles, plotted against the impact parameter β. We observe that $\Delta\mathcal{E}$ does not follow a simple power law. For comparison, we overplot the $\Delta\mathcal{E} \sim k\beta^2$ power law given by Eq. (2.17) (dashed black line), and the $\Delta\mathcal{E} \sim k\beta^0$ law given by Eq. (2.18) (horizontal dotted line). Empirically, we find $k \approx 2.05$ for our $\gamma = 5/3$ non-rotating polytrope. The data behind these plots came from our own simulations; the figure was published as Fig. 12 in Paper II.

for n (see Fig. 2.4 for results from our own Newtonian and relativistic simulations). We also point out that this definition is equivalent to that given by Zubovas *et al.* (2012), $\Delta\mathcal{E} \sim v_{\rm a}\Delta v_{\rm a}$, if we take $v_{\rm a}$ to be the parabolic velocity at the tidal radius ($\sim \sqrt{2Gm_{\rm bh}/r_{\rm t}}$) and $\Delta v_{\rm a}$ to be the escape velocity from the surface of the star ($\sim$

$\sqrt{2Gm_\star/r_\star}$). Then, ignoring factors of order unity, we obtain

$$\begin{aligned} \Delta\mathcal{E} &\sim \left(\frac{Gm_{\rm bh}}{r_{\rm t}}\right)^{1/2}\left(\frac{Gm_\star}{r_\star}\right)^{1/2} \\ &\overset{(2.9)}{=} G\left(\frac{m_{\rm bh}}{r_{\rm t}}\frac{{r_\star}^2 m_{\rm bh}}{{r_{\rm t}}^3}\right)^{1/2} \\ &= \frac{Gm_{\rm bh}}{r_{\rm t}}\frac{r_\star}{r_{\rm t}}. \end{aligned} \tag{2.19}$$

The apapsis[4] $r_{\rm a}$ (or apocentre) is the point of farthest excursion and is finite only for bound orbits. While the periapsides of various parcels of bound debris are compressed within a space no greater than $r_\star$ (this radial focussing of the orbits acts as an "effective nozzle", see Rosswog *et al.* 2009), the apapsides span an enormous region of space, from the most bound orbit ($r_{\rm a} \sim {r_{\rm p}}^2/r_\star$) to infinity (for the marginally unbound debris, which is on a parabolic orbit). This translates into very different times of return to periapsis, from the shortest ($\tau \sim 1$ month) to infinity.

The apapsis of the most bound orbit can be calculated from the semimajor axis (Eq. 2.44) as

$$r_{\rm a} = -Gm_{\rm bh}/2\mathcal{E} - r_{\rm p}. \tag{2.20}$$

Then, by using Eq. (2.16) to calculate the energy $\mathcal{E}$ of the most bound orbit, $\mathcal{E} \sim -Gm_{\rm bh}r_\star/{r_{\rm p}}^2$, we obtain $r_{\rm a} \sim {r_{\rm p}}^2/2r_\star - r_{\rm p}$. Since $r_{\rm p}/r_\star \gg 1$, the second term is negligible, leaving $r_{\rm a} \sim {r_{\rm p}}^2/r_\star$. In order to get a meaningful scaling, we combine this result with Eq. (2.10) and Eq. (2.14), obtaining

$$r_{\rm a} \approx 100\, r_{\rm p}\, \beta^{-1}\left(\frac{r_\star}{R_\odot}\right)\left(\frac{m_{\rm bh}}{10^6\, M_\odot}\right)^{1/3}\left(\frac{m_\star}{M_\odot}\right)^{-1/3}, \tag{2.21}$$

which gives us an idea of the typical $r_{\rm a}/r_{\rm p}$ ratio.

The time of shortest return, $T_{\rm min}$, can be calculated by making the same assumptions and then applying Kepler's third law:

$$\begin{aligned} \omega^2 a^3 &= Gm_{\rm bh} \\ {T_{\rm min}}^2 &= \frac{(2\pi)^2 a^3}{Gm_{\rm bh}} \\ T_{\rm min} &\overset{(2.44)}{=} \frac{2\pi\left({r_{\rm p}}^2/2r_\star\right)^{3/2}}{(Gm_{\rm bh})^{1/2}} \\ &= \frac{2\pi {r_{\rm p}}^3}{(Gm_{\rm bh})^{1/2}(2r_\star)^{3/2}}, \end{aligned} \tag{2.22}$$

[4] The more common term *apoapsis* is not etymologically correct, because the Greek prefix *ἀπό-* 'away from' becomes *ἀπ-* or *ἀφ-* before unaspirated or aspirated vowels, respectively, and only keeps its final *ό* before consonants (*apocentre*, but *apapsis* and *aphelion*).

and by scaling r_p with r_t we get

$$T_\mathrm{min} \overset{(2.9)}{=} \frac{2\pi \left(r_\mathrm{p}/r_\mathrm{t}\right)^3 {r_\star}^3 m_\mathrm{bh}/m_\star}{(G m_\mathrm{bh})^{1/2}(2r_\star)^{3/2}} \approx 41 \text{ days} \left(\frac{r_\mathrm{p}}{r_\mathrm{t}}\right)^3 \left(\frac{r_\star}{R_\odot}\right)^{3/2} \left(\frac{m_\star}{M_\odot}\right)^{-1} \left(\frac{m_\mathrm{bh}}{10^6\, M_\odot}\right)^{1/2}. \tag{2.23}$$

Compare this number with Eq. 3 from Ulmer (1999), where they get ~ 0.11 yr (40 days) with essentially the same scaling, and with Eq. 2.1 from Strubbe 2011, where they get $\sim$ 20 min, but scale r_p with $3r_\mathrm{s}$. We prefer scaling with r_t because the $r_\mathrm{p}/r_\mathrm{t}$ ratio is more meaningful, as it defines the impact parameter of the encounter (Eq. 2.14).

In addition to establishing a time scale on which the tidal disruption event can become visible, the difference in the return times also has important implications for modelling stellar tidal disruptions, as will be discussed in Sec. 3.1.3 (briefly, if there is not enough resolution, simulation particles can return to periapsis one by one, at different times, causing problems related to their statistical nature).

2.1.8 Binary breakup radius

If a stellar binary system of total mass m_bin with initial separation a_0 approaches the SMBH, it will be broken apart if its centre of mass becomes closer than the breakup radius (Miller *et al.*, 2005; Sesana *et al.*, 2009)

$$r_\mathrm{br} \sim \left(3\frac{m_\mathrm{bh}}{m_\mathrm{bin}}\right)^{1/3} a_0, \tag{2.24}$$

an expression similar in form to the definition of the tidal radius (Eq. 2.9), but with $r_\star$ replaced by a_0. To order of magnitude, this distance can be estimated by Taylor-expanding the gravitational acceleration due to the black hole around the position of the closest star,

$$F(r+\delta r) = -\frac{G m_\mathrm{bh}}{r^2} + \frac{2G m_\mathrm{bh}}{r^3}\delta r. \tag{2.25}$$

We then assume the other star is at a distance $r + a_0$ from the black hole, and require the tidal acceleration on the binary system to be equal to the mutual acceleration of the two stars,

$$\begin{aligned} \frac{2G m_\mathrm{bh}}{r^3} a_0 &\sim \frac{G m_\mathrm{bin}}{{a_0}^2} \\ r^3 &\sim \frac{2m_\mathrm{bh}}{m_\mathrm{bin}} {a_0}^3, \end{aligned} \tag{2.26}$$

which is approximately $r_{\rm br}$ in Eq. (2.24). The exact prefactor depends, of course, on the mass ratio of the two stars and on their orbital motion. The factor of 3 above is correct for a prograde binary on a circular orbit around the SMBH (Miller *et al.*, 2005), but it changes to 4 for weakly hyperbolic prograde orbits, and roughly 2 for retrograde orbits (e.g., Hamilton & Burns, 1991, 1992).

2.2 Time scales

2.2.1 Dynamical time scale of a star

The dynamical time scale (also called free fall time scale) is the time in which a star would collapse in the absence of any internal pressure, and can be computed as the time it takes a test particle released at the surface ($r = r_\star$) to reach the centre ($r = 0$) under the influence of the star's gravitational acceleration ($a \sim -Gm_\star/{r_\star}^2$). From the equations of motion

$$r(t) = r_0 + v_0 t + \frac{at^2}{2} \tag{2.27}$$

we obtain, for $r(0) = r_\star$ and $r(\tau_{\rm dyn}) \equiv 0$,

$$\tau_{\rm dyn} = \sqrt{\frac{2{r_\star}^3}{Gm_\star}}. \tag{2.28}$$

Up to a factor of ~ 2, this is equivalent to the usual definition found in the literature, given in terms of the average density of the star,

$$\begin{aligned} \tau_{\rm dyn} &= \frac{1}{\sqrt{G\,\bar{\rho}_\star}} \\ &\approx 1\ {\rm hr} \left(\frac{m_\star}{M_\odot}\right)^{-1/2} \left(\frac{r_\star}{R_\odot}\right)^{3/2}. \end{aligned} \tag{2.29}$$

$\tau_{\rm dyn}$ is also the period of the fundamental oscillation mode of the star and, in general, is the shortest time scale on which the stellar fluid can hydrodynamically react to the processes in which it is involved.

2.2.2 Periapsis passage time scale

The time $\tau_{\rm per}$ spent by the star near periapsis can be estimated by calculating the time in which the star travels around half a circle with radius $r_{\rm p}$ ($\pi r_{\rm p}$) with velocity $v_{\rm p}$

$(\sqrt{2Gm_{\rm bh}/r_{\rm p}} = c\sqrt{r_{\rm s}/r_{\rm p}})$,

$$\begin{aligned}\tau_{\rm per} &\sim \frac{\pi r_{\rm p}}{v_{\rm p}} \\ &= \frac{\pi}{c}\left(\frac{{r_{\rm p}}^3}{r_{\rm s}}\right)^{1/2} \\ &\overset{(2.9)}{\approx} 1\ {\rm hr}\left(\frac{r_\star}{R_\odot}\right)^{3/2}\left(\frac{m_\star}{M_\odot}\right)^{-1/2}\left(\frac{\beta}{1}\right)^{-3/2}, \end{aligned} \tag{2.30}$$

comparable to the dynamical time scale of the star for $\beta \sim 1$.

2.2.3 Circularization time scale

As discussed in Sec. 2.1.7, return of the bound debris to periapsis begins after a time $T_{\rm min}$. Following Ulmer (1999), we define the circularization time scale as closely related to this orbital time scale of the most bound debris,

$$T_{\rm cir} \approx n_{\rm orb}\ T_{\rm min}, \tag{2.31}$$

with the small parameter $n_{\rm orb}$ being the number of orbits required for debris circularization, which depends on how well angular momentum can be dissipated. Typically, Eq. (2.23) gives

$$T_{\rm cir} \approx 0.1\ {\rm yr}\ n_{\rm orb}\left(\frac{r_{\rm p}}{r_{\rm t}}\right)^3\left(\frac{r_\star}{R_\odot}\right)^{3/2}\left(\frac{m_\star}{M_\odot}\right)^{-1}\left(\frac{m_{\rm bh}}{10^6\ M_\odot}\right)^{1/2}. \tag{2.32}$$

2.2.4 Radiation time scale

The radiation time scale is the time needed to accrete all of the bound debris (which is $\sim$ half the stellar mass) if the black hole accretes at the Eddington mass accretion rate (Eq. 2.57) with radiative efficiency ε,

$$\tau_{\rm rad} = \frac{1}{2}\frac{m_\star c^2 \varepsilon}{L_{\rm Edd}} \tag{2.33}$$

$$\approx 22.5\ {\rm yr}\left(\frac{m_\star}{M_\odot}\right)\left(\frac{m_{\rm bh}}{10^6\ M_\odot}\right)^{-1}\left(\frac{\varepsilon}{0.1}\right). \tag{2.34}$$

2.2.5 Two-body relaxation time scale

In the steep potential of the supermassive black hole, two-body stellar interactions can be thought of as weak Coulomb collision, a term borrowed from plasma physics, where the typical kinetic energy of the particles is too large for any individual ellastic collision to produce a significant deviation of their trajectories. Such a deviation,

however, can be the cumulative effect of many collisions over a typical relaxation time scale $\tau_{\rm rel}$.

The same arguments hold for stellar interactions within the black hole's radius of influence $r_{\rm h}$ (Eq. 2.7), and we will derive $\tau_{\rm rel}$ in the same spirit as Rosswog & Brüggen (2007, Sec. 2.1.2). Let us assume that stars inside $r_{\rm h}$ have an isotropic velocity distribution, with the typical velocity v given as a function of the distance r to the black hole by Eq. (2.39),

$$v \sim \left(\frac{Gm_{\rm bh}}{r}\right)^{1/2}. \tag{2.35}$$

During a stellar two-body encounter with impact parameter b, let us use the impulse approximation: the gravitational acceleration is $a \sim Gm_\star/b^2$, the relative velocity of the two stars is $v_{\rm rel} \sim v$, the time scale for the interaction is $\delta t \sim b/v_{\rm rel}$. The encounter will then modify the velocity of the stars by

$$\delta v \sim a\ \delta t \sim \frac{Gm_\star}{b^2}\frac{b}{v_{\rm rel}} \sim \frac{Gm_\star}{bv}, \tag{2.36}$$

although the square of this quantity is more meaningful, as δv itself can be both positive and negative. In a time interval $\mathrm{d}t$, a star collides at impact parameter b with all the stars in a cylindrical shell of radius b, thickness $\mathrm{d}b$, and length $v\ \mathrm{d}t$, which is the length covered by a star with typical velocity v in the time $\mathrm{d}t$. The number of interacting stars, assuming a number density n, is then $2\pi n\, b\, \mathrm{d}b\, v\, \mathrm{d}t$, giving the total rate of change of $(\delta v)^2$ as the integral

$$\begin{aligned}\frac{\mathrm{d}(\delta v)^2}{\mathrm{d}t} &= 2\pi n v \int_{b_{\rm min}}^{b_{\rm max}} (\delta v)^2\, b\, \mathrm{d}b \\ &\overset{(2.36)}{\sim} 2\pi n \frac{G^2 {m_\star}^2}{v} \left[\ln b\right]_{b_{\rm min}}^{b_{\rm max}}\end{aligned} \tag{2.37}$$

The logarithm on the right is called the Coulomb logarithm and is usually represented by the symbol $\ln\Lambda \equiv \ln(b_{\rm max}/b_{\rm min})$. For tidal disruptions, $b_{\rm max} \sim r_{\rm h} \sim Gm_{\rm bh}/\sigma^2$ is the radius at which stars no longer feel the gravitational influence of the black hole, while $b_{\rm min} \sim Gm_\star/v^2$ is the radius at which the weak encounter approximation no longer holds (so this perturbative approach, as well as the Fokker-Planck approximation, break down). Ignoring factors of order unity, the time it takes for the cumulative influences of the small δv's to amount to a significant change of order $\sim v$ is

$$\begin{aligned}\tau_{\rm rel} &= \frac{v^2}{\mathrm{d}(\delta v)^2/\mathrm{d}t} \\ &\overset{(2.37)}{\sim} \frac{v^3}{G^2 {m_\star}^2 n \ln\Lambda} \\ &\approx \frac{5\times10^{10}\ \mathrm{yr}}{\ln\Lambda}\left(\frac{v}{100\ \mathrm{km\ s^{-1}}}\right)^3\left(\frac{m_\star}{M_\odot}\right)^{-2}\left(\frac{n}{10^6\ \mathrm{pc^{-3}}}\right)^{-1}\end{aligned} \tag{2.38}$$

about an order of magnitude larger than the life span of a solar-type star.

2.3 Physical quantities

2.3.1 Specific orbital energy

The specific orbital energy $\mathcal{E}$ of a binary system is defined as the sum of their mutual potential energy and total kinetic energy, divided by the reduced mass, $\mu = m_{\rm bh} m_\star/(m_{\rm bh}+m_\star)$. Using the assumptions $v_{\rm bh} = 0$ and $m_{\rm bh} \gg m_\star$ (valid for TDEs),

$$\begin{aligned} \mathcal{E} &= \frac{\left(m_\star {v_\star}^2 + m_{\rm bh}{v_{\rm bh}}^2\right)/2 - G m_{\rm bh} m_\star / r}{m_\star} \\ &= \frac{{v_\star}^2}{2} - \frac{G m_{\rm bh}}{r} \qquad (2.39) \\ &\overset{(2.47)}{=} \frac{1}{2}{v_{\rm r}}^2 + \frac{1}{2}\frac{\mathcal{L}^2}{r^2} - \frac{G m_{\rm bh}}{r}. \qquad (2.40) \end{aligned}$$

The decomposition of $v_\star$ into radial ($v_{\rm r}$) and transverse ($v_{\rm t}$) velocities, and the replacement of the latter according to Eq. (2.47), will prove useful later on. The conservation law of $\mathcal{E}$, historically known as the *vis-viva* equation, can be used to simplify the above expression, by using the fact that $\mathcal{E}$ is the same at both apsides ($r = r_{\rm a}$ and $r = r_{\rm p}$ for an elliptic orbit):

$$\begin{aligned} \frac{{v_{\rm a}}^2}{2} - \frac{G m_{\rm bh}}{r_{\rm a}} &= \frac{{v_{\rm p}}^2}{2} - \frac{G m_{\rm bh}}{r_{\rm p}} \\ \frac{{v_{\rm a}}^2}{2} - \frac{{v_{\rm p}}^2}{2} &= \frac{G m_{\rm bh}}{r_{\rm a}} - \frac{G m_{\rm bh}}{r_{\rm p}}, \end{aligned} \qquad (2.41)$$

and since at both apsides the velocity and position vectors are aligned, i.e. $v_\star \equiv v_{\rm t}$, Eq. (2.47) gives $\mathcal{L} = r_{\rm a} v_{\rm a} = r_{\rm p} v_{\rm p}$ and so

$$\begin{aligned} \frac{1}{2}{v_{\rm a}}^2\left(1 - \frac{{v_{\rm p}}^2}{{v_{\rm a}}^2}\right) &= G m_{\rm bh}\frac{r_{\rm p} - r_{\rm a}}{r_{\rm p} r_{\rm a}} \\ \frac{1}{2}{v_{\rm a}}^2\frac{{r_{\rm p}}^2 - {r_{\rm a}}^2}{{r_{\rm p}}^2} &= G m_{\rm bh}\frac{r_{\rm p}({r_{\rm p}}^2 - {r_{\rm a}}^2)}{{r_{\rm p}}^2 r_{\rm a}(r_{\rm p} + r_{\rm a})} \\ \frac{1}{2}{v_{\rm a}}^2 &= G m_{\rm bh}\frac{r_{\rm p}}{r_{\rm a}(r_{\rm p} + r_{\rm a})}. \end{aligned} \qquad (2.42)$$

By using the definition of the semimajor axis, $2a = r_{\rm p} + r_{\rm a}$, we obtain

$$\frac{1}{2}{v_{\rm a}}^2 = G m_{\rm bh}\frac{2a - r_{\rm a}}{2a r_{\rm a}}, \qquad (2.43)$$

and back-substitution into Eq. (2.39) gives

$$\begin{aligned}\mathcal{E} &= Gm_{\rm bh}\frac{2a-r_{\rm a}}{2ar_{\rm a}}-\frac{Gm_{\rm bh}}{r_{\rm a}}\\ &= Gm_{\rm bh}\frac{2a-r_{\rm a}-2a}{2ar_{\rm a}}\\ &= -\frac{Gm_{\rm bh}}{2a}.\end{aligned} \tag{2.44}$$

This expression of the orbital energy as a function of just the semimajor axis, and in particular the equivalent $a = -Gm_{\rm bh}/2\mathcal{E}$, will prove useful in computing the orbital characteristics of the stellar debris after disruption.

2.3.2 Specific relative angular momentum

The specific relative angular momentum $\mathcal{L}$ of two bodies is the cross product between their relative position and their relative velocity. For a bound orbit, according to Kepler's second law of planetary motion, the specific angular momentum is twice the area swept out per unit time by a chord from the primary to the secondary. Since the total area of the ellipse (πab) is swept out in one orbital period ($T = 2\pi\sqrt{a^3/Gm}$), the specific angular momentum $\mathcal{L}$ will be equal to twice the area of the ellipse divided by the orbital period, and using the definition of ellipse eccentricity,

$$e = \left(1-\frac{b^2}{a^2}\right)^{1/2}, \tag{2.45}$$

we obtain

$$\begin{aligned}\mathcal{L} &= \frac{2\pi ab}{2\pi\sqrt{\frac{a^3}{G(m_{\rm bh}+m_\star)}}}\\ &= b\sqrt{\frac{G(m_{\rm bh}+m_\star)}{a}}\\ &= a\sqrt{1-e^2}\sqrt{\frac{G(m_{\rm bh}+m_\star)}{a}}\\ &\approx \sqrt{Gm_{\rm bh}a(1-e^2)},\end{aligned} \tag{2.46}$$

where we assumed the central body to be much more massive ($m_{\rm bh} \gg m_\star$). The black hole is essentially at rest, the motion of the star is restricted to a plane, and the (constant) orbital angular momentum is equal to the angular momentum of the star with respect to the black hole, written in terms of its transverse velocity $v_{\rm t}$ and distance r to the black hole as

$$\mathcal{L} = rv_{\rm t}. \tag{2.47}$$

We will also use the angular momentum of a circular orbit with energy $\mathcal{E}$,

$$\mathcal{L}_c{}^2 = r^2 \frac{G m_{\rm bh}}{r} \overset{(2.44)}{=} \frac{G^2 m_{\rm bh}{}^2}{2\mathcal{E}}. \tag{2.48}$$

2.3.3 Light curve

The light curve of a tidal disruption event has a characteristic "outburst-like" evolution (fast rise and slow decay) and is powered by fall-back accretion, whose rate can be estimated using simple analytic arguments (Rees, 1988; Evans & Kochanek, 1989; Phinney, 1989), which we will re-derive here. First, the bound fluid elements return to periapsis after a Keplerian period T linked to their semimajor axis a by Kepler's third law,

$$a^3 = G m_{\rm bh} \left(\frac{T}{2\pi}\right)^2. \tag{2.49}$$

Since the orbital energy $\mathcal{E}$ is directly related to a by Eq. (2.44), one can also write it as a function of T,

$$\begin{aligned} \mathcal{E} &\overset{(2.44),(2.49)}{=} -\frac{1}{2} G m_{\rm bh} \left(G m_{\rm bh}\right)^{-1/3} \left(\frac{T}{2\pi}\right)^{-2/3} \\ &= -\frac{1}{2} \left(\frac{2\pi G m_{\rm bh}}{T}\right)^{2/3}. \end{aligned} \tag{2.50}$$

In order to estimate the accretion rate $\dot{m}$ one needs to make a number of fundamental assumptions. First, the material that comes back to periapsis loses energy and angular momentum on a time scale much shorter than T, thus suddenly accreting on to the SMBH. This translates into the mass accretion rate $\dot{m} \equiv \mathrm{d}m/\mathrm{d}t$ being equal to the mass distribution of return times, which is given by

$$\begin{aligned} \frac{\mathrm{d}m}{\mathrm{d}T} &\equiv \frac{\mathrm{d}m}{\mathrm{d}\mathcal{E}} \frac{\mathrm{d}\mathcal{E}}{\mathrm{d}T} \\ &\overset{(2.50)}{=} -\frac{\mathrm{d}m}{\mathrm{d}\mathcal{E}} \frac{1}{2} \frac{2}{3} \left(\frac{2\pi G m_{\rm bh}}{T}\right)^{-1/3} \left(-\frac{2\pi G m_{\rm bh}}{T^2}\right) \\ &= \frac{\left(2\pi G m_{\rm bh}\right)^{2/3}}{3} \frac{\mathrm{d}m}{\mathrm{d}\mathcal{E}} T^{-5/3}. \end{aligned} \tag{2.51}$$

The second assumption is that the energy distribution is uniform, i.e. $\mathrm{d}m/\mathrm{d}\mathcal{E}$ is approximately constant. This was only implied by Rees (1988); Phinney (1989) argued that $\mathcal{E} = 0$ (around which the distribution of specific energies is centred) is not special, therefore $\mathrm{d}m/\mathrm{d}\mathcal{E}$ should be roughly constant around it; later on, numerical simulations confirmed the assumption (e.g., Evans & Kochanek, 1989; Ayal *et al.*, 2000; Ramirez-Ruiz & Rosswog, 2009), with some caveats discussed below. If the

derivative is constant, it can be easily computed from the energy spread of the entire stellar mass,

$$\frac{\mathrm{d}m}{\mathrm{d}\mathcal{E}} \approx \frac{m_\star}{2\Delta\mathcal{E}}, \tag{2.52}$$

where the factor of 2, taken from Evans & Kochanek (1989), corresponds to $k = 2$ in Eq. (2.16). Using Eq. (2.16) to explicitely write $\Delta\mathcal{E}$, we obtain

$$\frac{\mathrm{d}m}{\mathrm{d}T} \overset{(2.51),(2.52)}{=} \frac{(2\pi G m_{\mathrm{bh}})^{2/3}}{3} \frac{m_\star {r_{\mathrm{p}}}^2}{2 G m_{\mathrm{bh}} r_\star} T^{-5/3}, \tag{2.53}$$

and by writing $G m_{\mathrm{bh}}$ in terms of T_{min} using Eq. (2.22), i.e.

$$(G m_{\mathrm{bh}})^{-1/3} = \frac{(2\pi)^{-2/3} {r_{\mathrm{p}}}^{-2}}{(2r_\star)^{-1} {T_{\mathrm{min}}}^{-2/3}}, \tag{2.54}$$

we get

$$\begin{aligned} \frac{dm}{dT} &\overset{(2.53),(2.54)}{=} \frac{(2\pi)^{2/3} m_\star {r_{\mathrm{p}}}^2}{3 \times 2 r_\star} \frac{(2\pi)^{-2/3} {r_{\mathrm{p}}}^{-2}}{(2r_\star)^{-1} {T_{\mathrm{min}}}^{-2/3}} T^{-5/3}, \\ &= \frac{1}{3} \frac{m_\star}{T_{\mathrm{min}}} \left(\frac{T}{T_{\mathrm{min}}}\right)^{-5/3} \\ &\approx 3\, M_\odot\ \mathrm{yr}^{-1} \left(\frac{r_{\mathrm{p}}}{r_{\mathrm{t}}}\right)^{-3} \left(\frac{r_\star}{R_\odot}\right)^{-3/2} \left(\frac{m_\star}{M_\odot}\right)^{2} \\ &\quad \left(\frac{m_{\mathrm{bh}}}{10^6\, M_\odot}\right)^{-1/2} \left(\frac{T}{T_{\mathrm{min}}}\right)^{-5/3}, \end{aligned} \tag{2.55}$$

similar to Eq. 3 in Evans & Kochanek (1989).

This value should be compared with the Eddington accretion rate, calculated from the Eddington (1921) luminosity for pure ionised hydrogen,

$$\begin{aligned} L_{\mathrm{Edd}} &= \frac{4\pi G m_{\mathrm{bh}} m_{\mathrm{p}} c}{\sigma_{\mathrm{T}}} \\ &\approx 1.25 \times 10^{44}\ \mathrm{erg\,s^{-1}} \left(\frac{m_{\mathrm{bh}}}{10^6\, M_\odot}\right), \end{aligned} \tag{2.56}$$

according to

$$\begin{aligned} L_{\mathrm{Edd}} &= \varepsilon\, \dot{m}_{\mathrm{Edd}} c^2 \\ \dot{m}_{\mathrm{Edd}} &\approx 0.022\, M_\odot\ \mathrm{yr}^{-1} \left(\frac{m_{\mathrm{bh}}}{10^6\, M_\odot}\right) \left(\frac{\varepsilon}{0.1}\right)^{-1}, \end{aligned} \tag{2.57}$$

where ε is the efficiency of conversion of gravitational binding energy into radiation during the accretion process.

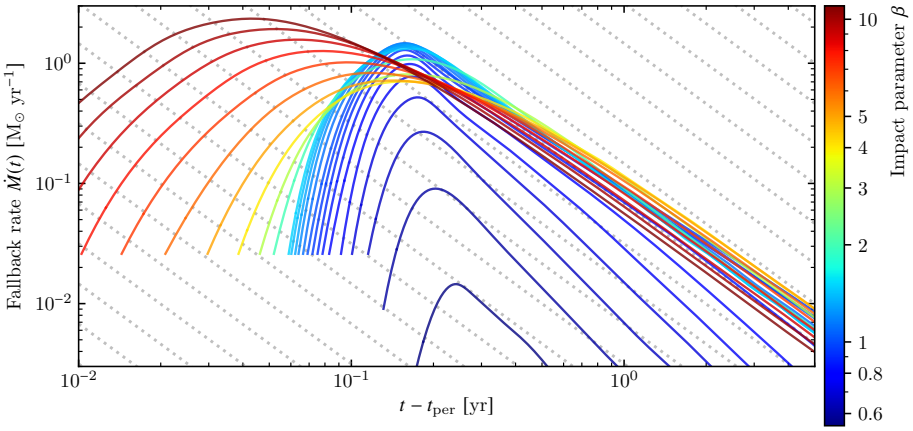

Figure 2.5: The return rate of the debris exhibits a characteristic "outburst-like" evolution, consisting of a fast rise (of the order of days) and a slow decay (of the order of years). If the circularization time scale is much shorter than the fallback time scale – and this question, far from being answered, is currently being pursued by a number of groups –, the light curve will exhibit a very similar behaviour. This plot shows the $\dot{M}$ curves for TDEs with $0.55 \leq \beta \leq 11$. While β has an obvious influence on the rise of the $\dot{M}$ curve (in both slope and maximum value), all curves with $\beta \gtrsim 1$ exhibit essentially the same decay governed by a $t^{-5/3}$ power law (oblique, gray dotted lines). This figure was produced by the author, using data from our own simulations, and is essentially a simplified version of the Newtonian panel of Fig. 8 in Paper I.

More recently, it has been shown that the energy distribution need not be, and is in fact in general not uniform, but depends on the internal structure of the star (e.g. Lodato *et al.*, 2009, Ramirez-Ruiz & Rosswog, 2009; see also our results presented in Fig. 2.3). This produces deviations from the canonical scaling at early times, but the light curve eventually "settles" into the equilibrium $t^{-5/3}$. Hayasaki *et al.* (2012) found that for elliptic orbits there exists a critical value of the orbital eccentricity e below which all the stellar debris remains bound to the black hole. This is because $\mathcal{E}$ is a function of a (Eq. 2.44), which depends on e as $a = r_{\rm p}/(1-e)$, thus $\mathcal{E} = -Gm_{\rm bh}\beta(1-e)/2r_{\rm t}$. For a parabolic orbit $\mathcal{E} = 0$, but for an elliptic one it can be smaller than $\Delta\mathcal{E}$ if

$$-\frac{Gm_{\rm bh}}{2r_{\rm t}}\beta(1-e) \overset{(2.16)}{<} -\frac{Gm_{\rm bh}}{r_{\rm t}}r_\star r_{\rm t} \tag{2.58}$$

$$-\beta(1-e) \overset{(2.9)}{<} -2\left(\frac{m_\star}{m_{\rm bh}}\right)^{1/3} \tag{2.59}$$

$$e < 1 - \frac{2}{\beta}\left(\frac{m_\star}{m_{\rm bh}}\right)^{1/3}. \tag{2.60}$$

In such cases, even a spread $\Delta\mathcal{E}$ in specific energies will not unbind any debris. Al-

though we argued that most tidal disruptions involve nearly parabolic orbits, the critical e given above is very close to 1: for $\beta = 1$, $m_\star = M_\odot$ and $m_{\rm bh} = 10^6\, M_\odot$, the condition becomes $e < 0.98$, which gives a plausible orbit. For high, but sub-critical eccentricities, Hayasaki *et al.* (2012) find a significant deviation from the canonical $t^{-5/3}$ mass fallback rate, caused by the fact that debris falls back much faster than in the standard parabolic scenario. In some of their simulations, the resulting accretion rate exceeds the Eddington rate by as much as 4 orders of magnitude.

2.3.4 Optical depth

In what follows we will derive an order-of-magnitude estimate for the typical photon optical depth of a tidal disruption debris "cloud". For simplicity, we will assume a spherical cloud of uniform density and only consider Thomson scattering.

For a typical $\beta = 1$, we would expect the size of the debris cloud to be of the order of a tidal radius. This is indeed confirmed by our simulations, and appears to hold true even for deeper encounters (e.g., $\beta = 5$). We will therefore take the characteristic size to be $L \sim 10^{13}$ cm.

The simplest analytical estimate for the typical density after disruption is obtained by imagining that the entire stellar mass is spread uniformly over a sphere of radius L. For $m_\star = M_\odot$ and the value of L considered above, we obtain $\rho = m_\star/(4\pi L^3/3) \sim 10^{-6}\,\mathrm{g\,cm^{-3}}$. Detailed numerical simulation evidently result in a more complex profile, but the typical density of the resulting disc is of the order of $\sim 10^{-7}\,\mathrm{g\,cm^{-3}}$. We will consider the latter, since it is the smaller of the two, and leads to a lower optical depth.

For the typical cross-section we take the Thomson cross-section for electron scattering: $\sigma \equiv \sigma_{\rm T} = 8\pi/3\left(\alpha\hbar c/m_{\rm e}c^2\right)^2 \sim 6.65 \times 10^{-29}\,\mathrm{m^2}$. The number density of the debris can be computed from its mass density by assuming e.g. that it is composed entirely of hydrogen, such that $n = \rho/m_{\rm p} \sim 6 \times 10^{16}\,\mathrm{cm^{-3}}$. The typical mean free path of a photon is then simply given by $l = 1/(n\sigma) \sim 10^7$ cm. This leads to a typical optical depth of $\tau \sim L/l \sim 10^6$, which justifies the usual assumption that the resulting debris is completely optically thick.

2.3.5 Peak wavelength

As the matter plunges towards the black hole, the intense frictional heating can raise the fluid temperature up to $\gtrsim 10^6$ K in the vicinity of the event horizon (e.g., Bonning *et al.*, 2007). Following Wien's displacement law, we can compute the wavelength of the peak blackbody emission as

$$\begin{aligned} \lambda_{\rm max} &= \frac{b}{T} \\ &\approx 2.9\ \mathrm{nm} \left(\frac{T}{10^6\ \mathrm{K}}\right)^{-1}, \end{aligned} \tag{2.61}$$

corresponding to 0.43 keV, which is in the soft X-ray part of the spectrum (approximately 0.1 to 5 keV, or 0.2 to 10 nm; for reference, the hard X-rays have energies from 5 to 10 keV, or wavelengths from 0.01 to 0.2 nm). On the other hand, the effective temperature of material radiating at Eddington luminosity from the tidal radius can be computed with the Stefan–Boltzmann law,

$$T_{\rm eff} \approx \left(\frac{L_{\rm Edd}}{4\pi {r_{\rm t}}^2 \sigma_{\rm SB}}\right)^{1/4} \overset{(2.9),(2.56)}{\approx} 2.5\times10^5\ {\rm K} \left(\frac{m_{\rm bh}}{10^6\ M_\odot}\right)^{1/12} \left(\frac{r_\star}{R_\odot}\right)^{-1/2} \left(\frac{m_\star}{M_\odot}\right)^{-1/6} \quad (2.62)$$

(compare with Eq. 8 in Ulmer 1999). This corresponds to blackbody radiation peaking at 11.6 nm, or 0.1 keV, in the far UV part of the spectrum. Eq. (2.62) reveals a very weak scaling of the effective temperature with the black hole mass, so all flares caused by disruptions of similar stars would have comparable temperatures.

Loeb & Ulmer (1997) present a more realistic post-disruption model, in which the rotating, radiation-pressure dominated torus at $r_{\rm p}$ is surrounded by an Eddington envelope: a quasi-spherical, optically thick cloud. Since the envelope has a very low density ($\lesssim 10^{-12}$ g cm^{-3}), Thompson opacity dominates, with bound-bound, bound-free, and free-free opacities being relatively unimportant (e.g., Burger & Lamers, 1989). Even though the emission from the torus is mainly in the X-rays and far UV as shown above, this radiation is processed through the surrounding envelope, and re-emitted mostly in the optical-UV band. Because of the very high opacity of the envelope, its emission spectrum is expected to be thermal to first order. Assuming the radius of the envelope to be $\sim 10^2\ r_{\rm t}$, its effective temperature can be calculated using Eq. (2.62) as

$$T_{\rm eff} \sim 1.4\times10^4\ {\rm K}, \quad (2.63)$$

peaking in the UV.

2.4 Disruption rates

2.4.1 The stellar cluster model

The mutual interactions between various stellar distributions and a central supermassive black hole have been studied in detail ever since the pioneering work of Bahcall & Wolf (1976, 1977), who computed a quasi-steady-state solution for the stellar distribution by solving the one-dimensional, steady-state Fokker-Planck equation.

> An approximation to the collisional Boltzmann equation, the Fokker-Planck equation describes the cumulative effect of two-body relaxation and energy

exchange between stars and the black hole on the stellar distribution function, in the limit where gravitational interactions between stars are assumed to be weak. We will derive its simplest form in the next section.

Their resulting stellar density profile shows a characteristic "cusp" (a density distribution that formally diverges at the origin), now called a Bahcall-Wolf cusp, which scales as $n(r) \propto r^{-7/4}$ inside the black hole's radius of influence.

The model was then refined by introducing the concept of loss cone (Frank & Rees 1976; see next section) and using the Fokker-Planck equation to calculate the rate at which the loss cone, depleted by stellar distruptions, is refilled (e.g., Lightman & Shapiro, 1977). More recently, Magorrian *et al.* (1998) used high-resolution imaging and spectroscopic results from the Hubble Space Telescope to estimate masses for the stellar distributions and SMBHs of 36 nearby galaxies. Syer & Ulmer (1999) used these results together with the Fokker-Planck formalism to calculate tidal disruption rates for real galaxies, assuming spherical symmetry and isotropic velocity dispersions. Later on, Magorrian & Tremaine (1999) performed similar calculations assuming axisymmetry, obtaining more optimistic disruption rates. The most recent disruption rate calculations for real galaxies were performed by Wang & Merritt (2004), following the revision of the aforementioned observational results.

Studies based on the Fokker-Planck method have been verified by numerical methods, such as Monte-Carlo integrations (e.g., Shapiro & Marchant, 1978; Shapiro, 1985) and N-body simulations (e.g., Brockamp *et al.*, 2011; Vasiliev & Merritt, 2013). The latter are so computationally expensive that they have only become feasible in recent years.

Theory predicts that under the gravitational influence of the black hole a high density cusp is formed at the centre of the surrounding star cluster, up to $\sim$ the radius of influence (Eq. 2.7). Beyond this distance, the gravitational influence of the black hole is so small that the distribution function of the stellar orbits is close to that of an isothermal sphere, with stellar density scaling as $n(r) \propto r^{-2}$. The ubiquity of high-density cusps is nowadays well established by observations (e.g., Alexander, 1999; Genzel *et al.*, 2003).

In what follows we will derive a typical tidal disruption rate through order-of-magnitude calculations, by assuming a spherically symmetric gravitational potential, a linear stellar distribution within the radius of influence, $n(r) = n_0(r_\mathrm{h}/r)$, and isotropic stellar velocity dispersions at the radius of influence.

2.4.2 Loss cone theory

Having defined the specific orbital energy and angular momentum, let us briefly summarize the loss cone theory, widely used to estimate tidal disruption rates (e.g., Magorrian & Tremaine, 1999; Wang & Merritt, 2004; Brockamp *et al.*, 2011), using the simple stellar cluster model described above.

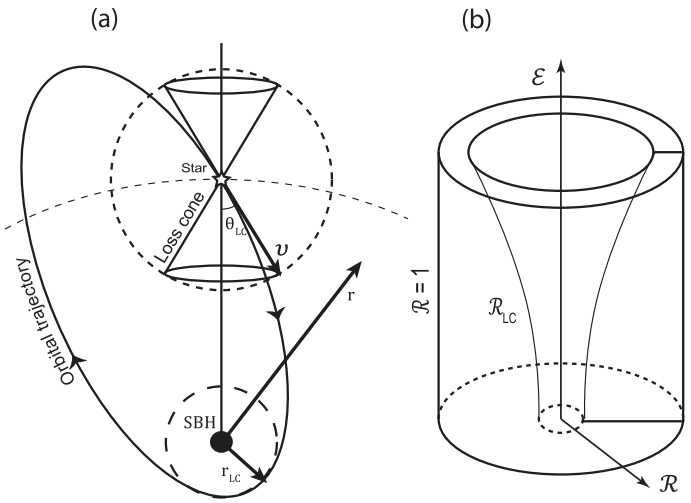

Figure 2.6: Two representations of the loss cone: a) A star with a given orbital trajectory lies within the loss cone if the angle ϑ between the position and the velocity vectors falls within the range of the critical $\vartheta_{\rm lc}$; b) In the space spanned by the energy and angular momentum, the loss cone contains orbits with angular momenta $L \leq L_{\rm lc}$, given in terms of $\mathcal{R} \equiv L^2/L_{\rm lc}(\mathcal{E})^2$. This figure reproduces Fig. 1 of Merritt (2013).

Let each star be described by its specific energy $\mathcal{E}$ and angular momentum L. The concept of "loss cone", first applied to tidal disruptions of stars by Frank & Rees (1976), refers to the portion of the $(\mathcal{E}, L)$ phase space containing orbits with periapsides $r_{\rm p} \leq r_{\rm t}$, in other words containing stars that will be captured by the black hole. For stars not bound to the black hole, the loss cone is essentially a "loss column", because the fate of the star depends on whether L is smaller than a critical value $L_{\rm lc}$, independent of its energy $\mathcal{E}$ (e.g., Cohn & Kulsrud, 1978).

A star with given specific energy $\mathcal{E}$ reaches a periapsis velocity given by

$$v_{\rm p}{}^2 \overset{(2.39)}{=} 2\left(\mathcal{E} + \frac{Gm_{\rm bh}}{r_{\rm p}}\right). \tag{2.64}$$

In order for the star to have a certain impact parameter β, the periapsis distance must be $r_{\rm p} = r_{\rm t}/\beta$, which places a constraint on the specific angular momentum,

$$\begin{aligned} L_{\rm lc}{}^2 &\overset{(2.47)}{=} r_{\rm p}{}^2 v_{\rm p}{}^2 \\ &\overset{(2.39)}{=} 2\left(\mathcal{E} + \frac{Gm_{\rm bh}}{r_{\rm p}}\right) r_{\rm p}{}^2 \\ &\approx 2Gm_{\rm bh} r_{\rm t}/\beta, \end{aligned} \tag{2.65}$$

where the term $\mathcal{E}$ (of order σ^2) is much smaller than $Gm_{\rm bh}/r_{\rm p}$ for a solar-type star,

$$\mathcal{E} \ll Gm_{\rm bh}/r_{\rm p}. \tag{2.66}$$

Thus, stars with energies $\mathcal{E}$ and angular momenta $\mathcal{L} \leq \mathcal{L}_{\rm lc}$ will be captured by the black hole. Evidently, only a fraction of these stars will be disrupted (as some may plunge directly into the black hole, if $r_{\rm p} < r_{\rm e}$), but to simplify matters we will ignore this aspect in the following discussion.

We will demonstrate the use of the loss cone theory in predicting disruption rates by using the simplest possible steady-state scenario – the spherical galaxy model presented in the previous section. Let the stellar distribution in phase space be represented by the distribution function $f(\boldsymbol{r}, \boldsymbol{v})$, defined such that

$$f(\boldsymbol{r}, \boldsymbol{v})\ \mathrm{d}^3\boldsymbol{r}\ \mathrm{d}^3\boldsymbol{v} \tag{2.67}$$

is the probability of finding a star within a phase space volume $\mathrm{d}^3\boldsymbol{r}\ \mathrm{d}^3\boldsymbol{v}$. Jean's theorem (see, e.g., Sec. 4.2 of Binney & Tremaine, 2008) states that in a spherical potential, the distribution function will only depend on the phase-space coordinates through the integrals of motion $\mathcal{E}$ and $\mathcal{L}$: $f(\boldsymbol{r}, \boldsymbol{v})$ can be written as $f(\mathcal{E}, \mathcal{L})$. We already have constraints on these quantities for the stars that are in the loss cone, see Eqs. (2.65) and (2.66). We can then write the number of stars $N(\mathcal{E}, \mathcal{L})$ with energies between $\mathcal{E}$ and $\mathcal{E} + d\mathcal{E}$ and angular momenta between $\mathcal{L}$ and $\mathcal{L} + d\mathcal{L}$ as

$$N(\mathcal{E}, \mathcal{L})\mathrm{d}\mathcal{E}\ \mathrm{d}\mathcal{L} = \int_{\mathcal{V}} f(\mathcal{E}, \mathcal{L})\ \mathrm{d}^3\boldsymbol{r}\ \mathrm{d}^3\boldsymbol{v} \tag{2.68}$$

Following Lightman & Shapiro (1977), we write the volume elements $\mathrm{d}^3\boldsymbol{r}$ and $\mathrm{d}^3\boldsymbol{v}$ in coordinate space and velocity space, respectively, as follows. For the coordinate space, we assume spherical symmetry, hence $\oint \mathrm{d}\Omega = 4\pi$ and the only spatial coordinate left is r,

$$\mathrm{d}^3\boldsymbol{r} = 4\pi\, r^2 \mathrm{d}r. \tag{2.69}$$

For a given spatial location $\boldsymbol{r}$, the velocity can be projected along three directions: $v_{\rm r}$ parallel to $\boldsymbol{r}$, $v_{\rm t}$ perpendicular to $\boldsymbol{r}$, and an angle φ between $v_{\rm t}$ and a reference direction. We assume the distribution function to be independent of φ, thus taking $\int \mathrm{d}\varphi = 2\pi$ out of the integral, and leaving the volume element in velocity space as a thin ring of height $\mathrm{d}v_{\rm r}$, radius $v_{\rm t}$ and thickness $\mathrm{d}v_{\rm t}$,

$$\begin{aligned} \mathrm{d}^3\boldsymbol{v} &= 2\pi\, v_{\rm t}\, \mathrm{d}v_{\rm t}\, \mathrm{d}v_{\rm r} \\ &\overset{(2.47),(2.40)}{=} 2\pi \frac{\mathcal{L}\mathrm{d}\mathcal{L}}{r^2} \frac{\mathrm{d}\mathcal{E}}{v_r} \end{aligned} \tag{2.70}$$

Using this result[5], we can rewrite Eq. (2.68) as

$$\begin{aligned} N(\mathcal{E}, \mathcal{L})\, \mathrm{d}\mathcal{E}\, \mathrm{d}\mathcal{L} &= 8\pi^2 \int f(\mathcal{E}, \mathcal{L})\, r^2 \mathrm{d}r \frac{\mathcal{L}\, \mathrm{d}\mathcal{L}}{r^2} \frac{\mathrm{d}\mathcal{E}}{v_\mathrm{r}} \\ &= 8\pi^2 f(\mathcal{E}, \mathcal{L})\, \mathcal{L}\, \mathrm{d}\mathcal{L}\, \mathrm{d}\mathcal{E} \int \frac{\mathrm{d}r}{v_\mathrm{r}}. \end{aligned} \tag{2.71}$$

To calculate the integral on the right, let us consider the orbital velocity as a function of radius. The function is then defined on the interval $[r_\mathrm{p}, r_\mathrm{a}]$. At each point r, by choosing a sufficiently small $\mathrm{d}r$, we can approximate the time in which the star travels the distance $\mathrm{d}r$ by $\mathrm{d}r/v_\mathrm{r}(r)$. The integral of this quantity, from r_p to r_a, gives half of the orbital period, which needs to be multiplied by two to account for the return trip back to r_p:

$$2 \int_{r_\mathrm{p}}^{r_\mathrm{a}} \frac{\mathrm{d}r}{v_\mathrm{r}(r)} = T(\mathcal{E}, \mathcal{L}). \tag{2.72}$$

We therefore replace the integral by the half-period of the orbit,

$$N(\mathcal{E}, \mathcal{L})\, \mathrm{d}\mathcal{E}\, \mathrm{d}\mathcal{L} = 4\pi^2 f(\mathcal{E}, \mathcal{L}) T(\mathcal{E}, \mathcal{L})\, \mathcal{L}\, \mathrm{d}\mathcal{L}\, \mathrm{d}\mathcal{E}, \tag{2.73}$$

where $T(\mathcal{E}, \mathcal{L})$ is the radial period of an orbit with energy $\mathcal{E}$ and angular momentum $\mathcal{L}$. For nearly radial orbits, we can approximate $T(\mathcal{E}, \mathcal{L})$ by $T(\mathcal{E}) \equiv T(\mathcal{E}, 0)$, which is given by Eq. (2.50) (compare with Eqs. 3, 4 in Magorrian & Tremaine 1999). We also used the fact that $f(\mathcal{E}, \mathcal{L})$ is essentially constant around the orbit of a star to pull it out of the integral. In order to find the number of stars N_lc in the (full) loss cone we need to integrate Eq. (2.73) with respect to $\mathcal{L}$, from $\mathcal{L} = 0$ to $\mathcal{L} = \mathcal{L}_\mathrm{lc}$, obtaining

$$N_\mathrm{lc}(\mathcal{E})\, \mathrm{d}\mathcal{E} = 2\pi^2 f(\mathcal{E}, \mathcal{L})\, T(\mathcal{E})\, {\mathcal{L}_\mathrm{lc}}^2\, \mathrm{d}\mathcal{E}. \tag{2.74}$$

In order to estimate its numerical value, we approximate the distribution function according to Eq. 9 in Magorrian & Tremaine (1999) (for a more detailed derivation see Strubbe, 2011, Sec. 4.3.1); we set the parameter $\alpha = 0$, such that the number density of stars is $n(r) = n_0(r_\mathrm{h}/r)$:

$$f(\mathcal{E}) \sim (2\pi {\sigma_\star}^2)^{-3/2}\, n_0 \left(\frac{\mathcal{E}}{{\sigma_\star}^2}\right)^{-3/2}, \tag{2.75}$$

[5] There seems to be a factor of 2 "magically" appearing here, from time to time, throughout the literature. For instance, Lightman & Shapiro (1977, Eq. 30) give 2π, as derived above; one year later, Shapiro & Marchant (1978, Eq. 8) present the exact same equations but give 4π; more recently, Magorrian & Tremaine (1999, Eq. 4) and Strubbe (2011, Eq. 4.14) also use 2π, but write $\mathcal{L}\mathrm{d}\mathcal{L}$ as ${\mathcal{L}_\mathrm{c}}^2 \mathrm{d}(\mathcal{L}^2/{\mathcal{L}_\mathrm{c}}^2) \equiv 2\mathcal{L}\mathrm{d}\mathcal{L}$, which effectively gives a 4π as well. This distinction modifies all subsequent equations and the disruption rate by a factor of two.

and using $T(\mathcal{E})$ from Eq. (2.50) and ${\mathcal{L}_{\rm lc}}^2$ from Eq. (2.65) we write $N_{\rm lc}(\mathcal{E})$ as

$$\begin{aligned} N_{\rm lc}(\mathcal{E}) &= 2\pi^2(2\pi{\sigma_\star}^2)^{-3/2}\, n_0 \left(\frac{\mathcal{E}}{{\sigma_\star}^2}\right)^{-3/2} \frac{2\pi G m_{\rm bh}}{(-2\mathcal{E})^{3/2}} \\ &\quad \frac{2Gm_{\rm bh}}{\beta} r_\star \left(\frac{m_{\rm bh}}{m_\star}\right)^{1/3} \\ &= \sqrt{\pi} G^2 n_0 {m_{\rm bh}}^{7/3} \mathcal{E}^{-3} r_\star {m_\star}^{-1/3} \beta^{-1} \\ &\approx 0.1 \left(\frac{n_0}{10^6\ {\rm pc}^{-3}}\right) \left(\frac{m_{\rm bh}}{10^6\ M_\odot}\right)^{\frac{7}{3}} \left(\frac{\mathcal{E}}{{\sigma_\star}^2}\right)^{-3} \left(\frac{\sigma_\star}{100\ {\rm km/s}}\right)^{-6} \\ &\quad \left(\frac{r_\star}{R_\odot}\right) \left(\frac{m_\star}{M_\odot}\right)^{-\frac{1}{3}} (\beta)^{-1}\,, \end{aligned} \tag{2.76}$$

which only differs by a factor of ~ 5 from the result of the more involved calculations presented by Magorrian & Tremaine (1999) in their Eq. 10. The last thing needed to compute the disruption rates is the typical time-scale for emptying a full loss cone, which is approximately the Keplerian period of an orbit at $r_{\rm h}$,

$$\begin{aligned} {T_{\rm lc}}^2(\mathcal{E}) &= \frac{(2\pi)^2 {r_{\rm h}}^3}{G m_{\rm bh}} \\ &\overset{(2.7)}{=} (2\pi)^2 (G m_{\rm bh})^2 \sigma^{-6} \\ T_{\rm lc}(\mathcal{E}) &\sim 10^4\ {\rm yr} \left(\frac{m_{\rm bh}}{10^6\ M_\odot}\right) \left(\frac{\sigma}{100\ {\rm km\ s^{-1}}}\right)^{-3}. \end{aligned} \tag{2.77}$$

Finally, the flux of stars into the tidal radius when the loss cone is full is simply $F(\mathcal{E}) = N_{\rm lc}(\mathcal{E})/T_{\rm lc}(\mathcal{E})$,

$$\begin{aligned} F(\mathcal{E}) \sim\ & 10^{-5}\ {\rm yr}^{-1} \left(\frac{n_0}{10^6\ {\rm pc}^{-3}}\right) \left(\frac{m_{\rm bh}}{10^6\ M_\odot}\right)^{\frac{4}{3}} \left(\frac{\mathcal{E}}{{\sigma_\star}^2}\right)^{-3} \\ & \left(\frac{\sigma_\star}{100\ {\rm km/s}}\right)^{-3} \left(\frac{r_\star}{R_\odot}\right) \left(\frac{m_\star}{M_\odot}\right)^{-\frac{1}{3}}. \end{aligned}$$

Integration over $\mathcal{E}/{\sigma_\star}^2$ from 0 to 1 then gives the stellar disruption rate,

$$F \sim 10^{-5}\ {\rm yr}^{-1} \left(\frac{n_0}{10^6\ {\rm pc}^{-3}}\right) \left(\frac{m_{\rm bh}}{10^6\ M_\odot}\right)^{\frac{4}{3}} \left(\frac{\sigma_\star}{100\ {\rm km/s}}\right)^{-1} \left(\frac{r_\star}{R_\odot}\right) \left(\frac{m_\star}{M_\odot}\right)^{-\frac{1}{3}}, \tag{2.78}$$

which is comparable to Eq. (2) presented by Rees (1988).

We point out the steep inverse dependence of $N_{\rm lc}$ on $\mathcal{E}$ in Eq. (2.76): the density of the stars in the loss cone declines at large $\mathcal{E}$ (i.e., close to the black hole). It turns

out that the same happens for very small $\mathcal{E}$ (mainly because the number of stars bound tightly to the hole is extremely small), and that there is a critical energy corresponding to the critical distance r_h where N_lc peaks (e.g., Magorrian & Tremaine, 1999). This means that most disrupted stars come from a distance $\sim r_\mathrm{h}$ (of the order of parsecs) and have an orbital energy $\sim \mathcal{E}_\mathrm{h} = -Gm_\mathrm{bh}/2r_\mathrm{h}$. Comparing this with the energy spread of the debris (Eq. 2.16), $\Delta\mathcal{E} \sim Gm_\mathrm{bh}r_\star/{r_\mathrm{t}}^2$, and using $r_\mathrm{t}/r_\star \sim 10^2$ (Eq. 2.10), we conclude that the typical orbital energy of a disrupted star is smaller than the energy spread after disruption by a factor of $\sim r_\mathrm{h}/(10^2\ r_\mathrm{t})$, more than 6 orders of magnitude for a solar-type star. This justifies the usual assumption that disrupted stars approach the black hole on parabolic orbits, since the energy of the debris after periapsis crossing, ranging from $-\Delta\mathcal{E}$ to $+\Delta\mathcal{E}$, is essentially centred around $\mathcal{E}_\mathrm{h}$. It also explains the statement made by Rees (1988) that half of the debris becomes bound to the hole, while the other half escapes, regardless of any other details of the encounter.

> It should be noted, though, that massive perturbers (e.g., a cluster of stellar black holes formed by mass segregation) may kick marginally unbound stars just enough to place them on an elliptic orbit.

Our simple estimations assumed spherical symmetry, isotropy of $\sigma_\star$ at r_h, a thermal distribution of the stars, and that the loss cone was replenished with stars at least as fast as it was depleted through disruptions. In general, the stellar distribution is not thermal: if the most important mechanism for loss cone replenishment is two-body relaxation, the cause is that the two-body relaxation time scale – larger than the Hubble time, see Eq. (2.38) – is longer than the age of the system. In particular, close to the black hole, where the stellar population is dominated by young B stars, the relaxation time is much longer than the maximum stellar lifespan ($\sim 10^8$ yr). If there are other processes at play, they may refill the loss cone faster by sending stars on chaotic orbits, but in that case the chance for thermalization is even smaller.

> A note on how the Fokker-Planck equation is used to compute the flux of stars into the loss cone at each energy (this is treated in detail in Sec. 7.4 of Binney & Tremaine, 2008). Let the distribution function $f(\boldsymbol{r}, \mathcal{E}, \mathcal{L}, t)$ represent the stellar distribution $(\mathcal{E}, \mathcal{L})$ in the smooth potential $\Phi(\boldsymbol{r})$ of a central supermassive black hole at time t. In the absence of collisions, f obeys the collisionless Boltzmann equation $\mathrm{d}f/\mathrm{d}t = 0$, with the derivative taken along the phase-space path of the star. The equation can be written in a more familiar form (while also taking into account symmetries like $\partial f/\partial\varphi = 0$) as
>
> $$\frac{\partial f}{\partial t} + v_\mathrm{r}\frac{\partial f}{\partial r} + \dot{\mathcal{E}}\frac{\partial f}{\partial \mathcal{E}} + \dot{\mathcal{L}}\frac{\partial f}{\partial \mathcal{L}} = 0. \tag{2.79}$$
>
> However, in a dense stellar environment, collisions between stars occur sufficiently often to change the phase-space density on the time scale of the

relaxation time, and can be quantified through an encounter operator $\Gamma[f]$. Using this operator, one can then solve the full Boltzmann equation $\mathrm{d}f/\mathrm{d}t = \Gamma[f]$ (see Eqs. 7.46–7.47 in Binney & Tremaine 2008). This is a complicated problem, given the integro-differential character of the Boltzmann equation, and simpler expressions have been developed based on physical arguments. The Fokker-Plank equation, borrowed from plasma physics, is a good approximation in situations where gravitational encounters are weak, i.e. their impact parameter obeys $b \gg b_{\min}$, with $b_{\min} \equiv Gm_\star/{v_\star}^2$ being the impact parameter required to produce a change in velocity of order unity. In other words, any two-body collision is assumed not to alter the velocities of the stars too much (this is true since, by definition, significant cumulative alterations occur on the two-body relaxation time scale). The weak encounters approximation allows us to Taylor expand the collision operator $\Gamma[f]$ in powers of $(\Delta\mathcal{E}/\mathcal{E})$, $(\Delta\mathcal{L}/\mathcal{L})$ and $(\Delta t/t)$ (see, e.g., Lightman & Shapiro, 1977, Sec. IIIb),

$$\begin{aligned}\Gamma[f] \approx & -\frac{\partial}{\partial\mathcal{E}}[f\langle\Delta\mathcal{E}\rangle] - \frac{\partial}{\partial\mathcal{L}}[f\langle\Delta\mathcal{L}\rangle] + \frac{1}{2}\frac{\partial^2}{\partial\mathcal{E}^2}[f\langle(\Delta\mathcal{E})^2\rangle] \\ & + \frac{1}{2}\frac{\partial^2}{\partial\mathcal{L}^2}[f\langle(\Delta\mathcal{L})^2\rangle] + \frac{1}{2}\frac{\partial^2}{\partial\mathcal{E}\partial\mathcal{L}}[f\langle(\Delta\mathcal{E}\Delta\mathcal{L})\rangle] \end{aligned} \tag{2.80}$$

A further simplifying assumption has been proven in Eq. (2.65): the configuration of the loss cone is virtually independent of $\mathcal{E}$, except for the most tightly bound stars (which are very few). Dropping all terms containing $\partial/\partial\mathcal{E}$, one can therefore write the Fokker-Planck equation in its most common form, as

$$\frac{\mathrm{d}f}{\mathrm{d}t} = -\frac{\partial}{\partial\mathcal{L}}[f\langle\Delta\mathcal{L}\rangle] + \frac{1}{2}\frac{\partial^2}{\partial\mathcal{L}^2}[f\langle(\Delta\mathcal{L})^2\rangle]. \tag{2.81}$$

Further continuation of the derivation is beyond the scope of this thesis: it suffices to say that one either solves Eq. (2.81) numerically (e.g., through a Monte-Carlo simulation, see Shapiro & Marchant, 1978, Sec. III), or approaches it analytically by making further assumptions about the terms $\langle\Delta\mathcal{L}\rangle$ and $\langle(\Delta\mathcal{L})^2\rangle$ (which are diffusion coefficients, since they measure the expected rate of change in stellar velocities) (e.g., Strubbe, 2011, Sec. 4.3).

2.4.3 The inner parsec of the Galactic Centre

The inner parsec of the Galactic Centre lies completely within the radius of influence of the black hole, see Eq. (2.7). Measurements of the surface density distribution of stars (i.e., the number of stellar sources per square arcsecond) as a function of the projected separation from Sgr A* are best fitted by a broken power law,

$$\rho_\star(r) \sim r^{-\alpha}, \tag{2.82}$$

with $\alpha \approx 2$ for $r \gtrsim 0.4$ pc and $\alpha \approx 1.4$ inside the inner ~ 0.4 pc (Genzel *et al.*, 2003). This confirms the theoretically predicted stellar density cusp mentioned in Sec. 2.4.1. The region outside the cusp has a mixture of old, metal-rich stars (an extension of the old bulge population), and intermediate-age and young stars: the old stars are dynamically relaxed and follow general galactic rotation, while the young stars show counter-rotation (Genzel *et al.*, 1996). The inner cusp, however, exhibits a featureless luminosity function due to a lack of old, low-mass stars, and is dominated by unrelaxed blue supergiants (Genzel *et al.*, 2000). Spectrally, these stars present distinctive helium emission lines and a lack of hydrogen lines, specific of Wolf-Rayet stars: massive ($m_\star \sim$ few $\times\, 10\ M_\odot$) stars with lifespans of few $\times\, 10^6$ yr undergoing rapid mass loss by strong stellar winds, which remove their hydrogen envelopes and reveal the helium-rich cores. In our Galaxy, these young stars are grouped in two counter-rotating disc-like structures around the black hole, strongly inclined relative to each other, but with the same stellar content, indicating that they formed at the same time. A plausible scenario for their formation is that 5–8 million years ago two gas clouds fell towards the Galactic Centre, collided, were shock compressed and subsequently formed two rotating accretion discs orbiting the SMBH (Genzel *et al.*, 2003).

The inner 0.04 pc does not host any bright giants, red or blue, nor discs of stars, but is home to some tens of isotropically distributed faint blue stars called "S-stars", after their identifying labels. Spectroscopically, the S-stars are B0–B9 main-sequence stars with spins similar to those of Solar neighbourhood B-type stars. Of particular importance is the brightest S-star, labelled S2 or S0-2, orbiting the SMBH in 15.9 years on an eccentric ($e = 0.89$) orbit with periapsis $r_\mathrm{p} \approx 120$ AU and maximum orbital velocity in excess of 5000 km s^{-1}, and which was the first S-star to be observed for a full orbital period (Ghez *et al.*, 2008). S2 is a transitional O8-B8 star of mass $m_\star \sim 15\ M_\odot$, effective temperature $T \sim 3\times10^5$ K, intrinsic bolometric luminosity $L \sim 10^3\ L_\odot$ and a main-sequence life span of $\sim 10^7$ yr (Gillessen *et al.*, 2009b). All the other stars in the S-cluster are less massive and hence cooler, fainter and longer-lived: the "typical" S-star would be a B2 main-sequence star of mass $m_\star \sim 10\ M_\odot$, radius of $r_\star \sim 4.5\ R_\odot$ and main-sequence life span of $\sim 2 \times 10^7$ yr (Alexander, 2005).

The S-stars have been tracked since 1992 at the Very Large Telescope (VLT) and since 1995 at the Keck telescope (Eckart & Genzel, 1996; Ghez *et al.*, 1998), and are used as test particles for the gravitational potential of the black hole Sgr A*.

In 2012, a new S-star labelled S0-102 was discovered to have an even shorter period than S2 (Meyer *et al.*, 2012). S0-102 is on an eccentric ($e = 0.68$) orbit with period of only 11.5 years, which means it can reach orbital velocities in excess of ~ 12000 km s^{-1}. It is also the second S-star to have its orbit fully determined in three dimensions, and together with S2 is currently being used to observe post-Newtonian effects such as gravitational redshift, orbital precession, and frame-dragging.

Despite their importance, the formation and nature of these young stars is still a puzzle and subject of ongoing studies, both observationally (e.g., Perets & Gualandris, 2010) and numerically (e.g., De Colle *et al.*, 2012a).

2.4.4 Stellar processes near supermassive black holes

The large-scale dynamics within the black hole's radius of influence r_h (Eq. 2.7) is determined by the superposition of the black hole's smooth gravitational potential and the combined potential of all other stars. When two stars approach each other close enough for their mutual gravitational attraction to overcome the gradient of the background potential, they are involved in a two-body interaction, or stellar "collision", even if they do not physically collide. Since the stellar density in the Galactic Centre is unusually high ($\simeq 10^8\ M_\odot\ \mathrm{pc}^{-3}$ compared to $1\ M_\odot\ \mathrm{pc}^{-3}$ in the Solar neighbourhood), two-body interactions occur frequently by galactic standards, which led Alexander (2003) to coin the term "stellar collider" for the inner part of this region. The collision process is often also called two-body scattering because it leads to a redistribution of the orbits (technically, of energy and angular momentum). However, in the steep potential well of the SMBH, energy equipartition cannot be achieved: in the long term, two-body interactions will tend to slow down heavier stars and speed up lighter ones. Since the Keplerian orbital radius only depends on the velocity – as $r \sim Gm_\mathrm{bh}/v^2$, through the specific energy, see Eqs. (2.39) and (2.44) –, heavy stars will tend to "sink" towards the Galactic Centre, while lighter stars will drift outwards. In due time, this leads to mass segregation, with the vicinity of the SMBH becoming populated mainly by heavy stellar remnants (the exact steady-state solution has a dependence on heavy-to-light stellar ratio and the unbound population number ratio; this leads to a weak segregation and a strong segregation solution, with very different density profiles; see Alexander & Hopman, 2009 for a discussion). This effect is further enhanced by the essentially unlimited life span of these compact objects (much longer than the Hubble time) in comparison to the shorter stellar life spans.

> The existence of a cluster of $\sim 2 \times 10^4$ black holes at the Galactic Centre was speculated by Miralda-Escudé & Gould (2000) based on theoretical arguments, though it has not yet been observationally confirmed. This lack of observable X-ray emission, probably linked to radiatively inefficient accretion of the cold gas in the Galactic Centre, has been used to put an upper limit of $\sim 4\times10^4$ on the black hole population in this dense cusp (Deegan & Nayakshin, 2007). Other possible manifestations of these stellar black holes include gravitational microlensing (Chanamé *et al.*, 2001) and the dynamical effect on the stellar population (i.e., the mass segregation itself).
> To date, the closest magnetar detected in the vicinity of Sgr A* is SGR1745–2900 (with a period of 3.76 s, located at a distance of $\approx$ 2.4 arcseconds,

or 0.09 pc from the Galactic Centre; see Mori *et al.*, 2013; Kennea *et al.*, 2013). Its potential for novel tests of GR effects (such as the cosmic censorship conjecture and the no-hair theorem for Kerr black holes), independent of the distance R_0 to the Galactic Centre, is unprecedented (Liu *et al.*, 2012). Within a distance of ~ 200 pc from the SMBH, Lazio *et al.* (2003) report the detection of only 10 candidate pulsars. The scarcity of observations has been primarily explained by the extreme scattering of radio waves by the ionized interstellar medium in the inner hundred parsecs of the galaxy (Eatough *et al.*, 2013).
Simple estimates of the formation rate of black hole–pulsar binaries via three-body exchange interactions indicate that a handful of these systems should also be present in the central parsec of our galaxy (Faucher-Giguère & Loeb, 2011). The detection of such a system would be a significant event, since only recently LIGO may have started to directly observe such binaries, though still without a definitive confirmation (e.g., Castelvecchi, 2019).
A number of stellar black hole binaries are also expected to form out of gravitational wave emission during black hole encounters, with a detectable coalescence rate as high as $\sim 1-10^2\,\mathrm{yr}^{-1}$ (O'Leary *et al.*, 2009) with the upcoming Advanced LIGO gravitational wave detector (e.g., Waldman, 2011).

The relaxation process can however be accelerated by massive nearby perturbers such as star clusters, molecular clouds, stellar black hole clusters (Miralda-Escudé & Gould, 2000), intermediate mass black holes (Zhao *et al.*, 2002), or, where the orbits are nearly Keplerian, by resonant relaxation (Rauch & Tremaine, 1996).

Such self-gravitating systems have a "negative heat capacity" (i.e., if energy is removed from the system then its kinetic energy, or "temperature", actually increases): the virial theorem (Clausius, 1870) states that the average potential and kinetic energies are related by $\mathcal{E}_{\rm pot} = -2\mathcal{E}_{\rm kin}$, or, conversely, that $\mathcal{E}_{\rm tot} = \mathcal{E}_{\rm pot} + \mathcal{E}_{\rm kin} = -\mathcal{E}_{\rm kin}$, and so if $\mathcal{E}_{\rm tot}$ changes by $(-d\mathcal{E})$, $\mathcal{E}_{\rm kin}$ will increase by $(+d\mathcal{E})$. As two-body scattering processes draw energy out of the system, either by ejecting lighter stars or by diffusion to higher energies (evaporation), they lead to a more bound and compact system, with an increased collision rate, and therefore to even higher energy losses by the system. This runaway process, named "gravothermal catastrophe" or "core collapse", can lead to the formation of an extremely dense stellar core surrounded by a diffuse extended halo.

Closer to the black hole, as the density increases, effects related to the finite size of the stars become important. In particular, very close two-body interactions can lead to tidal waves, mass stripping, and even tidal capture of the two stars into a tightly bound binary. For a star in orbit around the SMBH, the Keplerian orbital velocity ($\sim \sqrt{Gm_{\rm bh}/r}$) exceeds the escape velocity from the star's surface ($\sim \sqrt{2Gm_\star/r_\star}$)

at a distance

$$r \sim 10^{-2}\,\mathrm{pc}\left(\frac{r_\star}{R_\odot}\right)\left(\frac{m_\star}{M_\odot}\right)^{-1}\left(\frac{m_{\mathrm{bh}}}{10^6\,M_\odot}\right). \tag{2.83}$$

All stars that orbit the SMBH closer than that will collide on hyperbolic orbits, extracting energy and angular momentum from their orbit but continuing on separate ways. The energy can be radiated away between subsequent encounters, but angular momentum is likely to be dissipated only on a time scale comparable to the stellar life span, leading to a stochastic spin-up of the high density cusp stars, up to a significant fraction of their breakup velocity (e.g., Alexander & Kumar, 2001).

Head-on collisions between stars are probably the rarest, but the Galactic Centre is the place where they are most likely to occur. In the previous section we have seen that the inner part of the cusp is mainly populated by massive, short-lived giant stars. Due to their sheer size, these stars also have the largest collision cross-sections. The expected outcome of such a collision is either the stripping of the relatively tenuous envelope of the giant leaving behind a hot thus bluer star, the formation of a common envelope binary, or even the creation of exotic collision products such as a Thorne-Żytkow object (Thorne & Żytkow, 1975), a giant star with a neutron star or black hole at its core.

2.5 Relativistic effects

Due to the very strong gravity of the supermassive black hole, measurements of stellar orbits around Sgr. A* can test a number of predictions made by general relativity (e.g., Merritt *et al.*, 2010). Along with deviations from a Keplerian orbit, there are prospects of probing more fundamental ideas such as the Einstein equivalence principle (Angélil & Saha, 2011), time dilation (Zucker *et al.*, 2006), or the no-hair conjecture (Will, 2008; Sadeghian & Will, 2011). The plausible presence of a large number of high-mass stellar black holes near the Galactic Centre due to mass segregation can complicate the interpretation of these observations, because such compact objects produce relativistic effects of their own.

A consistent (i.e., to the same order) expansion of the metric and of the energy-momentum tensor in the Einstein's field equations yields the so-called post-Newtonian corrections, which can be classified according to their dependence on the relativistic parameter $\beta \equiv v/c$, or, equivalently, by the compactness parameter $\Upsilon = r_{\mathrm{s}}/r$ (e.g., Maggiore, 2007, Sec. 5.1.2). From $v^2 \sim Gm_{\mathrm{bh}}/r$ and $r_{\mathrm{s}} = 2Gm_{\mathrm{bh}}/c^2$ we obtain directly $(v/c)^2 \sim r_{\mathrm{s}}/r$ hence the $O(\beta)$ corrections to the orbital motion are equivalent to the $O(\Upsilon^{1/2})$ corrections to the metric. Second order $O(\beta^2)$ effects include periapsis shift and gravitational redshift. Third order $O(\beta^3)$ effects include the Lense–Thirring effect (i.e., frame dragging; Lense & Thirring, 1918).

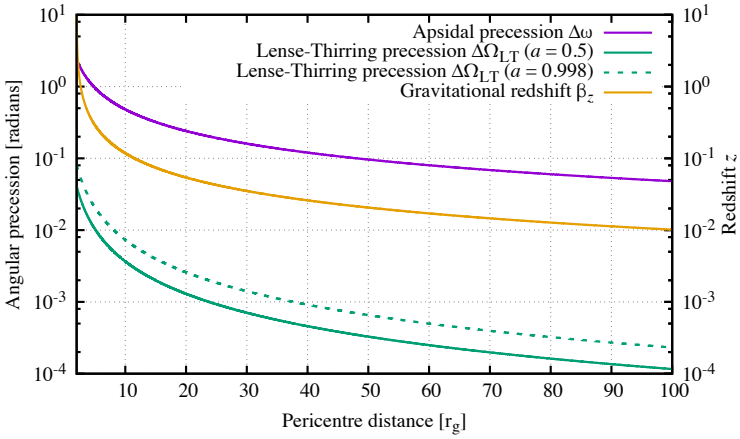

Figure 2.7: Magnitude of relativistic effects as a function of the periapsis distance r_p expressed in gravitational radii $r_g = Gm_{bh}/c^2$, as computed using Eqs. (2.84), (2.85) and (2.87), assuming an orbit with $e = 0.98$. Decreasing the eccentricity slightly increases the magnitude of the angular precessions (since it reduces the apocentre distance, which appears in the denominator), but most TDEs will have $e \approx 1$. Changing the black hole spin has a very small effect on the Lense–Thirring precession, as evidenced by the small difference between the green lines. We observe that all effects decrease by more than two orders of magnitude within $100\, r_g$, and that the third order effects (here, Lense–Thirring precession) is about two orders of magnitude weaker than the second-order effects (apsidal precession and gravitational redshift).

2.5.1 Apsidal motion.

The equations of orbital dynamics predict closed orbits for only two types of potential: the harmonic oscillator and the Keplerian gravitational potential (e.g., Rosswog & Brüggen, 2007, Sec. 6.2.1). Any deviations from the $1/r$ Keplerian potential (introduced by e.g. higher-order multipole moments, perturbations due to a third body, or general relativistic corrections) lead to a rosette-shaped orbit with a prograde shift $\Delta\omega$. For an orbit around a Schwarzschild black hole, $\Delta\omega$ is given by (e.g., Weinberg, 1972, Eq. 8.6.11)

$$\Delta\omega = \frac{3\pi}{(1-e^2)}\frac{r_s}{a}. \tag{2.84}$$

A putative cluster of compact objects around the black hole would have an opposite effect on stellar orbits, leading to retrograde periapsis shift. The cause is that as the star approaches periapsis, the stellar acceleration due to the dark objects decreases due to its scaling with the enclosed mass. Insofar as such a cluster exists (and mass segregation makes this very likely), the periapsis shifts will likely be entangled, and calculations show that measurements of at least three complete stellar orbits are needed in order to unambiguously solve for its separate components (Rubilar & Eckart, 2001).

2.5.2 Lense–Thirring precession.

A supermassive black hole with nonzero dimensionless spin parameter $a^\star$ ($0 \leq a^\star \leq 1$, note the difference between the spin parameter $a^\star$ and the semimajor axis a in the following equations) produces two secular changes in the trajectory of a test particle: a precession of the longitude of the ascending node Ω, and also a precession of the periapsis, in addition to the s-independent one given in Eq. (2.84). The former is given in the weak field limit by (Lense & Thirring, 1918)

$$\Delta\Omega_{\rm LT} = \frac{2}{\pi}\frac{a^\star}{(1-e^2)^{3/2}}\left(\frac{r_{\rm s}}{a}\right)^{3/2}, \tag{2.85}$$

while the latter is given by

$$\Delta\omega_{\rm LT} = -3\Delta\Omega_{\rm LT}\cos i, \tag{2.86}$$

with i being the angle between the orbital angular momentum of the star and the spin of the black hole. In a tidal disruption event, Lense–Thirring precession is mainly relevant after the star is disrupted, because frame dragging effects modify the spatial configuration of the debris. In principle, the precession of the debris stream under the influence of a fast-spinning black hole will either delay or prevent for several orbits the self-intersection and shocking of the stream due to periapsis shift (e.g., Hayasaki *et al.*, 2013; Guillochon & Ramirez-Ruiz, 2015), though a systematic numerical study of the parameter space (in at least impact parameter and black hole spin) is required to completely answer this question. Our parameter space exploration in Paper I does consider the influence of the BH spin on the morphology and energetics of tidal disruptions, but only around a $10^6\,M_\odot$ black hole, and without following the entire circularization process.

2.5.3 Gravitational redshift.

Photons with wavelength λ emitted at distance r from the black hole will lose energy as they escape the deep potential well of the SMBH. The redshift measured by an observer at infinity is given by

$$\beta_z = \left(1-\frac{r_{\rm s}}{r}\right)^{-1/2} - 1, \tag{2.87}$$

which can be Taylor-expanded as

$$z \approx \Upsilon/2 = \frac{1}{2}\left[\Upsilon_0 + \beta^2\right] \tag{2.88}$$

for sufficiently small compactness parameters Υ (introduced above).

In addition, there will be a Doppler-shift

$$\beta_{\mathrm{D}} = \frac{1+\beta\cos\vartheta}{\sqrt{1-\beta^2}} - 1 \approx \beta\cos\vartheta + \frac{1}{2}\beta^2, \tag{2.89}$$

with a classical component dependent on the angle ϑ between the direction of motion and the line of sight, and a second order transverse relativistic component with the same magnitude as the second-order term of the gravitational redshift.

A third source of redshift is the Rømer time delay, a Newtonian effect caused by variations in the distance between source and observer for orbits that are not completely face-on. Its exact form depends on the orbital parameters, but results in second-order corrections $\beta_{\mathrm{R}} \approx B_{\mathrm{R}}\beta^2$ (Alexander, 2005).

Summing up all these contributions, one obtains the observed radial velocity expanded in terms of the magnitude of the true stellar velocity β,

$$\beta_{\mathrm{r}} = \left(\beta_{\odot} + \beta_{\mathrm{z,gal}} + \beta_{\mathrm{z},\star} + \frac{1}{2}\Upsilon_0\right) + (\cos\vartheta)\,\beta + (1+B_{\mathrm{R}})\,\beta^2 + O(\beta^3), \tag{2.90}$$

with the constant term written in terms of the local velocity shift $\beta_{\odot}$ (caused both by the Doppler shift due to the motion of the Sun and the Earth, and the the gravitational blueshift by the Sun, Earth, and other planets), the galactic gravitational redshift $\beta_{\mathrm{z,gal}}$, the gravitational redshift $\beta_{\mathrm{z},\star}$ due to the star's potential well, and the constant part of the gravitational redshift due to the SMBH in Eq. (2.88).

3

Modeling relativistic tidal disruptions

We have to remember that what we observe is not nature herself, but nature exposed to our method of questioning.
Werner Heisenberg

3.1 Using SPH in modeling TDEs

3.1.1 A brief overview of SPH

Lagrangian schemes are more suited for the numerical modelling of tidal disruptions than Eulerian ones, since the interpolation points move with the fluid, provide a natural adaptive 'mesh', eliminate the need to follow a multitude of empty grid cells, and ensure exact advection of the fluid elements. If well-formulated, they also ensure exact conservation of energy and (most importantly for this kind of problem) angular momentum. The calculations can thus be just as easily conducted in the rest frame of the black hole instead of the star. One of the more successful Lagrangian methods, the so-called "smoothed particle hydrodynamics" (SPH; see Monaghan 1992; Rosswog 2009 for reviews), discretises the fluid into a set of interpolation points, traditionally called 'particles', which can be thought of as fluid parcels. Each particle a has assigned to it certain physical properties (e.g., mass m_a, density ρ_a, internal energy u_a, position $\boldsymbol{r}_a$) and a smoothing length h_a. Continuous or 'smoothed' physical quantities f are computed at any given position $\boldsymbol{r}$ using a kernel-weighted interpolation:

$$(f)_{\mathrm{SPH}}(\boldsymbol{r}) = \sum_b V_b f_b W(|\boldsymbol{r} - \boldsymbol{r}_b|, h), \tag{3.1}$$

where V_b is a volume element (commonly taken as m_b/ρ_b, with m_b and ρ_b being, respectively, the mass and density of a neighbouring particle b), and W is the so-called 'smoothing kernel', whose 'support' (or in layman's terms, radius of influence) is determined by the smoothing length h. The summation is done over all particles b that fall within the range of the kernel (usually, but not always, taken as $2h$). In other words, $(f)_{\mathrm{SPH}}$ is the kernel-weighted average of the properties f_b of all the particles for which the given point $\boldsymbol{r}$ is within the range of their kernel. Similarly, gradients of fluid

properties can be calculated as sums over the analytically known kernel gradient:

$$(\nabla f)_{\mathrm{SPH}}(\boldsymbol{r}) = \sum_b V_b f_b \nabla W(|\boldsymbol{r} - \boldsymbol{r}_a|, h). \tag{3.2}$$

The evolution equations for a perfect fluid (i.e., the Euler equations) can be written in the SPH formalism as follows; note that we shall give the simplest, "vanilla ice" version of the equations for a perfect fluid; while suitable for academic purposes, this formulation lacks the additional terms resulting from the variable smoothing length (the so-called "grad-h" terms), viscosity, and self-gravity.

The mass conservation equation can be written in Lagrangian form as

$$\frac{\mathrm{d}\rho}{\mathrm{d}t} = -\rho \nabla \cdot \boldsymbol{v}. \tag{3.3}$$

The standard practice in SPH is to keep the particle masses fixed, in which case mass conservation is perfect by construction, and there is no need to solve Eq. (3.3) explicitly.

The momentum conservation equations, given in Lagrangian form as

$$\frac{\mathrm{d}\boldsymbol{v}}{\mathrm{d}t} = -\frac{\nabla P}{\rho} \tag{3.4}$$

can be discretized as

$$\frac{\mathrm{d}\boldsymbol{v}_a}{\mathrm{d}t} = -\sum_b m_b \left(\frac{P_a}{{\rho_a}^2} + \frac{P_b}{{\rho_b}^2} \right) \nabla_a W_{ab}. \tag{3.5}$$

Since this equation is manifestly symmetric in a and b, and $\nabla_a W_{ab} = -\nabla_b W_{ba}$ (as long as W_{ab} uses the mean of h_a and h_b), this form of the momentum equation conserves total and angular momentum by construction.

Finally, the energy equation stems directly from the first law of thermodynamics, $(\partial u/\partial \rho)_s = P/\rho^2$, and Eq. (3.3) as:

$$\frac{\mathrm{d}u}{\mathrm{d}t} = -\frac{P}{\rho} \nabla \cdot \boldsymbol{v}, \tag{3.6}$$

and can be discretized as

$$\frac{\mathrm{d}u_a}{\mathrm{d}t} = \frac{P_a}{{\rho_a}^2} \sum_b m_b \boldsymbol{v}_{ab} \cdot \nabla_a W_{ab}. \tag{3.7}$$

Certain aspects of this standard formulation can be greatly improved (Rosswog, 2015): by choosing better volume elements than m/ρ (e.g. Hopkins, 2013) one can prevent the occurence of spurious surface tension forces; by using integral-based gradient

estimators (e.g. García-Senz *et al.*, 2012) one can improve the gradient estimate by several orders of magnitude; by using a kernel with certain mathematical properties (e.g., peaked kernels, or kernels with a non-negative Fourier transform such as Wendland, 1995, first discussed in an SPH context by Dehnen & Aly, 2012) one can prevent particles from forming pairs, which would reduce the effective resolution of the simulation.

All these modifications would result in subtle improvements, particularly in resolving small-scale structures or making the simulation less noisy. Unfortunately, the issues that appear in simulating tidal disruptions (with SPH, or with any other particle- or grid-based code), discussed below, cannot be alleviated by such improvements, so for our simulations we used a "standard SPH" code, as described in detail by Rosswog *et al.* (2009).

3.1.2 Choosing the time steps

We use a predictor–corrector time stepping scheme with individual time steps (see, e.g., Press *et al.*, 1992, Sec. 16.7, for a general description of such integrators), with the following time step criteria in place:

- a CFL stability criterion (Courant, Friedrichs & Lewy, 1928), stating that information propagated at the sound speed should not travel more than a certain fraction of a smoothing length within a time step:

$$(\Delta t)_{\mathrm{CFL}} \lesssim h/c_s; \tag{3.8}$$

- a relative "total force" criterion of the form

$$(\Delta t)_{\mathrm{f}} \lesssim \left(\frac{h}{f_{\mathrm{tot}}}\right)^{1/2}; \tag{3.9}$$

- a SMBH criterion that is switched on when particles are close to the black hole (e.g., several Schwarzschild radii), acting as a "safety net" when the relative force criterion (which is primarily used for hydro forces) does not react sufficiently fast to the extremely fast-changing acceleration along an orbit close to the black hole:

$$(\Delta t)_{\mathrm{bh}} \lesssim \left(\frac{r^3}{Gm_{\mathrm{bh}}}\right)^{1/2}. \tag{3.10}$$

The time step of each particle is then computed as a fraction (e.g., 0.1) of the minimum of these three quantities. In principle, any evolved quantity q may have its own generalized time step criterion, based on

$$(\Delta t)_q < \left(q/q^{(n)}\right)^{1/n}, \tag{3.11}$$

(where $^{(n)}$ denotes the n^{th} time derivative). Obvious candidates for q would be the internal energies and the smoothing lengths, though in various experiments we have not observed these additional criteria to significantly modify the minimum time step.

In the case of fully relativistic simulations, an additional challenge comes from the fact that the relevant signal velocity that enters the CFL stability criterion is the speed of light, so that the numerical time step is restricted to

$$\Delta t < 0.02 \text{ s} \left(\frac{\Delta x}{r_\star/100} \right), \tag{3.12}$$

where Δx symbolises the smallest length-scale that needs to be resolved. This restriction may be relaxed after a disruption has occurred, but if the encounter is only weak and a stellar core survives, similar time step restrictions still apply after the encounter. Therefore, a full simulation – starting from several tidal radii and following the spreading of the stellar debris to large distances, the return of a fraction of the debris to the BH, and the subsequent circularization and formation of an accretion disc – is prohibitively expensive for a fully relativistic treatment. Together with the enormous mass ratio between the SMBH and the star (which makes stellar self-gravity only a tiny perturbation on top of the BH metric), this explains why canonical tidal disruptions have not yet been modeled, from beginning to end, using a fully general-relativistic code.

3.1.3 Technical challenges

In the first stage of a tidal disruption, the star approaches the black hole. Here, the time step is limited by the internal time step of the star (set by the Courant and the relative force criteria, which in this stage are normally of roughly the same order), so for large particle numbers this may well be the most expensive part of the simulation, depending on the initial distance. For most low- and medium-resolution simulations, we initially place the star at 5 tidal radii, such that the tidal force at the beginning of the simulation is negligible (as discussed in Sec. 1 of Paper II), and only gradually increases as the star approaches the SMBH. For particle numbers $\gtrsim 10^6$, we start with the star at 3 tidal radii.

During the periapsis passage, the Courant and the force time step decrease due to tidal compression, but the SMBH criterion also kicks in, and for deep encounters it may actually determine the time step at periapsis. It is crucial to have a sufficiently small time step here, especially for the (pseudo-)relativistic simulations, where the periapsis shift is only accurately reproduced if Δt is sufficiently small.

As the star recedes from the black hole and the tidal debris expands, the time step greatly increases, until the most delicate part of the simulation begins: the second periapsis passage. As the bound tail approaches the SMBH (while the centre of mass continues to recede along the parabolic trajectory), it becomes stretched along the

length of the stream (in the radial direction) and compressed across the stream. The spatial distribution thus becomes essentially one-dimensional. In addition, due to the expansion, the density drops by several orders of magnitude (compared to the original star). Due to the energy distribution that dictates the rise of the $\dot{M}$-curve, if this rise is not steep enough (as in the case of parabolic encounters) then the width of the head of the debris stream cannot be resolved, independently of the resolution: particles will return to periapsis "one by one" (see Figure 3.1).

In the course of all our simulations we use adaptive smoothing lengths, which increase or decrease at every time step in order to maintain between 50 and 90 neighbours per particle. This is absolutely necessary given the geometrical constraints of the problem (after disruption the star may expand to thousands of times its original size, and the density contrast between the most and the least dense parts of the debris stream may span many orders of magnitude), but leads to problems during the second periapsis passage: since the head of the stream is one-dimensional, the smoothing length of these particles will increase far more than the width of the stream, and these particles will have very distant neighbours downstream, leading to unresolved interactions between the head and the rest of the stream . This effect is particularly problematic once the stream "turns" at periapsis: the isolated particles, having huge smoothing lengths, may suddenly detect the rest of the stream approaching from the opposite direction, which triggers the $\nabla \cdot \boldsymbol{v}$ artificial viscosity term for shock heating, leading to a questionably large heating of the few isolated particles (while they are still far away from the rest of the stream)[6]. In relativistic encounters, once the stream self-intersects due to periapsis shift, the high temperature and internal energy of the head of the stream will affect the hydrodynamic properties of all the particles close to the self-intersection point, which drastically reduces our confidence in the accuracy of the thermodynamical results past this point. The orbital motion and the geometry of the stream remain virtually unaffected by this effect, so density and velocity plots are always "well-behaved".

In Paper I and Paper IV we are interested in the energy distribution after the first periapsis passage, and therefore we do not run into these problems: the simulations are stopped after the energy freezes-in (approximately after the star exits the tidal radius, long before the second periapsis passage). However, when following the long-term evolution of a TDE one will always encounter these issues, unless: a) the orbital eccentricity is small enough to steepen the rise of the $\dot{M}$ curve and result in a thicker stream that can be properly resolved across, or b) special preventive measures are taken (e.g., the gravitational force due to the BH is "smoothed" so that the head of

[6]This issue may in part be due to the individual time steps, but running a simulation with global time steps is, at the moment, prohibitively expensive. A solution would be to run only the problematic part of the simulation, i.e., the beginning of the second periapsis passage, with global time steps, while using individual time steps for the rest of the simulation. We plan to investigate this option in future works.

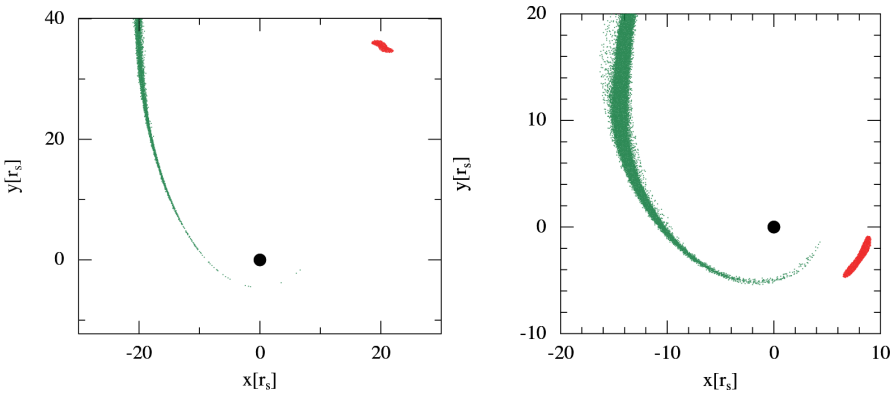

Figure 3.1: Spatial distribution of the tidal debris shortly after the first periapsis passage (red particles), and at the beginning of the second periapsis passage (green particles), in a parabolic ($e = 1$; *left panel*) and an elliptical ($e = 0.8$; *right panel*) encounter. The figure reveals the virtually one-dimensional nature of the stream as it returns to the SMBH and starts the circularization process. The effect is much more pronounced in parabolic encounters, while in elliptical encounters the width of the stream can often be resolved satisfactorily. If not carefully handled, the head of the debris stream (consisting of single particles returning to periapsis one by one) may cause serious problems to the simulation, as discussed in the main text.

the stream does not follow its normal orbit around the black hole, but is cut off from the rest of the stream at periapsis; this force smoothing would also solve the problem of a few isolated particles close to the black hole slowing down the entire simulation due to their impractically small time steps).

Needless to say, grid-based codes have their own types of problems with such complicated geometries. The only feasible way of performing such computations is in the rest frame of the centre of mass of the fluid (e.g., Guillochon *et al.*, 2009; Guillochon & Ramirez-Ruiz, 2013), since advection of such a thin stream of gas, possibly along a complicated, self-intersecting orbit, while conserving angular momentum, is close to impossible, unless an impractically fine grid is used. The code also needs a dynamically-adapting AMR scheme that continuously refines the grid as the stream geometry evolves.

To date, full simulations (i.e., with second periapsis passage and possibly disc formation) of tidal disruptions have either: a) run the entire disruption and disc formation with SPH, but considered an elliptical encounter (e.g. Bonnerot *et al.*, 2015; Hayasaki *et al.*, 2015), in which the debris returns to periapsis in a much shorter time; b) simulated a system with a less extreme $m_{\rm bh}/m_\star$ ratio (e.g., intermediate-mass black holes and white dwarfs), for which the dynamic ranges of length- and timescales were more manageable (e.g. Rosswog *et al.*, 2009; Shiokawa *et al.*, 2015); or c) performed different simulations for the two parts of the TDE, i.e., before and

after the second periapsis passage: the former can be easily run with a grid code in the rest frame of the star (e.g. Shiokawa *et al.*, 2015) or with SPH; the results are then mapped onto a grid (or used as a boundary condition), and the formation of the disc is then followed with a grid-based code in the rest frame of the black hole[7]. Nevertheless, to date, none of the simulations we are aware of have followed the entire process of stellar disruption followed by disc formation for the most "typical" TDE (solar-type star on a parabolic orbit with $\beta = 1$ around a $10^6\,M_\odot$ black hole).

3.2 Including relativistic effects

As argued above, a fully general relativistic treatment of TDEs is prohibitively expensive. For the numerical study of a TDE, this leaves a handful of options:

a) Use an entirely Newtonian approach and restrict the focus to encounters that can be treated as non-relativistic with a reasonable accuracy (this is the prevalent approach in the literature on TDEs; it works very well in the appropriate regime, but obviously ignores all relativistic effects).

b) Use a Newtonian hydrodynamics scheme together with a pseudo-Newtonian potential for approximately capturing some relativistic effects (e.g., Rosswog, 2009; Hayasaki *et al.*, 2013, 2015; Bonnerot *et al.*, 2015; Paper IV).
These pseudo-Newtonian potentials are usually tuned to reproduce special properties for the motion around a BH, but cannot reproduce all of the relevant relativistic effects simultaneously. Moreover, these kinds of potential have mostly been developed for non-rotating BHs (see e.g. Tejeda & Rosswog, 2013, for a comparison of some of the most commonly used pseudo-Newtonian potentials), and they have been less successful in modelling (the more realistic) rotating BHs.

c) Follow a post-Newtonian approach for mildly relativistic encounters (Ayal *et al.*, 2000, 2001; Hayasaki *et al.*, 2015); These approaches are computationally very demanding since they require the solution of several Poisson equations (nine for the full approach of Ayal *et al.*, 2001), while being unnecessary far from the BH and inaccurate close to it. In addition, the computational burden for solving the Poisson equations seriously restricts the numerical resolution that can be afforded for the hydrodynamics.

d) Use a full numerical relativity approach by solving the Einstein equations, and restrict the attention mainly to regions near the BH (e.g. East, 2014); we point out that all fully relativistic simulations (i.e., as opposed to a fixed-

[7] Note that "patching up" particle- and grid-based simulations for the various stages has its own share of drawbacks, including the addition of an artificial, non-zero "vacuum" for the "empty" cells of the grid-based simulation at the time when the transition is done, and the interpolation of the particle distribution to a grid, which is never perfect and may often be accompanied by a downscaling in resolution.

metric treatment) to date use a very restrictive subset of the parameter space, focusing on ultra-close encounters with small SMBH to stellar mass ratio.

e) Use a combination of some of the above approaches, as was done by, e.g., Shiokawa *et al.* (2015) and in Paper III.

In the following subsections we will present the new formalism for including the exact Kerr gravitational and hydrodynamic accelerations, together with an ad-hoc correction to the Newtonian self-gravity, into existing Newtonian codes, as introduced in Paper II.

3.2.1 Geodesic motion

In Newtonian SPH codes, the gravitational influence of the black hole is represented by the Newtonian potential,

$$\Phi_{\rm N}(r) = -\frac{Gm_{\rm bh}}{r}. \tag{3.13}$$

The acceleration is then simply the negative gradient of the gravitational potential,

$$\left(\frac{{\rm d}^2 x_i}{{\rm d}t^2}\right)_{\rm bh,N} = -\partial_i \Phi_{\rm N}(r) \overset{(3.13)}{=} -\frac{Gm_{\rm bh}x_i}{r^3}. \tag{3.14}$$

Pseudo-Newtonian potential work by modifying Eq. (3.13) – and consequently Eq. (3.14) – with additional, higher-order terms. The rest of the code is left virtually unchanged, which makes this approach easy to implement and therefore attractive. Several such potentials have been reviewed and diligently compared by Tejeda & Rosswog (2013), so in what follows we will only give the expressions for three widely-used pseudo-Newtonian potentials. The oldest and simplest expression is due to Paczyński & Wiita (1980; see also Abramowicz, 2009 for a step-by-step derivation), which makes the deceptively simple choice of replacing the r in Eq. (3.13) by $r - 2r_{\rm g}$,

$$\Phi_{\rm PW}(r) = -\frac{Gm_{\rm bh}}{r - 2r_{\rm g}}, \tag{3.15}$$

though by doing so it reproduces exactly the locations of the innermost stable circular orbit and the marginally bound orbit.

An example of pseudo-Newtonian potential used to approximate test particle motion around Kerr black holes is due to Nowak & Wagoner (1991):

$$\Phi_{\rm NW}(r) = -\frac{Gm_{\rm bh}}{r}\left(1 - \frac{3r_{\rm g}}{r} + \frac{12{r_{\rm g}}^2}{r^2}\right) \tag{3.16}$$

The Tejeda & Rosswog (2013) potential achieves much better accuracy for Schwarzschild black holes than all the other available options, and reproduces exactly several

relativistic features of the motion of test particles in Schwarzschild spacetime such as: the location of the photon, marginally bound and marginally stable circular orbits; the radial dependence of the energy and angular momentum of circular orbits; the ratio between the orbital and epicyclic frequencies; the time evolution of parabolic-like trajectories; the spatial projection of general trajectories as function of the constants of motion and their periapsis advance. The full expression of the TR potential is:

$$\Phi_{\rm TR}(r,\dot{r},\dot{\varphi}) = -\frac{Gm_{\rm bh}}{r} - \left(\frac{2r_{\rm g}}{r-2r_{\rm g}}\right)\left[\left(\frac{r-r_{\rm g}}{r-2r_{\rm g}}\right)\dot{r}^2 + \frac{r^2\dot{\varphi}^2}{2}\right]. \tag{3.17}$$

By taking the gradient of this last expression, we obtain the gravitational acceleration in a TR potential (Paper IV, Eq. A1),

$$\left(\frac{{\rm d}^2x_i}{{\rm d}t^2}\right)_{\rm bh,TR} = -\frac{Gm_{\rm bh}x_i}{r^3}\left(1-\frac{r_{\rm s}}{r}\right)^2 + \frac{r_{\rm s}\dot{x}_i\dot{r}}{r(r-r_{\rm s})} - \frac{3}{2}\frac{r_{\rm s}x_i\dot{\varphi}^2}{r}, \tag{3.18}$$

while the full-relativistic expression for the acceleration on a test particle in Schwarzschild space time is (Paper IV, Eq. A9),

$$\left(\frac{{\rm d}^2x_i}{{\rm d}t^2}\right)_{\rm bh,S} = -\frac{Gm_{\rm bh}x_i}{r^3}\left(1-\frac{r_{\rm s}}{r}\right)^2 + \frac{r_{\rm s}\dot{x}_i\dot{r}}{r(r-r_{\rm s})} + \frac{r_{\rm s}x_i\dot{r}^2}{2(r-r_{\rm s})r^2} - \frac{r_{\rm s}x_i\dot{\varphi}^2}{r}. \tag{3.19}$$

The exact Schwarzschild expression has one extra term and a missing $3/2$ factor, but apart from that it is the same as the pseudo-Newtonian expression. It is also only slightly more complicated than the PW, NW or Newtonian accelerations, yet it gives exact geodesic motion of test particles in Schwarzschild spacetime!

At the time Paper IV was published, we (much like all the authors before us) had not realised the true meaning of this fact. In the case of a Newtonian SPH code, the acceleration due to the BH is computed for each individual particle, but the expression for the potential is not used in the evolution equations. Of course, Eq. (3.19) does not have an associated "potential", but since that is not used in the code, the Newtonian (or pseudo-Newtonian) forces in the code can be replaced directly with Eq. (3.19), which then yields *exact* geodesic motion for all the SPH particles, at virtually zero additional computational cost. Furthermore, the expression in Eq. (3.19) can be replaced by the full expression in Kerr spacetime (which involves similar, but many more terms, and includes the BH spin; see the Appendix of Paper II). This completely obviates the need to use pseudo-Newtonian potentials (which simply modify the BH acceleration but not the hydrodynamic or self-gravity terms), since the exact acceleration can be used instead.

As a result of this realisation after the publication of Paper IV, we have set out to calculate the Kerr expression, including the hydrodynamics terms and, as best as

possible, self-gravity (which is non-obvious, since the mere notion of "self-gravity" is only an approximation to general relativity), and to test this approach and its applicability to tidal disruptions. This work is presented in Paper II, and in what follows we will summarize the expressions for the hydrodynamic and self-gravity forces.

3.2.2 Hydrodynamics

The Newtonian Euler equation, expressing the conservation of momentum for an ideal fluid and representing the contribution of hydrodynamic (i.e., pressure) forces to the acceleration, is given by

$$\left(\frac{\mathrm{d}^2 x_i}{\mathrm{d}t^2}\right)_{\mathrm{hy,N}} = -\frac{1}{\rho}\frac{\partial P}{\partial x^i}. \tag{3.20}$$

In Sec. 3 of Paper II, the relativistic version of this expression is derived step-by-step, resulting in

$$\left(\frac{\mathrm{d}^2 x^i}{\mathrm{d}t^2}\right)_{\mathrm{hy,rel}} = -\left(g^{i\lambda} - \dot{x}^i g^{0\lambda}\right)\frac{1}{\Gamma^2 \varrho\, \omega}\frac{\partial P}{\partial x^\lambda}. \tag{3.21}$$

The expression is given in coordinate-independent terms, but in order to use it in a code, a particular choice of coordinate system must be done. The two common choices for a Kerr black hole are: the Boyer–Lindquist coordinate system (Boyer & Lindquist, 1967), which is a generalization of the Schwarzschild coordinate system, and the Kerr–Schild coordinate system (Kerr & Schild, 2009). The expression for the hydrodynamic acceleration in the two coordinates are given in Appendices B and C, respectively, of Paper II, and we will not repeat them here. It is, however, instructive to have a look at, e.g., Eq. (C.15), representing the hydrodynamic acceleration in the x-direction in Kerr–Schild coordinates, and analyse its terms and prefactors (we will reproduce Eq. C.15 below to make it easier to follow the discussion; the same exercise could be done for any of the similar expressions in Appendices B and C):

$$\left(\frac{\mathrm{d}^2 x^i}{\mathrm{d}t^2}\right)_{\mathrm{hy,KS}} = -\frac{1}{\Gamma^2 \varrho\, \omega}\left[\frac{\partial P}{\partial x} + \dot{x}\frac{\partial P}{\partial t} + \frac{2Mr}{\rho^2}\left(\dot{x} + \frac{rx + ay}{r^2 + a^2}\right)\mathcal{A}\right], \tag{3.22}$$

where

$$\mathcal{A} = \frac{\partial P}{\partial t} - \frac{\partial P}{\partial x}\left(\frac{rx + ay}{r^2 + a^2}\right) - \frac{\partial P}{\partial y}\left(\frac{ry - ax}{r^2 + a^2}\right) - \frac{\partial P}{\partial z}\frac{z}{r}. \tag{3.23}$$

The prefactor is $-1/\left(\Gamma^2 \rho\omega\right)$, where Γ is the generalized Lorentz factor (which is a straightforward expression in terms of the particle's position and velocity, and the BH mass and spin), ω is the relativistic enthalpy (which is a function of the particle's internal energy, pressure, and density), and ρ is the prefactor for the Newtonian

expression, as shown in Eq. (3.20). The $1/\left(\Gamma^2\omega\right)$ term effectively introduces a gravitational redshift effect close to the BH.

Eq. (3.22) also contains three terms in the square bracket: the first one, $\partial P/\partial x$, is just the Newtonian term from Eq. (3.20). The second one introduces a velocity dependence, while the third and also most complex one contains non-trivial combinations of all the time and spatial derivatives of the pressure and the BH mass and spin, introducing non-linearity in the equation: unlike in the Newtonian case, where the acceleration in the x direction simply depends on the pressure derivative in the x direction, in the Kerr case it depends on all the pressure derivatives (including the time derivative). The Boyer–Lindquist expressions contain similar terms.

An important observation is that in spite of its complexity, Eq. (3.22) can be computed after the Newtonian terms, $\partial_i P/\rho$, are computed. The extra terms and prefactors only require particle properties (such as density, internal energy, velocity, position) and the BH mass and spin, but no interpolated quantities that would need neighbour loops, other than the ones already computed in the Newtonian calculation of the pressure forces. Since the most expensive part of an SPH computation is, by far, the loop over the neighbouring particles (see Gafton & Rosswog, 2011), this means that the computational cost of the additional terms is negligible (as detailed in Sec. 3.2 of Paper II), and that the corrections are virtually a "post-processing" step that can be written as a separate subroutine, and can be turned on or off at will, without modifications to the underlying, Newtonian code.

3.2.3 Self-gravity

As mentioned above, including self-gravity in a relativistic simulation is not an obvious or easy step, since the concept of "self-gravity" is a Newtonian approximation. In principle, a fully consistent general-relativistic code would solve the Einstein equations, and would therefore not need to explicitly include self-gravity. This consistent approach, however, is extremely expensive and, in the case of a TDE, is also numerically very challenging: given the ratio of the SMBH to stellar mass, the star's contribution to the spacetime is but a tiny perturbation on top of the underlying metric; yet on the length scale of the star, it cannot be neglected. In the particular case of partial tidal disruptions, this aspect becomes even more important, as self-gravity is crucial in determining the evolution of the self-bound stellar core as it recedes from the black hole, but if the surviving core is very small it can be an even tinier perturbation on top of of the background metric than in the case of the original star.

Whenever the Einstein equations are *not* solved (e.g., in all the fixed-metric simulations, regardless of how they compute the BH accelerations), self-gravity should be included, and the (mostly tacit) assumption throughout the literature is that Newtonian self-gravity should be used. This is generally acceptable in simulations performed in the rest frame of the star, though only as long as the spacetime can be

considered flat across the space occupied by the star. In Paper II, however, we realised that in a global coordinate system (Kerr–Schild or Boyer–Lindquist), where the hydrodynamic acceleration contains gravitational redshift and non-linear effects, the self-gravity acceleration should be modified in a similar way. This changes Eq. (3.21) to:

$$\left(\frac{\mathrm{d}^2 x^i}{\mathrm{d}t^2}\right)_{\mathrm{hy+sg,rel}} = -\left(g^{i\lambda} - \dot{x}^i g^{0\lambda}\right)\left[\frac{1}{\Gamma^2\omega}\left(\frac{1}{\varrho}\frac{\partial P}{\partial x^\lambda} + \frac{\partial \Phi_{\mathrm{sg}}}{\partial x^\lambda}\right)\right]. \tag{3.24}$$

This, in turn, modifies both Eqs. (3.22) and (3.23) by replacing all occurrences of $\partial_i P/\rho$ by $\partial_i(P/\rho + \Phi_{\mathrm{sg}})$. Obviously, this comes at no additional computational cost, since $\partial_i \Phi_{\mathrm{sg}}$ is already computed in a Newtonian code, and all the relativistic prefactors and terms are already computed for the hydrodynamic forces. It is also worth noting in Eq. (3.24) that, since self-gravity and pressure forces always enter the evolution equation together, hydrostatic equilibrium will be guaranteed as long as the two forces are comparable, and in the regime in which both are much larger than the tidal forces due to the BH. This would not necessarily be the case if the fully relativistic hydrodynamic forces (in particular, with the $1/\Gamma^2\omega$ prefactor) would be used alongside the unmodified Newtonian self-gravity.

3.3 Test results

Apart from the way in which we treat self-gravity, which depends on the particular choice of spatial coordinates – and hence is at odds with general relativity's covariance principle –, our particular implementation of the method also makes a number of assumptions and approximations.

The most important one is discussed in Paper II, and concerns the use of Euclidean distances for the calculation of all inter-particle separations. In an SPH code this distance is critical for building the tree itself (which is then used for computing the hydrodynamic and self-gravity accelerations), and then appears in all of the expressions that contain the SPH kernel or its derivatives, such as those for: gas density, momentum equation, energy equation, artificial viscosity and shock heating terms, and self-gravity acceleration. One could, in principle, also calculate the inter-particle separation via the proper spatial distance using the spatial metric tensor γ_{ij} (rather than the Euclidean, flat-space distance that we are using). This would only be an extra layer of complexity on top of an already approximate method, and we have chosen not to implement it since the effects are likely negligible, as argued in Paper II (although it is not a property of the method itself, but of our implementation).

Similarly, we have chosen to not calculate the time derivative of the self-gravitational potential, which appears in Eqs. (3.22) and (3.23) alongside the time derivative of the pressure, but instead set it to zero. This is technically not correct, but we have not at the time found a way to easily and stably calculate its value, and tests showed

that the contribution of $\dot{\Phi}_{sg}$ does not affect the overall evolution of the system (e.g., in a tidal disruption simulation). This, of course, is a matter of implementation and not a shortcoming of the method itself, and is still much more consistent than to forgo all corrections and use purely Newtonian self-gravity together with relativistic hydrodynamics. In any event, the time derivative of the potential is a negligible contribution when compared to the other terms in Eq. (3.24).

In Paper II, we tested the validity of our approximative approach through a long suite of tests, including comparison with previous results in the literature, and of identical simulations run in both Boyer–Lindquist and Kerr–Schild coordinates, and we found that in all cases it performs extremely well, even for very deep encounters.

4 Results and discussion

There is nothing more deceptive than an obvious fact.
Sherlock Holmes

4.1 Relativistic partial disruptions

In Paper IV, we found that for a given impact parameter β, relativistic effects become increasingly important for larger black hole masses. This was to be expected on analytical grounds (since β is defined in a very simple way, based only on the Newtonian tidal forces), but had not been observed in a systematic numerical study before.

In particular, we found two interesting effects: a) the range of β in which partial disruptions occur is severely diminished as the BH mass increases (since due to relativistic effects the tidal forces increase in strength for a given β); b) the kick velocity increases with the black hole mass, making larger kicks more common than in the Newtonian case, as low-β encounters are statistically more likely than high-β encounters.

The first effect also implies that characterizing the strength of TDEs in terms of β alone is no longer sufficient when relativistic effects are accounted for. Apart from the $r_\mathrm{p}/r_\mathrm{t}$ ratio (related to β), the $r_\mathrm{p}/r_\mathrm{g}$ ratio also becomes important, and it is the (complex) interplay between these two scales that determines the outcome of the disruption. This has an important impact on the ability to extract fit formulae from simulations, or generalize results to encounters with BHs of different masses, as explained in the Appendix A of Paper I.

4.2 Energy distribution after disruption

In Paper I, we found that the energy distribution ($\mathrm{d}M/\mathrm{d}\mathcal{E}$) is not flat around $\mathcal{E} = 0$ (as normally assumed in the literature), except for a narrow range of impact parameters around $\beta \sim 1$ (Fig. 6 in Paper I), when most of the matter resides in the thin and dense tidal bridge. For weaker encounters, when the core of the star survives, $\mathrm{d}M/\mathrm{d}\mathcal{E}$ exhibits a sharp central peak (corresponding to the core) and broad wings (corresponding to the tidal arms) that may evolve at late times under the gravitational

influence of the self-bound core (see, for example, the left panel of Fig. 2.3); for strong disruptions, above $\beta \sim 4$, the logarithmic histogram of $\mathrm{d}M/\mathrm{d}\mathcal{E}$ can be fitted remarkably well by a generalized Gaussian function whose parameters appear to be smooth functions of β, as shown in Appendix A of Paper I.

The spread in orbital mechanical energies, calculated as the standard deviation of the energy distribution, $\sigma_{\mathcal{E}}$, exhibits little variation with β until after $\beta \sim 4$, where it starts approaching the theoretical predictions of the standard frozen-in model, $\sigma_{\mathcal{E}} \propto \beta^2$ (Fig. 7 of Paper I). These results are somewhat in contradiction with those recently presented by Steinberg *et al.* (2019), who found that above $\beta \sim 5$ the spread in energy is nearly insensitive with β. Apart from using very different codes and computing the energy spread in different ways, it is difficult to understand well the origin of this difference, as they do not present histograms of the energy distribution. (Note also the difference between Fig. 7 of Paper I and Fig. 2.4 in this thesis, for which we used the same data but computed the energy spread in two different ways! It is certainly more instructive to look at $\mathrm{d}M/\mathrm{d}\mathcal{E}$ instead of just at the "width" of this distribution, which can be arbitrarily defined.) We strongly emphasize that the energy spread, in itself, does not offer much information about the disruption, in general, or the fallback rate, in particular, unless it is coupled with the (quite erroneous unless $\beta \approx 1$) assumption that the energy distribution is flat.

Concerning the possible relativistic effects on $\mathrm{d}M/\mathrm{d}\mathcal{E}$, for $m_{\mathrm{bh}} = 10^6\, M_\odot$ we did not detect a significant change from the Newtonian picture of the spread or distribution of energies, even for deep encounters. In Sec. 4.5 of Paper I we explained this with an argument first put forward by Servin & Kesden (2017): when comparing Newtonian and relativistic simulations with the same β, there are two competing effects – a relativistic disruption occurs in a steeper potential but higher in the potential well, i.e. further from the black hole – that partially cancel out to yield relatively similar energy distributions and, consequently, return rates. In principle we would expect a bigger difference for larger BH masses, although – given that the two competing effects would still be in play – the answer would best be settled via numerical simulations, which we have not yet performed.

4.3 Relativistic effects

In Paper I, we found that general relativity particularly affects deep encounters, within a few event horizon radii, as follows: the strong (periapsis and nodal) precession creates debris stream geometries impossible to obtain with the Newtonian equations (such as three-dimensional spirals winding multiple times around the black hole, Fig. 4); part of the fluid can be launched on plunging orbits, which reduces the fallback rate and decreases the mass of the resulting accretion disc (by as much as 80 per cent in the deepest encounters with retrograde spin, Fig. 16); a suite of compression and bounce episodes at periapsis in very deep relativistic encounters

(Fig. 2) may generate distinctive X-ray signatures resulting from the associated shock breakout; we also found that disruptions can even occur inside the marginally bound radius, if the enhanced angular momentum spread launches part of the debris on non-plunging orbits (as is the case of all the simulations with $a^\star = -0.99$ and $\beta > 8$).

Perhaps surprisingly, we also found relativistic effects to be important in weak disruptions, where the balance between self-gravity and the tidal force is very close to equilibrium. In this case, the otherwise minor relativistic effects can have decisive consequences on the qualitative outcome of the disruption. This effect is greatly enhanced for larger black hole masses, and perhaps the clearest proof of this was shown in the right panel of Fig. 3 in Paper IV: for $m_{\rm bh} = 4 \times 10^7\, M_\odot$, for instance, the star will be completely disrupted at $\beta \approx 0.72$ in a relativistic simulation, while in the Newtonian picture the limit for disruption is independent of the BH mass.

In between, where the star is fully disrupted but relativistic effects are not extreme, the difference is less conspicuous and resides mostly in a gentler rise of the fallback rate, a later peak and a broader return rate curve, in agreement with the few previous relativistic simulations. However, even in the case of moderately strong encounters, we found that the differential periapsis shift creates much thicker debris streams than in the Newtonian case, both in the bound part (possibly speeding up the circularization) and in the unbound part (speeding up the production of the recombination transient by a factor of two, and enhancing the interaction of the ejecta with the interstellar medium).

4.3.1 Shape of the debris stream

Our simulations produced a large variety of morphological classes for the tidal debris stream, some of which had not been presented in the literature. Based on geometry alone, we find that tidal disruptions may result in seven distinct morphological classes (see Fig. 4.1), as described in Sec. 3.2.2 of Paper I.

At low β, the Newtonian and relativistic encounters are similar, passing progressively through stages A, B, and C; however, in so far as the relativistic encounters are more disruptive in terms of the mass removed from the star, they reach stages B and C at lower impact parameters.

After $\beta \sim 2$ ($r_{\rm p}/r_{\rm g} \approx 23.5$), Newtonian and relativistic encounters become qualitatively different: the Newtonian encounters with $\beta \gtrsim 4$ are similar, resulting in virtually identical airfoil-shaped debris streams that expand adiabatically (type D). For the encounters in Kerr, however, we observe several new morphological classes, all of them ultimately linked to the individual relativistic precession of the fluid elements: up to $\beta \approx 5$, the tidal tails merge into a single, double-triangular shaped stream with no tidal bridge (type E). After that, up until $\beta \approx 9$, the debris takes the shape of a very thick, banana-shaped stream that accretes from its inner part

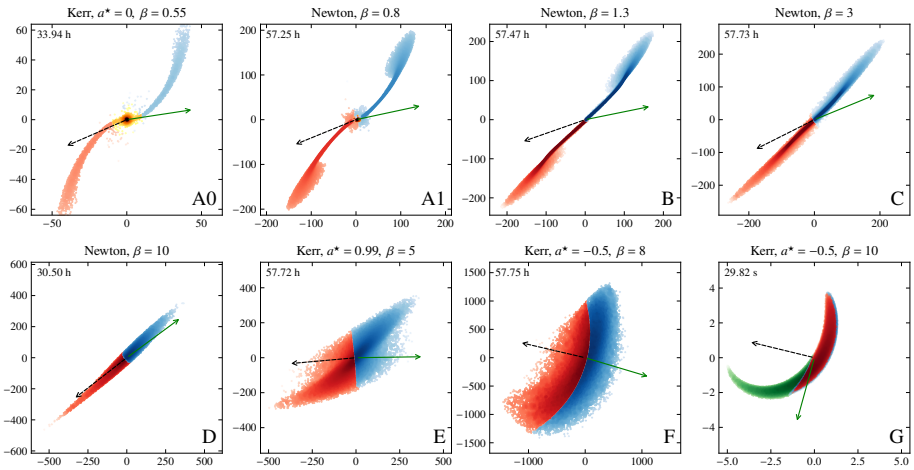

Figure 4.1: Morphological types of debris stream seen in our simulations. The colour coding denotes self-bound (yellow), bound (red), unbound (blue) and plunging (green) particles, with the colour intensity being related to the logarithm of the density. Types E, F and G are only seen in relativistic simulations. The axes are given in units of GM/c^2 and with the origin in the centre of mass of the debris. The dashed black arrow points in the direction of the black hole, while the solid green arrow points in the direction of motion of the centre of mass. This figure was produced by the author, using data from our own simulations, and was included as Fig. 3 in Paper I.

(type F). Above $\beta \sim 9$, the stream becomes a spiral (type G).

For case G, the spiral eventually ends up winding multiple times around the BH (e.g., Fig. 13 in Paper II). The debris stream shown for class G is much thinner than for classes E and F, but note that the time of the snapshot is a mere $\sim$ 30 seconds after the periapsis passage, right before the plunge of the most bound particle into the event horizon, as compared with $\sim$ 57 hours for E and F. The spiral, however, continues to expand because of the differential periapsis shift, and it eventually reaches a comparable width to cases E and F (based on ballistic extrapolation). Running the full simulation, however, would be problematic, due to the imperative of accurately treating the plunge and the second periapsis passage.

We also note that we have found the bound and unbound debris to be mixed (as previously observed in the simulations of Cheng & Bogdanović, 2014), under the action of the different periapsis shifts. This contrasts with the Newtonian case, where the bound and unbound debris are always separated by the initial trajectory of the centre of mass. The effect only appears in very close ($r_\mathrm{p}/r_\mathrm{g} \lesssim 5$) encounters, where a crescent-shape debris stream is formed (as seen before in Laguna *et al.*, 1993; Kobayashi *et al.*, 2004; Cheng & Bogdanović, 2014; Paper II). Due to the same mixing, a significant part of the plunging material (which is marked with green in plot G of Fig. 4.1) may be energetically unbound, invalidating the premise (otherwise

valid for the Newtonian case) that "half" of the debris always escapes. Nevertheless, we observed that the ratio of bound to unbound plunging material is not 1, but ranges from $\sim$ 1.4 (for $a^\star = -0.99$) to $\sim$ 2.3 (for $a^\star = 0.5$). The $a^\star = 0.99$ case produces a negligible amount of plunging material, since the periapsis is furthest from the radius of the marginally bound circular orbit, see Eq. (2.6).

4.3.2 Thickness of the debris stream

We observed that in the Kerr case the debris stream tends to puff up due to both periapsis shift and Lense–Thirring precession, two effects that do not exist in Newtonian simulations. This may have implications on how long such a TDE can avoid detection, as the general prediction is that a thin-enough stream will avoid self-intersection for many orbital periods (Guillochon & Ramirez-Ruiz, 2015).

While reviewing how nodal precession may prevent the self-intersection of the debris stream, Stone *et al.* (2019) pointed out that streams in SPH simulations with adiabatic Equations of State (EOS) tend to puff up quickly due to heating from internal shocks, and quickly circularize, while streams with isothermal EOS tend to remain narrower for a longer time, avoiding circularization for up to 10 orbital periods of the most-bound debris ($T_{\rm min}$, see Eq. 2.23). Based on the typical temperatures, densities and opacities of the bound TDE debris stream, it is unlikely that it could be well described by an isothermal EOS, since it is highly opaque to radiation, as estimated in Sec. 2.3.4. Nevertheless, the concern that SPH simulations tend to produce puffed-up TDE debris streams is valid, and we addressed it in some detail in Sec. 3.2.2 of Paper I, and will reproduce the main points of that discussion here.

In our simulations, since we only treat the first stage of the disruption, internal shocks only occur during the strong compression experienced during the first periapsis passage. In addition, the debris streams we obtain are much narrower in the vertical direction than in the orbital plane (with typical ratios between 10 and 100), and in any case remain much narrower in the Newtonian case than in Kerr (with typical ratios $\sim$ 10 for classes E and F vs class D, see Fig. 4.1), all pointing towards the thickening being a relativistic, rather than hydrodynamic effect.

Still, in order to test numerically that the puffing up is solely the result of geodesic motion, and that hydrodynamic forces do not affect the stream's evolution (at least not before the second periapsis passage), we have also run three control simulations of a complete disruption (Kerr, $a^\star = 0.99$, $\beta = 6$), by taking a snapshot: a) as the star exits the tidal radius after disruption, b) just after the first periapsis passage, and c) as the star enters the tidal radius before disruption, switching off the self-gravity and hydrodynamic forces, and letting the particles evolve on ballistic trajectories alone. The results at the end of the simulations (at the same time as the SPH case, $\approx$ 57 hours after the periapsis passage) are shown in Fig. 5 of Paper I. We observe that cases a) and b) yield similar results, but only case a) is virtually identical to the original

simulation, showing that the constants of motion do evolve for some time after the bounce, but settle in by the time the star exits the tidal radius. The case c) utterly fails to reproduce the geometry of the debris stream, proving that the periapsis passage is crucial in determining how the energy and angular momentum are redistributed, and so the frozen-in model cannot be applied when entering $r_{\rm tid}$ to determine the stream geometry, at least for deep encounters. The results also show that the expansion of the debris stream is due to geodesic motion alone, as even if the constants of motion are frozen at periapsis, the resulting debris stream has a comparable thickness to the one from the full simulation, and is any case much thicker than in the Newtonian case.

4.3.3 Mass return rates and fallback curves

In Fig. 8 of Paper I we presented the fallback rates, $\dot{M}(t)$, for the Newtonian simulations (left panel) and for the Kerr case with $a^\star = 0.5$ (right panel). The procedure for binning the data is discussed at length in Appendix B. The log–log plot is similar to the one presented in Fig. 5 of Guillochon & Ramirez-Ruiz (2013), although the parameter range is now extended to $\beta = 11$. The fact that, up to $\beta \sim 2$, the results match so well the ones from the reference paper is a non-trivial test of both, since the two sets of simulations have been performed with different codes, using different formalisms (high-resolution, grid-based simulations, with a multipole gravity solver, in the rest frame of the star, vs medium-resolution, global, tree-based SPH particle simulation), different ways of setting up the initial conditions and of postprocessing the data, etc. We even reproduced the feature of $\dot{M}_{\rm peak}$ discovered by Guillochon & Ramirez-Ruiz (2013) around $\beta \sim 1$, where the initial trend at low β, towards earlier and higher peaks with increasing β, reverses to later and lower ones. We find, however, that the trend reverses again around $\beta \sim 3$, where the peak starts shifting to significantly higher accretion rates and to earlier times. Our explanation for this behaviour is related to the occurrence of shocks during the periapsis passage, which does not happen at lower β (this was discussed at length in Sec. 4.4 of Paper I).

In Fig. 9 we presented the times of the peak fallback rate $t_{\rm peak}$ and the peak fallback rate $\dot{M}_{\rm peak}$. For $\beta < 2$, the results for the Newtonian simulations are in agreement with Fig. 12 of Guillochon & Ramirez-Ruiz (2013), whose fit curves are overplotted with a dashed purple line. Our results also agree with the $\beta = 1$ tidal disruptions of Cheng & Bogdanović (2014), who concluded that Newtonian rates have a slightly earlier rise, while GR rates exhibit: a more gradual rise, a higher peak, and a later rise above the Eddington luminosity.

In Fig. 11 of the same paper we presented the times of rise from 10% of $\dot{M}_{\rm peak}$ to peak, and of decay from $\dot{M}_{\rm peak}$ back to 10%. This is probably where we notice the biggest difference between relativistic and Newtonian simulations: around $\beta \sim 4$, where the largest differences occur, Newtonian simulations rise to peak a few days

faster, but also decay a few months earlier. These quantities, although not customarily presented in numerical studies of TDEs, may be of interest for the analysis of observational data, as they are a good representation of how broad the fallback curves are, and of how quickly they rise and fall.

4.3.4 Transients from the unbound debris

We note that the relativistic debris in panels E and F in Fig. 4.1 exhibits a considerably larger width than in the Newtonian case, due to the differential periapsis shifts imparted on the different fluid streams during the periapsis passage. The prospect of observing such debris streams are promising: the unbound material keeps expanding and cooling adiabatically, generating an optical transient from hydrogen recombination (Kasen & Ramirez-Ruiz, 2010). It would be plausible to make the assumption that the axis ratio of the debris in the orbital plane, in the presence of strong periapsis shift, is of the order of $\sim$ 1, as can be seen in classes E and F, instead of $\sim$ 10, as was assumed by Kasen & Ramirez-Ruiz (2010), and which is in agreement with our Newtonian simulations represented by class D. In this case, both the expansion time t_e, defined by Kasen & Ramirez-Ruiz (2010) in their Eq. (8) as scaling with $\propto E_t^{1/3}$, and the time at which the transient is expected to occur, t_t, given in their Eq. (19) with the same scaling, would be reduced by a factor of ~ 2. In order to test this, we extract the times at which the mean and the maximum temperatures of the debris stream drop below 10^4 K in two simulations with $\beta = 6$ (Newtonian and Kerr with $a^\star = 0$). For the mean temperatures, we find the Newtonian time to be $\sim$ 24 hr, compared to $\sim$ 8.8 hr for Kerr, representing a speed-up of $\sim$ 2.7, in agreement with our very simple order-of-magnitude analytical estimate. If, instead, we consider the maximum temperature, the contrast is much larger: in the Newtonian case, the maximum temperature, in the very centre of the debris stream, only drops below 10^4 K in $\sim$ 160 days, while in the Kerr case it takes merely $\sim$ 1.5 days, representing a speed-up of more than 10^2. In any case, both effects are greatly diminished for $\beta \lesssim 3$, where the periapsis shift is not strong enough to generate the $\sim$ 1:1 aspect ratio of the debris in the orbital plane.

Another scenario is the production of a γ-ray afterglow following the collision of the expanding debris with molecular clouds (Chen *et al.*, 2016). The effect of relativistic periapsis shift is to significantly increase the solid angle of the unbound ejecta, reducing the time it takes to end the free expansion and begin the Sedov-like phase, as predicted by Khokhlov & Melia (1996) though never followed-up with three-dimensional relativistic simulations.

4.3.5 Circularization

In Paper III we have studied the disruption, fallback and circularization of a red dwarf ($m_\star = 0.1\,M_\odot$, $r_\star = 0.15\,R_\odot$) in an elliptical ($e = 0.97$) orbit around

a $10^5\,M_\odot$ black hole. The somewhat improbable set of parameters was chosen to alleviate the computational burden, as discussed in Sec. 3.1.3 and as often employed in the literature. We ran the first part of the simulation, up to the second periapsis passage, with the relativistic SPH code presented in Paper II, then followed the fall-back and circularization with a grid-based, GR-MHD code employing a fixed Kerr metric (although, for simplicity, we only considered a non-rotating black hole).

In this study we observed the formation of a self-crossing shock that drives a quasi-spherical outflow of hot, optically thick gas carrying significant kinetic energy. The transfer of energy from the head of the stream to its tail generates a feedback loop with a Keplerian period, modulating the dissipation in the self-crossing shock. The rotating disc that forms is thick and highly turbulent, close to marginally bound (and thus well approximated by a zero-Bernoulli accretion flow), and remains turbulent for many dynamical time scales. We found the influence of magnetic fields to be negligible, since hydrodynamic turbulent viscosity completely dominates over the viscosity mediated by magnetic fields. Finally, the estimated luminosity expected to reach an observer is modest, both from the energetic outflow and from the bound debris falling back on to the BH.

4.4 Further work

The numerical tool that we have contributed to as part of the work for this thesis (Paper II) seems well-suited for tackling a broad range of problems, including tidal disruptions and compact binary mergers. Some foreseeable improvements would be:

a) to use a more modern SPH formulation, including a better kernel with a higher number of neighbours, and more accurate kernel derivatives (Rosswog, 2015);

b) to improve the formulation of the artificial viscosity term, for instance by making it trigger on the time derivative of $\nabla \cdot \boldsymbol{v}$ instead of on $\nabla \cdot \boldsymbol{v}$ itself, which may be too dissipative in strong compression without a shock (e.g., Cullen & Dehnen, 2010);

c) to include, in a numerically stable way, the time derivative of the self-gravitational potential $\partial_t \Phi_{\rm sg}$ in Eq. (3.24);

d) to use a faster, MPI-parallel tree (Gafton & Rosswog, 2011), as this will significantly increase the performance and allow us to incorporate the last and most important improvement:

e) to keep increasing the number of particles. While SPH is truly remarkable in its ability to capture the dynamics of a system with an extremely low resolution[8], it benefits tremendously from a (much) higher number of particles in resolving the small-scale thermodynamic evolution of the fluid.

[8] The first SPH simulations in the 1970s (Lucy, 1977; Gingold & Monaghan, 1977) used less than 100 particles, and the first relativistic simulations in the 1990s (Laguna *et al.*, 1993) used 3000 particles, yet they accurately reproduced the stellar structure and dynamical evolution to within a few per cent.

Bibliography

Abramowicz, M.A. (2009). *The Paczyński–Wiita potential. A step-by-step "derivation"*. A&A **500**, 213, doi: 10.1051/0004-6361/200912155. 50

Abramowicz, M.A., Czerny, B., Lasota, J.P. *et al.* (1988). *Slim accretion disks*. ApJ **332**, 646, doi: 10.1086/166683. 4

Alexander, T. (1999). *The distribution of stars near the supermassive black hole in the Galactic center*. ApJ **527**, 835, doi: 10.1086/308129. 28

Alexander, T. (2003). *Stars and singularities: stellar phenomena near a massive black hole*, 246–275. arXiv: astro-ph/0202242. 3, 36

Alexander, T. (2005). *Stellar processes near the massive black hole in the Galactic center*. Physics Reports **419**, 65, doi: 10.1016/j.physrep.2005.08.002. 35, 41

Alexander, T. (2012). *Stellar dynamics and tidal disruption events in galactic nuclei*. EPJ Web of Conferences **39**, 05001, doi: 10.1051/epjconf/20123905001. 10

Alexander, T. & Hopman, C. (2009). *Strong mass segregation around a massive black hole*. ApJ **697**, 1861, doi: 10.1088/0004-637X/697/2/1861. 36

Alexander, T. & Kumar, P. (2001). *Tidal spin-up of stars in dense stellar cusps around massive black holes*. ApJ **549**, 948, doi: 10.1086/319436. 38

Alexander, T. & Livio, M. (2001). *Tidal scattering of stars on supermassive black holes in galactic centers*. ApJL **560**, L143, doi: 10.1086/324324. 11

Alexander, T. & Morris, M. (2003). *Squeezars: tidally powered stars orbiting a massive black hole*. ApJL **590**, L25, doi: 10.1086/376671. 13

Angélil, R. & Saha, P. (2011). *Galactic-center S stars as a prospective test of the Einstein equivalence principle*. ApJL **734**, L19, doi: 10.1088/2041-8205/734/1/L19. 38

Antonini, F., Faber, J., Gualandris, A. *et al.* (2010). *Tidal breakup of binary stars at the galactic center and its consequences*. ApJ **713**, 90, doi: 10.1088/0004-637X/713/1/90. 6

Atkinson, J.W., Collett, J.L., Marconi, A. *et al.* (2005). *Supermassive black hole mass measurements for NGC 1300 and 2748 based on Hubble Space Telescope emission-line gas kinematics*. MNRAS **359**, 504, doi: 10.1111/j.1365-2966.2005.08904.x. 4

Ayal, S., Livio, M. & Piran, T. (2000). *Tidal disruption of a solar-type star by a supermassive black hole*. ApJ **545**, 772, doi: 10.1086/317835. 23, 49

Ayal, S., Piran, T., Oechslin, R. *et al.* (2001). *Post–Newtonian smoothed particle hydrodynamics*. ApJ **550**, 846, doi: 10.1086/319769. 49

Bahcall, J.N. & Wolf, R.A. (1976). *Star distribution around a massive black hole in a globular cluster*. ApJ **209**, 214, doi: 10.1086/154711. 27

Bahcall, J.N. & Wolf, R.A. (1977). *The star distribution around a massive black hole in a globular cluster. II. Unequal star masses*. ApJ **216**, 883, doi: 10.1086/155534. 27

Bardeen, J.M., Press, W.H. & Teukolsky, S.A. (1972). *Rotating Black Holes: Locally Nonrotating Frames, Energy Extraction, and Scalar Synchrotron Radiation*. ApJ **178**, 347, doi: 10.1086/151796. 8

Beifiori, A., Courteau, S., Corsini, E.M. *et al.* (2012). *On the correlations between galaxy properties and supermassive black hole mass*. MNRAS **419**, 2497, doi: 10.1111/j.1365-2966.2011.19903.x. arXiv: 1109.6265. xv, 5

Beloborodov, A.M., Illarionov, A.F., Ivanov, P.B. *et al.* (1992). *Angular momentum of a supermassive black hole in a dense star cluster*. MNRAS **259**, 209, doi: 10.1093/mnras/259.2.209. 11

Bender, R., Kormendy, J., Bower, G. *et al.* (2005). *HST STIS spectroscopy of the triple nucleus of M31: two nested disks in Keplerian rotation around a supermassive black hole*. ApJ **631**, 280, doi: 10.1086/432434. 1

Binney, J. & Tremaine, S. (2008). *Galactic dynamics*. Princeton University Press, USA, 2nd edition edition. ads: 20008gady.book.....b08. 9, 30, 33, 34

Blaauw, A. (1961). *On the origin of the O- and B-type stars with high velocities (the "run-away" stars), and some related problems*. Bulletin Astron. Inst. Netherlands **15**, 265. ads: 1961ban....15..265b. 6

Bonnerot, C., Rossi, E.M., Lodato, G. *et al.* (2015). *Disc formation from stellar tidal disruptions*. ArXiv, arXiv: 1501.04635. 48, 49

Bonning, E.W., Cheng, L., Shields, G.A. *et al.* (2007). *Accretion disk temperatures and continuum colors in QSOs*. ApJ **659**, 211, doi: 10.1086/510712. 26

Boyer, R.H. & Lindquist, R.W. (1967). *Maximal Analytic Extension of the Kerr Metric*. Journal of Mathematical Physics **8**, 265, doi: 10.1063/1.1705193. 52

Brockamp, M., Baumgardt, H. & Kroupa, P. (2011). *Tidal disruption rate of stars by supermassive black holes obtained by direct N-body simulations*. MNRAS **418**, 1308, doi: 10.1111/j.1365-2966.2011.19580.x. 3, 28

Bromley, B.C., Kenyon, S.J., Geller, M.J. *et al.* (2012). *Binary disruption by massive black holes: hypervelocity stars, S stars, and tidal disruption events*. ApJ **749**, L42, doi: 10.1088/2041-8205/749/2/L42. 6

Burger, P. & Lamers, H.J.G.L.M. (1989). *Analytical expressions for the Rosseland-mean opacity and electron scattering in stellar atmospheres*. A&A **218**, 161. ads: 1989A%26A...218..161B. 27

Burkert, A. & Tremaine, S. (2010). *A correlation between central supermassive black holes and the globular cluster systems of early-type galaxies*. ApJ **720**, 516, doi: 10.1088/0004-637X/720/1/516. 5

Carter, B. & Luminet, J.P. (1983). *Tidal compression of a star by a large black hole. I. Mechanical evolution and nuclear energy release by proton capture*. A&A **121**, 97. ads: 1983A&A...121...97C. 12

Carter, B. & Luminet, J.P. (1985). *Mechanics of the affine star model*. MNRAS **212**, 23. ads: 1985mnras.212...23c. 12

Castelvecchi, D. (2019). *Gravitational waves hint at detection of black hole eating star*. Nature **569**, 15, doi: 10.1038/d41586-019-01377-2. 37

Chanamé, J., Gould, A. & Miralda-Escudé, J. (2001). *Microlensing by stellar black holes around Sagittarius A**. ApJ **563**, 793, doi: 10.1086/323986. 36

Chen, X., Gómez-Vargas, G.A. & Guillochon, J. (2016). *The γ-ray afterglows of tidal disruption events*. MNRAS **458**, 3314, doi: 10.1093/mnras/stw437. arXiv: 1512.06124. 63

Chen, X. & Liu, F.K. (2013). *Is there an intermediate massive black hole in the Galactic center: imprints on the stellar tidal-disruption rate*. ApJ **762**, 95, doi: 10.1088/0004-637X/762/2/95. 3

Chen, X., Madau, P., Sesana, A. *et al.* (2009). *Enhanced tidal disruption rates from massive black hole binaries*. ApJL **697**, L149, doi: 10.1088/0004-637X/697/2/L149. 6

Cheng, R.M. & Bogdanović, T. (2014). *Tidal disruption of a star in the Schwarzschild spacetime: Relativistic effects in the return rate of debris*. Phys. Rev. D **90**, 064020, doi: 10.1103/PhysRevD.90.064020. arXiv: 1407.3266. 60, 62

Clausius, R. (1870). *On a mechanical theorem applicable to heat*. Philosophical Magazine Series 4 **40**, 122, doi: 10.1080/14786447008640370. 37

Cohn, H. & Kulsrud, R.M. (1978). *The stellar distribution around a black hole - Numerical integration of the Fokker-Planck equation*. ApJ **226**, 1087, doi: 10.1086/156685. 29

Courant, R., Friedrichs, K. & Lewy, H. (1928). *Über die partiellen Differenzengleichungen der mathematischen Physik*. Mathematische Annalen **100**, 32, doi: 10.1007/BF01448839. 45

Cuadra, J., Nayakshin, S., Springel, V. *et al.* (2006). *Galactic centre stellar winds and Sgr A* accretion*. MNRAS **366**, 358, doi: 10.1111/j.1365-2966.2005.09837.x. 2

Cullen, L. & Dehnen, W. (2010). *Inviscid smoothed particle hydrodynamics*. MNRAS **408**, 669, doi: 10.1111/j.1365-2966.2010.17158.x. arXiv: 1006.1524. 64

De Colle, F., Guillochon, J., Naiman, J. *et al.* (2012a). *The dynamics, appearance, and demographics of relativistic jets triggered by tidal disruption of stars in quiescent supermassive black holes*. ApJ **760**, 103, doi: 10.1088/0004-637X/760/2/103. 36

Deegan, P. & Nayakshin, S. (2007). *Constraining the number of compact remnants near Sgr A**. MNRAS **377**, 897, doi: 10.1111/j.1365-2966.2007.11659.x. 36

Dehnen, W. & Aly, H. (2012). *Improving convergence in smoothed particle hydrodynamics simulations without pairing instability*. MNRAS **425**, 1068, doi: 10.1111/j.1365-2966.2012.21439.x. arXiv: 1204.2471. 45

Di Matteo, T., Springel, V. & Hernquist, L. (2005). *Energy input from quasars regulates the growth and activity of black holes and their host galaxies*. Nature **433**, 604, doi: 10.1038/nature03335. 6

Diener, P., Kosovichev, A.G., Kotok, E.V. *et al.* (1995). *Non-linear effects at tidal capture of stars by a massive black hole - II. Compressible affine models and tidal interaction after capture*. MNRAS **275**, 498, doi: 10.1093/mnras/275.2.498. 10, 12

Donley, J.L., Brandt, W.N., Eracleous, M. *et al.* (2002). *Large-amplitude X-ray outbursts from galactic nuclei: a systematic survey using ROSAT archival data*. AJ **124**, 1308, doi: 10.1086/342280. 3

East, W.E. (2014). *Gravitational Waves from the Collision of Tidally Disrupted Stars with Massive Black Holes*. ApJ **795**, 135, doi: 10.1088/0004-637X/795/2/135. arXiv: 1408.1695. 49

Eatough, R.P., Kramer, M., Klein, B. *et al.* (2013). *Can we see pulsars around Sgr A*? The latest searches with the Effelsberg telescope.* In *IAU Symposium*, volume 291 of *IAU Symposium*, 382–384. doi: 10.1017/S1743921312024209. 37

Eckart, A. & Genzel, R. (1996). *Observations of stellar proper motions near the Galactic centre*. Nature **383**, 415, doi: 10.1038/383415a0. 35

Eddington, A.S. (1921). *Das Strahlungsgleichgewicht der Sterne*. Zeitschrift für Physik **7**, 351, doi: 10.1007/BF01332806. 24

Eisenhauer, F., Genzel, R., Alexander, T. *et al.* (2005). *SINFONI in the Galactic center: young stars and infrared flares in the central light-month*. ApJ **628**, 246, doi: 10.1086/430667. 6

Eisenhauer, F., Schödel, R., Genzel, R. *et al.* (2003). *A Geometric Determination of the Distance to the Galactic Center*. ApJL **597**, L121, doi: 10.1086/380188. 7

Esin, A.A., McClintock, J.E. & Narayan, R. (1997). *Advection-dominated accretion and the spectral states of black hole X-ray binaries: application to Nova MUSCAE 1991*. ApJ **489**, 865, doi: 10.1086/304829. 5

Evans, C.R. & Kochanek, C.S. (1989). *The tidal disruption of a star by a massive black hole*. ApJ **346**, L13, doi: 10.1086/185567. 23, 24

Event Horizon Telescope Collaboration, Akiyama, K., Alberdi, A. *et al.* (2019). *First M87 Event Horizon Telescope Results. I. The Shadow of the Supermassive Black Hole*. ApJL **875**, L1, doi: 10.3847/2041-8213/ab0ec7. arXiv: 1906.11238. 1

Faber, S.M., Tremaine, S., Ajhar, E.A. *et al.* (1997). *The centers of early-type galaxies with HST. IV. Central parameter relations*. AJ **114**, 1771, doi: 10.1086/118606. 5

Faucher-Giguère, C.A. & Loeb, A. (2011). *Pulsar-black hole binaries in the Galactic centre*. MNRAS **415**, 3951, doi: 10.1111/j.1365-2966.2011.19019.x. 37

Ferrarese, L. & Ford, H. (2005). *Supermassive black holes in galactic nuclei: past, present and future research*. Space Science Reviews **116**, 523, doi: 10.1007/s11214-005-3947-6. 5

Ferrarese, L. & Merritt, D. (2000). *A fundamental relation between supermassive black holes and their host galaxies*. ApJL **539**, L9, doi: 10.1086/312838. 5

Frank, J. (1978). *Tidal disruption by a massive black hole and collisions in galactic nuclei*. MNRAS **184**, 87. ads: 1978mnras.184...87f. 2

Frank, J., King, A. & Raine, D.J. (2002). *Accretion power in astrophysics*. Cambridge University Press, UK, 3rd edition edition. ads: http://adsabs.harvard.edu/abs/2002apa..book.....F. 4

Frank, J. & Rees, M.J. (1976). *Effects of massive central black holes on dense stellar systems*. MNRAS **176**, 633. ads: 1976mnras.176..633f. 2, 6, 28, 29

Frolov, V.P. & Novikov, I.D. (1998). *Black Hole Physics: Basic Concepts and New Developments*. Kluwer Academic. 8

Gafton, E. & Rosswog, S. (2011). *A fast recursive coordinate bisection tree for neighbour search and gravity*. MNRAS **418**, 770, doi: 10.1111/j.1365-2966.2011.19528.x. arXiv: 1108.0028. 53, 64

Garcia, M.R., Hextall, R., Baganoff, F.K. *et al.* (2010). *X-ray and radio variability of M31*, the Andromeda galaxy nuclear supermassive black hole*. ApJ **710**, 755, doi: 10.1088/0004-637X/710/1/755. 1, 2

García-Senz, D., Cabezón, R.M. & Escartín, J.A. (2012). *Improving smoothed particle hydrodynamics with an integral approach to calculating gradients*. A&A **538**, A9, doi: 10.1051/0004-6361/201117939. arXiv: 1111.3261. 45

Gebhardt, K., Bender, R., Bower, G. *et al.* (2000). *A relationship between nuclear black hole mass and galaxy velocity dispersion*. ApJ **539**, L13, doi: 10.1086/312840. 4, 5

Genzel, R., Eisenhauer, F. & Gillessen, S. (2010). *The Galactic center massive black hole and nuclear star cluster*. Rev. Mod. Phys. **82**, 3121, doi: 10.1103/RevModPhys.82.3121. 1, 3

Genzel, R., Pichon, C., Eckart, A. *et al.* (2000). *Stellar dynamics in the Galactic centre: proper motions and anisotropy*. MNRAS **317**, 348, doi: 10.1046/j.1365-8711.2000.03582.x. 35

Genzel, R., Schödel, R., Ott, T. *et al.* (2003). *The stellar cusp around the supermassive black hole in the Galactic center*. ApJ **594**, 812, doi: 10.1086/377127. 28, 35

Genzel, R., Thatte, N., Krabbe, A. *et al.* (1996). *The dark mass concentration in the central parsec of the Milky Way*. ApJ **472**, 153, doi: 10.1086/178051. 35

Ghez, A.M., Klein, B.L., Morris, M. *et al.* (1998). *High proper-motion stars in the vicinity of Sagittarius A*: evidence for a supermassive black hole at the center of our Galaxy*. ApJ **509**, 678, doi: 10.1086/306528. 35

Ghez, A.M., Salim, S., Weinberg, N.N. *et al.* (2008). *Measuring distance and properties of the Milky Way's central supermassive black hole with stellar orbits*. ApJ **689**, 1044, doi: 10.1086/592738. 1, 2, 3, 35

Gillessen, S., Eisenhauer, F., Fritz, T.K. *et al.* (2009a). *The orbit of the star S2 around Sgr A* from Very Large Telescope and Keck data*. ApJ **707**, L114, doi: 10.1088/0004-637X/707/2/L114. 3

Gillessen, S., Eisenhauer, F., Trippe, S. *et al.* (2009b). *Monitoring stellar orbits around the massive black hole in the Galactic center*. ApJ **692**, 1075, doi: 10.1088/0004-637X/692/2/1075. 6, 35

Gingold, R.A. & Monaghan, J.J. (1977). *Smoothed particle hydrodynamics - Theory and application to non-spherical stars*. MNRAS **181**, 375. 64

Greene, J.E., Peng, C.Y., Kim, M. *et al.* (2010). *Precise black hole masses from megamaser disks: black hole–bulge relations at low mass*. ApJ **721**, 26, doi: 10.1088/0004-637X/721/1/26. 4

Guillochon, J. & Ramirez-Ruiz, E. (2013). *Hydrodynamical simulations to determine the feeding rate of black holes by the tidal disruption of stars: The importance of the impact parameter and stellar structure*. ApJ **767**, 25, doi: 10.1088/0004-637X/767/1/25. 10, 12, 48, 62

Guillochon, J. & Ramirez-Ruiz, E. (2015). *A Dark Year for Tidal Disruption Events*. ArXiv, arXiv: 1501.05306. 40, 61

Guillochon, J., Ramirez-Ruiz, E., Rosswog, S. *et al.* (2009). *Three-dimensional simulations of tidally disrupted solar-type stars and the observational signatures of shock breakout*. ApJ **705**, 844, doi: 10.1088/0004-637X/705/1/844. 48

Hamilton, D.P. & Burns, J.A. (1991). *Orbital stability zones about asteroids*. Icarus **92**, 118, doi: 10.1016/0019-1035(91)90039-V. 18

Hamilton, D.P. & Burns, J.A. (1992). *Orbital stability zones about asteroids. II - The destabilizing effects of eccentric orbits and of solar radiation*. Icarus **96**, 43, doi: 10.1016/0019-1035(92)90005-R. 18

Häring, N. & Rix, H.W. (2004). *On the black hole mass-bulge mass relation*. ApJ **604**, L89, doi: 10.1086/383567. 5

Hayasaki, K., Stone, N. & Loeb, A. (2012). *Tidal disruption flares from stars on eccentric orbits*. In *European Physical Journal Web of Conferences*, volume 39 of *European Physical Journal Web of Conferences*, 1004. doi: 10.1051/epjconf/20123901004. 25, 26

Hayasaki, K., Stone, N. & Loeb, A. (2013). *Finite, intense accretion bursts from tidal disruption of stars on bound orbits*. MNRAS **434**, 909, doi: 10.1093/mnras/stt871. arXiv: 1210.1333. 40, 49

Hayasaki, K., Stone, N.C. & Loeb, A. (2015). *Circularization of Tidally Disrupted Stars around Spinning Supermassive Black Holes*. ArXiv, arXiv: 1501.05207. 48, 49

Hills, J.G. (1975). *Possible power source of Seyfert galaxies and QSOs*. Nature **254**, 295, doi: 10.1038/254295a0. 2

Ho, L.C. (2008). *Nuclear activity in nearby galaxies*. Annual Review of Astronomy and Astrophysics **46**, 475, doi: 10.1146/annurev.astro.45.051806.110546. 1

Hopkins, P.F. (2013). *A general class of Lagrangian smoothed particle hydrodynamics methods and implications for fluid mixing problems*. MNRAS **428**, 2840, doi: 10.1093/mnras/sts210. arXiv: 1206.5006. 44

Hopkins, P.F. & Hernquist, L. (2010). *A non-parametric estimate of mass 'scoured' in galaxy cores*. MNRAS **407**, 447, doi: 10.1111/j.1365-2966.2010.16915.x. 5

Hunter, J.D. (2007). *Matplotlib: A 2D Graphics Environment*. Comput. Sci. Eng. **9**, 90, doi: 10.1109/MCSE.2007.55. 75

Jones, E., Oliphant, T., Peterson, P. *et al.* (2001). *SciPy: Open source scientific tools for Python*. 75

Kasen, D. & Ramirez-Ruiz, E. (2010). *Optical transients from the unbound debris of tidal disruption*. ApJ **714**, 155, doi: 10.1088/0004-637X/714/1/155. 14, 63

Kennea, J.A., Burrows, D.N., Kouveliotou, C. *et al.* (2013). *Swift Discovery of a New Soft Gamma Repeater, SGR J1745-29, near Sagittarius A**. ApJL **770**, L24, doi: 10.1088/2041-8205/770/2/L24. arXiv: 1305.2128. 37

Kerr, R.P. & Schild, A. (2009). *Republication of: A new class of vacuum solutions of the Einstein field equations*. General Relativity and Gravitation **41**, 2485, doi: 10.1007/s10714-009-0857-z. 52

Khokhlov, A. & Melia, F. (1996). *Powerful Ejection of Matter from Tidally Disrupted Stars near Massive Black Holes and a Possible Application to Sagittarius A East*. ApJL **457**, L61, doi: 10.1086/309895. 63

King, A.R. & Pounds, K.A. (2003). *Black hole winds*. MNRAS **345**, 657, doi: 10.1046/j.1365-8711.2003.06980.x. 4

Kobayashi, S., Laguna, P., Phinney, E.S. *et al.* (2004). *Gravitational waves and X-ray signals from stellar disruption by a massive black hole*. ApJ **615**, 855, doi: 10.1086/424684. 11, 60

Kochanek, C.S. (1994). *The aftermath of tidal disruption: The dynamics of thin gas streams*. ApJ **422**, 508, doi: 10.1086/173745. 14

Kollmeier, J.A., Onken, C.A., Kochanek, C.S. *et al.* (2006). *Black hole masses and Eddington ratios at* $0.3 < z < 4$. ApJ **648**, 128, doi: 10.1086/505646. 5

Kormendy, J. & Bender, R. (1999). *The double nucleus and central black hole of M31*. ApJ **522**, 772, doi: 10.1086/307665. 1

Kormendy, J. & Richstone, D. (1995). *Inward bound – The search for supermassive black holes in galactic nuclei*. ARA&A **33**, 581, doi: 10.1146/annurev.aa.33.090195.003053. 1, 5

Krolik, J.H. (1999). *Active galactic nuclei: from the central black hole to the galactic environment*. Princeton University Press, USA. ads: http://adsabs.harvard.edu/abs/1999agnc.book.....K. 4

Lacy, J.H., Townes, C.H. & Hollenbach, D.J. (1982). *The nature of the central parsec of the Galaxy*. ApJ **262**, 120, doi: 10.1086/160402. 3, 14

Laguna, P., Miller, W.A., Zurek, W.H. *et al.* (1993). *Tidal disruptions by supermassive black holes - Hydrodynamic evolution of stars on a Schwarzschild background*. ApJ **410**, L83, doi: 10.1086/186885. 60, 64

Landt, H., Ward, M.J., Peterson, B.M. *et al.* (2013). *A near-infrared relationship for estimating black hole masses in active galactic nuclei*. MNRAS **432**, 113, doi: 10.1093/mnras/stt421. 4

Law-Smith, J., Guillochon, J. & Ramirez-Ruiz, E. (2019). *The Tidal Disruption of Sun-like Stars by Massive Black Holes*. arXiv e-prints arXiv:1907.04859. arXiv: 1907.04859. 13

Lazio, T.J.W., Cordes, J.M., Lang, C.C. *et al.* (2003). *Radio pulsars in the Galactic center*. Astronomische Nachrichten Supplement **324**, 333, doi: 10.1002/asna.200385106. 37

Lense, J. & Thirring, H. (1918). *Über den Einfluß der Eigenrotation der Zentralkörper auf die Bewegung der Planeten und Monde nach der Einsteinschen Gravitationstheorie*. Physikalische Zeitschrift **19**, 156. ads: 1918PhyZ...19..156L. 38, 40

Li, G. & Loeb, A. (2013). *Accumulated tidal heating of stars over multiple pericentre passages near Sgr A**. MNRAS **429**, 3040, doi: 10.1093/mnras/sts567. 11

Li, Z., Garcia, M.R., Forman, W.R. *et al.* (2011). *The murmur of the hidden monster: Chandra's decadal view of the supermassive black hole in M31*. ApJ **728**, L10, doi: 10.1088/2041-8205/728/1/L10. 2

Lidskii, V.V. & Ozernoi, L.M. (1979). *Tidal triggering of stellar flares by a massive black hole*. Soviet Astronomy Letters **5**, 16. ads: 1979SvAL....5...16L. 2

Lightman, A.P. & Shapiro, S.L. (1977). *The distribution and consumption rate of stars around a massive, collapsed object*. ApJ **211**, 244, doi: 10.1086/154925. 28, 30, 31, 34

Liu, K., Wex, N., Kramer, M. *et al.* (2012). *Prospects for probing the spacetime of Sgr A* with pulsars*. ApJ **747**, 1, doi: 10.1088/0004-637X/747/1/1. 37

Lodato, G., King, A.R. & Pringle, J.E. (2009). *Stellar disruption by a supermassive black hole: is the light curve really proportional to $t^{5/3}$?* MNRAS **392**, 332, doi: 10.1111/j.1365-2966.2008.14049.x. 25

Lodato, G. & Rossi, E.M. (2011). *Multiband light curves of tidal disruption events*. MNRAS **410**, 359, doi: 10.1111/j.1365-2966.2010.17448.x. 14

Loeb, A. & Ulmer, A. (1997). *Optical appearance of the debris of a star disrupted by a massive black hole*. ApJ **489**, 573, doi: 10.1086/304814. 27

Lucy, L.B. (1977). *A numerical approach to the testing of the fission hypothesis*. AJ **82**, 1013, doi: 10.1086/112164. 64

Luminet, J.P. & Carter, B. (1986). *Dynamics of an affine star model in a black hole tidal field*. ApJS **61**, 219, doi: 10.1086/191113. 10

Lynden-Bell, D. (1969). *Galactic nuclei as collapsed old quasars*. Nature **223**, 690, doi: 10.1038/223690a0. 1

MacLeod, M., Guillochon, J. & Ramirez-Ruiz, E. (2012). *The tidal disruption of giant stars and their contribution to the flaring supermassive black hole population*. ApJ **757**, 134, doi: 10.1088/0004-637X/757/2/134. xvi, 13

Madigan, A.M., Hopman, C. & Levin, Y. (2011). *Secular stellar dynamics near a massive black hole*. ApJ **738**, 99, doi: 10.1088/0004-637X/738/1/99. 6

Maggiore, M. (2007). *Gravitational Waves: Volume 1: Theory and Experiments*. Gravitational Waves. Oxford: OUP. 38

Magorrian, J. & Tremaine, S. (1999). *Rates of tidal disruption of stars by massive central black holes*. MNRAS **309**, 447, doi: 10.1046/j.1365-8711.1999.02853.x. 3, 6, 11, 28, 31, 32, 33

Magorrian, J., Tremaine, S., Richstone, D. *et al.* (1998). *The demography of massive dark objects in galaxy centers*. AJ **115**, 2285, doi: 10.1086/300353. 5, 28

Mainetti, D., Lupi, A., Campana, S. *et al.* (2017). *The fine line between total and partial tidal disruption events*. A&A **600**, A124, doi: 10.1051/0004-6361/201630092. arXiv: 1702.07730. 12

van der Marel, R.P., de Zeeuw, P.T., Rix, H.W. *et al.* (1997). *A massive black hole at the centre of the quiescent galaxy M32*. Nature **385**, 610, doi: 10.1038/385610a0. 1

Menou, K. & Quataert, E. (2001). *Activity From Tidal Disruptions in Galactic Nuclei*. ApJL **562**, L137, doi: 10.1086/338195. 1

Merritt, D. (2013). *Loss-cone dynamics*. Classical and Quantum Gravity **30**, 244005, doi: 10.1088/0264-9381/30/24/244005. arXiv: 1307.3268. xvii, 29

Merritt, D., Alexander, T., Mikkola, S. *et al.* (2010). *Testing properties of the Galactic center black hole using stellar orbits*. Phys. Rev. D **81**, 062002, doi: 10.1103/PhysRevD.81.062002. 38

Merritt, D., Berczik, P. & Laun, F. (2007). *Brownian motion of black holes in dense nuclei*. AJ **133**, 553, doi: 10.1086/510294. 11

Merritt, D. & Poon, M.Y. (2004). *Chaotic loss cones and black hole fueling*. ApJ **606**, 788, doi: 10.1086/382497. 6

Meyer, L., Ghez, A.M., Schödel, R. *et al.* (2012). *The shortest-known-period star orbiting our galaxy's supermassive black hole*. Science **338**, 84, doi: 10.1126/science.1225506. 35

Miller, M.C., Freitag, M., Hamilton, D.P. *et al.* (2005). *Binary encounters with supermassive black holes: Zero-eccentricity LISA Events*. ApJ **631**, L117, doi: 10.1086/497335. 17, 18

Milosavljević, M., Merritt, D. & Ho, L.C. (2006). *Contribution of stellar tidal disruptions to the X-ray luminosity function of active galaxies*. ApJ **652**, 120, doi: 10.1086/508134. 4

Miralda-Escudé, J. & Gould, A. (2000). *A cluster of black holes at the Galactic center*. ApJ **545**, 847, doi: 10.1086/317837. 3, 36, 37

Miralda-Escudé, J. & Kollmeier, J.A. (2005). *Star captures by quasar accretion disks: A possible explanation of the M–σ relation*. ApJ **619**, 30, doi: 10.1086/426467. 6

Misner, C.W., Thorne, K.S. & Wheeler, J.A. (1973). *Gravitation*. Freeman and Co., USA. ads: 19773grav.book.....m73. 8

Monaghan, J.J. (1992). *Smoothed particle hydrodynamics*. Annual Review of Astronomy and Astrophysics **30**, 543, doi: 10.1146/annurev.aa.30.090192.002551. 43

Mori, K., Gotthelf, E.V., Zhang, S. *et al.* (2013). *NuSTAR Discovery of a 3.76 s Transient Magnetar Near Sagittarius A**. ApJL **770**, L23, doi: 10.1088/2041-8205/770/2/L23. arXiv: 1305.1945. 37

Morris, M.R., Meyer, L. & Ghez, A.M. (2012). *Galactic center research: manifestations of the central black hole*. Research in Astron. and Astrophys. **12**, 995, doi: 10.1088/1674-4527/12/8/007. 1

Narayan, R. (2002). *Why do AGN lighthouses switch off?* In M. Gilfanov, R. Sunyaev & E. Churazov (editors), *Lighthouses of the universe: the most luminous celestial objects and their use for cosmology*, 405. doi: 10.1007/10856495_60. 1

Novikov, I.D., Pethick, C.J. & Polnarev, A.G. (1992). *Tidal capture of stars by a massive black hole*. MNRAS **255**, 276. ads: 1992mnras.255..276n. 10

Nowak, M.A. & Wagoner, R.V. (1991). *Diskoseismology: Probing accretion disks. I - Trapped adiabatic oscillations*. ApJ **378**, 656, doi: 10.1086/170465. 50

Ohsuga, K., Mori, M., Nakamoto, T. *et al.* (2005). *Supercritical accretion flows around black holes: two-dimensional, radiation pressure-dominated disks with photon trapping*. ApJ **628**, 368, doi: 10.1086/430728. 4

O'Leary, R.M., Kocsis, B. & Loeb, A. (2009). *Gravitational waves from scattering of stellar-mass black holes in galactic nuclei*. MNRAS **395**, 2127, doi: 10.1111/j.1365-2966.2009.14653.x. 37

Paczyński, B. & Wiita, P.J. (1980). *Thick accretion disks and supercritical luminosities*. A&A **88**, 23. ads: 1980A&A....88...23P. 50

Perets, H.B. & Gualandris, A. (2010). *Dynamical constraints on the origin of the young B-stars in the Galactic center*. ApJ **719**, 220, doi: 10.1088/0004-637X/719/1/220. 6, 36

Phinney, E.S. (1989). *Manifestations of a massive black hole in the Galactic center*. In M. Morris (editor), *The center of the Galaxy*, volume 136 of *IAU Symposium*, 543. ads: 1989IAUS..136..543P. 23

Pota, V., Graham, A.W., Forbes, D.A. *et al.* (2013). *The SLUGGS survey: probing the supermassive black hole connection with bulges and haloes using red and blue globular cluster systems*. MNRAS **AA**, doi: 10.1093/mnras/stt718. 5

Press, W.H. & Teukolsky, S.A. (1977). *On formation of close binaries by two-body tidal capture*. ApJ **213**, 183, doi: 10.1086/155143. 11

Press, W.H., Teukolsky, S.A., Vetterling, W.T. *et al.* (1992). *Numerical recipes in FORTRAN. The art of scientific computing*. Cambridge University Press. 45

Price, D.J. (2007). *splash: An Interactive Visualisation Tool for Smoothed Particle Hydrodynamics Simulations*. PASA **24**, 159, doi: 10.1071/AS07022. arXiv: 0709.0832. 75

Ramirez-Ruiz, E. & Rosswog, S. (2009). *The star ingesting luminosity of intermediate-mass black holes in globular clusters*. ApJ **697**, L77, doi: 10.1088/0004-637X/697/2/L77. 23, 25

Rauch, K.P. & Tremaine, S. (1996). *Resonant relaxation in stellar systems*. New Astronomy **1**, 149, doi: 10.1016/S1384-1076(96)00012-7. 37

Rees, M.J. (1988). *Tidal disruption of stars by black holes of* 10^6–10^8 *solar masses in nearby galaxies*. Nature **333**, 523, doi: 10.1038/333523a0. 3, 23, 32, 33

Rees, M.J. (1990). *"Dead quasars" in nearby galaxies?* Science **247**, 817, doi: 10.1126/science.247.4944.817. 1

Richstone, D., Ajhar, E.A., Bender, R. *et al.* (1998). *Supermassive black holes and the evolution of galaxies*. Nature **395**, A14. arXiv: 9810378. 1

Rosswog, S. (2009). *Astrophysical smooth particle hydrodynamics*. New Astronomy Reviews **53**, 78, doi: 10.1016/j.newar.2009.08.007. 43, 49

Rosswog, S. (2015). *Boosting the accuracy of SPH techniques: Newtonian and special-relativistic tests*. MNRAS **448**, 3628, doi: 10.1093/mnras/stv225. arXiv: 1405.6034. 44, 64

Rosswog, S. & Brüggen, M. (2007). *Introduction to high-energy astrophysics*. Cambridge University Press, UK. ads: 2007ihea.book.....R. 20, 39

Rosswog, S., Ramirez-Ruiz, E. & Hix, W.R. (2009). *Tidal disruption and ignition of white dwarfs by moderately massive black holes*. ApJ **695**, 404, doi: 10.1088/0004-637X/695/1/404. 16, 45, 48

Rubilar, G.F. & Eckart, A. (2001). *Periastron shifts of stellar orbits near the Galactic Center*. A&A **374**, 95, doi: 10.1051/0004-6361:20010640. 39

Sacchi, A. & Lodato, G. (2019). *'Failed' tidal disruption events and X-ray flares from the Galactic Centre*. MNRAS **486**, 1833, doi: 10.1093/mnras/stz981. arXiv: 1904.02424. 12

Sadeghian, L. & Will, C.M. (2011). *Testing the black hole no-hair theorem at the galactic center: perturbing effects of stars in the surrounding cluster*. Classical and Quantum Gravity **28**, 225029, doi: 10.1088/0264-9381/28/22/225029. 38

Sanders, R.H. (1984). *Seyfert nuclei as short-lived stochastic accretion events*. A&A **140**, 52. ads: 1984A%26A...140...52S. 2

Schawinski, K., Urry, C.M., Virani, S. *et al.* (2010). *Galaxy zoo: The fundamentally different co-evolution of supermassive black holes and their early- and late-type host galaxies*. ApJ **711**, 284, doi: 10.1088/0004-637X/711/1/284. 1

Schödel, R., Ott, T., Genzel, R. *et al.* (2003). *Stellar dynamics in the central arcsecond of our Galaxy*. ApJ **596**, 1015, doi: 10.1086/378122. 1, 9

Secrest, N.J., Satyapal, S., Gliozzi, M. *et al.* (2012). *The Chandra View of NGC 4178: The Lowest Mass Black Hole in a Bulgeless Disk Galaxy?* ApJ **753**, 38, doi: 10.1088/0004-637X/753/1/38. arXiv: 1205.0230. 1

Servin, J. & Kesden, M. (2017). *Unified treatment of tidal disruption by Schwarzschild black holes*. PRD **95**, 083001, doi: 10.1103/PhysRevD.95.083001. arXiv: 1611.03036. 58

Sesana, A., Haardt, F. & Madau, P. (2007). *Hypervelocity stars and the environment of Sgr A*. MNRAS **379**, L45, doi: 10.1111/j.1745-3933.2007.00331.x. 6

Sesana, A., Madau, P. & Haardt, F. (2009). *Ejection of hypervelocity binary stars by a black hole of intermediate mass orbiting Sgr A**. MNRAS **392**, L31, doi: 10.1111/j.1745-3933.2008.00578.x. 17

Shapiro, S.L. (1985). *Monte Carlo simulations of the 2 + 1 dimensional Fokker-Planck equation - Spherical star clusters containing massive, central black holes*. In J. Goodman & P. Hut (editors), *Dynamics of star clusters*, volume 113 of *IAU Symposium*, 373–412. ads: 1985IAUS..113..373S. 28

Shapiro, S.L. & Marchant, A.B. (1978). *Star clusters containing massive, central black holes - Monte Carlo simulations in two-dimensional phase space*. ApJ **225**, 603, doi: 10.1086/156521. 28, 31, 34

Shields, G.A. & Wheeler, J.C. (1978). *Sustenance of a black hole in a galactic nucleus*. ApJ **222**, 667, doi: 10.1086/156185. 2

Shiokawa, H., Krolik, J.H., Cheng, R.M. *et al.* (2015). *General Relativistic Hydrodynamic Simulation of Accretion Flow from a Stellar Tidal Disruption*. ApJ **804**, 85, doi: 10.1088/0004-637X/804/2/85. arXiv: 1501.04365. 48, 49, 50

Silk, J. & Rees, M.J. (1998). *Quasars and galaxy formation*. A&A **331**, L1. arXiv: 9801013. 6

Sridhar, S. & Tremaine, S. (1992). *Tidal disruption of viscous bodies*. Icarus **95**, 86, doi: 10.1016/0019-1035(92)90193-B. 10

Steinberg, E., Coughlin, E.R., Stone, N.C. *et al.* (2019). *Thawing the frozen-in approximation: implications for self-gravity in deeply plunging tidal disruption events*. ArXiv e-prints arXiv:1903.03898. arXiv: 1903.03898. 58

Stone, N., Sari, R. & Loeb, A. (2013). *Consequences of strong compression in tidal disruption events*. MNRAS **435**, 1809, doi: 10.1093/mnras/stt1270. arXiv: 1210.3374. 14

Stone, N.C., Kesden, M., Cheng, R.M. *et al.* (2019). *Stellar tidal disruption events in general relativity*. Gen. Relativ. Gravit. **51**, 30, doi: 10.1007/s10714-019-2510-9. arXiv: 1801.10180. 61

Strubbe, L.E. & Quataert, E. (2009). *Optical flares from the tidal disruption of stars by massive black holes*. MNRAS **400**, 2070, doi: 10.1111/j.1365-2966.2009.15599.x. 14

Strubbe, L.E. (2011). *Snacktime for hungry black holes: theoretical studies of the tidal disruption of stars*. Ph.D. thesis, University of California, Berkeley. ads: 2011PhDT.....385S. 4, 17, 31, 34

Syer, D. & Ulmer, A. (1999). *Tidal disruption rates of stars in observed galaxies*. MNRAS **306**, 35, doi: 10.1046/j.1365-8711.1999.02445.x. 3, 28

Tejeda, E. & Rosswog, S. (2013). *An accurate Newtonian description of particle motion around a Schwarzschild black hole*. MNRAS **433**, 1930, doi: 10.1093/mnras/stt853. arXiv: 1303.4068. 49, 50

Thorne, K.S. & Żytkow, A.N. (1975). *Red giants and supergiants with degenerate neutron cores*. ApJL **199**, L19, doi: 10.1086/181839. 38

Ulmer, A. (1999). *Flares from the tidal disruption of stars by massive black holes*. ApJ **514**, 180, doi: 10.1086/306909. 14, 17, 19, 27

van den Bosch, R.C.E., Gebhardt, K., Gültekin, K. *et al.* (2012). *An over-massive black hole in the compact lenticular galaxy NGC 1277*. Nature **491**, 729, doi: 10.1038/nature11592. arXiv: 1211.6429. 1

van der Walt, S., Colbert, S.C. & Varoquaux, G. (2011). *The NumPy Array: A Structure for Efficient Numerical Computation*. Comput. Sci. Eng. **13**, 22, doi: 10.1109/MCSE.2011.37. arXiv: 1102.1523. 75

Vasiliev, E. & Merritt, D. (2013). *The loss cone problem in axisymmetric nuclei*. ApJ **774**, 87, doi: 10.1088/0004-637X/774/1/87. arXiv: 1301.3150. 28

Volonteri, M. (2012). *The formation and evolution of massive black holes*. Science **337**, 544, doi: 10.1126/science.1220843. 1

Waldman, S.J. (2011). *The Advanced LIGO gravitational wave detector*. e-print, arXiv: 1103.2728. 37

Wang, J. & Merritt, D. (2004). *Revised rates of stellar disruption in galactic nuclei*. ApJ **600**, 149, doi: 10.1086/379767. 3, 6, 28

Wang, J.M., Du, P., Valls-Gabaud, D. *et al.* (2013). *Super-Eddington accreting massive black holes as long-lived cosmological standards*. PRL **110**, 081301, doi: 10.1103/PhysRevLett.110.081301. 5

Weinberg, S. (1972). *Gravitation and cosmology: principles and applications of the general theory of relativity*. NY:Wiley, USA. ads: 1972gcpa.book.....W. 39

Wendland, H. (1995). *Piecewise polynomial, positive definite and compactly supported radial functions of minimal degree*. Advances in Computational Mathematics **4**, 389, doi: 10.1007/BF02123482. 45

Will, C.M. (2008). *Testing the general relativistic "no-hair" theorems using the Galactic center black hole sagittarius A**. ApJL **674**, L25, doi: 10.1086/528847. 38

Young, P.J., Shields, G.A. & Wheeler, J.C. (1977). *The black tide model of QSOs*. ApJ **212**, 367, doi: 10.1086/155056. 13

Younger, J.D., Hayward, C.C., Narayanan, D. *et al.* (2009). *The merger-driven evolution of warm infrared luminous galaxies*. MNRAS **396**, L66, doi: 10.1111/j.1745-3933.2009.00663.x. 2

Zhao, H., Haehnelt, M.G. & Rees, M.J. (2002). *Feeding black holes at galactic centres by capture from isothermal cusps*. New Astronomy **7**, 385, doi: 10.1016/S1384-1076(02)00107-0. 6, 37

Zubovas, K., Nayakshin, S. & Markoff, S. (2012). *Sgr A* flares: tidal disruption of asteroids and planets?* MNRAS **421**, 1315, doi: 10.1111/j.1365-2966.2011.20389.x. 2, 15

Zucker, S., Alexander, T., Gillessen, S. *et al.* (2006). *Probing post-Newtonian physics near the Galactic black hole with stellar redshift measurements*. ApJL **639**, L21, doi: 10.1086/501436. 38

Acknowledgements

I don't know half of you half as well as I should like;
and I like less than half of you half as well as you deserve.
Bilbo Baggins

I would like to thank the Nordic Institute for Theoretical Physics (NORDITA) and the Oskar Klein Centre (OKC) in Stockholm, the Nordic Optical Telescope (NOT) and the Isaac Newton Group of Telescopes (ING) on La Palma, the Niels Bohr Institute (NBI) in Copenhagen, and the Harvard-Smithsonian Center for Astrophysics (CfA) in Cambridge, MA for their hospitality, in various forms and on various occasions during my PhD studies. This research has benefited from an Alva and Lennart Dahlmark research grant.

The simulations and postprocessing in this thesis have in part been carried out on the facilities of the North-German Supercomputing Alliance (HLRN) in Hannover, Göttingen and Berlin, and of the PDC Centre for High Performance Computing (PDC–HPC) in Stockholm. This work has also benefited from digital storage space provided by the Swedish National Infrastructure for Computing (SNIC) through the Swestore project.

Our research has made extensive use of NASA's Astrophysics Data System (ADS; it's a pity they have completely given up the "classic" version for the "new ADS" – it might be a matter of taste, that doesn't make it any less appalling; I had to say it somewhere) and of Cornell University's arXiv repository, of NUMPY (van der Walt *et al.*, 2011), SCIPY (Jones *et al.*, 2001), MATPLOTLIB (Hunter, 2007) and SPLASH (Price, 2007).

Now on to the most read part of the thesis.

This journey started a long, long time ago, at the end of 2011, when Stephan proposed that I finish my two-year MSc degree in Bremen within one year, and that I start a PhD in Stockholm the very next year. The decision was swift and enthusiastic, because although (as always) I didn't have clear long-term plans, I knew that I wanted to work with him! Plus, I've naively said to myself, Sweden cannot possibly be that much different than Germany, which I was enjoying so much, right? Not so, as I'd quickly come to realise, and in all fairness I've never really called the place home

(but more on that later). But the decision to continue to work with Stephan I have never regretted. So, herzlichsten Dank, Stephan! For being my mentor for more than a decade, since the beginning of my university studies. For showing me paths and opening doors that took me from Basel to Trieste, from Oxford to Harvard, from Bremen to Stockholm; the only limits to the breadth and depth of our work were the ones I put, but even in that I had your support, or at least acceptance. For working enthusiastically and at a fast pace with me in the better moments, and patiently hearing me out over a pint in the worse ones. I've come to know many scientists – and academia in general – and it was late that I fully realised the luck I'd had so many years ago, when – seemingly randomly, maybe due to what Ancient Greeks would have called Μοῖραι –, after a defining trip to the observatory in Crete, I had chosen to do my BSc thesis with you; we've started with a code and now end with a code. Somewhat self-exiled from the academia – at least in its traditional (or rather, modern) paradigm –, I owe both my continued interest in science, astronomy, astrophysics and SPH, and the little nostalgia I still have about working in Stockholm, to you. Equally I owe you, to a larger extent than I probably realise, the job and the life that I have in La Palma now. Thank you for all my successes; the failures are mine. I hope we will continue to work and write (both code and articles) together for another long, long time.

Thank you, John, my second supervisor – maybe not in a traditional hands-on way, but always the first person to read each article or thesis with painstaking carefulness, always asking for just the right clarification, without missing even the tiniest detail, either in the science or in any departure from the purest Oxford English. It has always been a pleasure to meet with you, whether in any of your two home cities, or in Stockholm, and I've always had a lot to learn – the science itself can always be found in books and articles, but your way of asking the right questions and your composed way of doing complicated calculations, those cannot be learnt but by example. Thank you!

I am grateful to Göran S. for being a very interested PhD mentor, always encouraging me to finish my thesis – I will probably not forget the glimpse and twinkle of happiness in your eyes when I told you the work is complete and that I have a date for the defence (I wouldn't blame anyone for giving up hope, as it seemed that in going away I had given it all up). Sorry for the boring – in your case – job of being a mediator between the PhD and the supervisor, though I guess this is one of those duties where the less you have to do, the better it means the situation is.

⋆

As I mentioned, the journey through my new home after the beginning of my PhD, particularly on the social side, was not quite easy. We've probably discovered the "How To Be A Swede" book a few years too late. Fika helped, and I think it is an institution that should be exported everywhere. But I owe a big debt of gratitude to

our post-fika fika group: Kai Yan, Florent, Illa and Cecilia, in no particular order. It started with having a good time and laughing (mostly at the Swedes, or at Florent) instead of going back to work at 4 pm, but we ended up becoming friends, having trips, excursions, dinners, parties, hangovers, superficial and deep conversations, Wii contests, laser tag games, kayaking incidents, and so much more! You made it easier to live here, and harder to be in a grumpy mood! Keep in touch; you'll always have a home wherever I am.

Thanks to all the PhD students and postdocs I have crossed paths with (but mostly to those with whom I got along well), and in particular to Matteo, Veronica, Francesco, Gianni, and Emir. Most of you have finished your PhDs well before me, and are now dispersed throughout the world, but I still have the memory of our times together, be it a fika, a board games session with pizza, an excursion, or a PhD activity; all these made my life better, and for that I thank you.

From the department I also have to thank Emilio, who was one of the best coworkers anyone could have asked for, full of great ideas and always a whiz at analytical calculations (the things he can do with just a Mathematica notebook!). Of my collaborators, I would like to thank James in particular: although we haven't interacted a lot, you've always been a model for the uniquely insightful way of thinking about TDEs, and your dedication to the field; also, thank you for the warm hospitality at Harvard! Many thanks to all my other collaborators and coauthors – I have learnt as much as I could from each of you.

I will always be grateful to Andreas, Göran Ö. and Matthew, the principal instigators (did I spell that right?) behind my many, many observing trips to La Palma. Those trips have slowly opened a wonderful door for me, which in the end materialized in my getting first a studentship at the NOT, and then a job at the ING and a life in La Palma. Ultimately this is thanks to you, though I cannot leave out that it was Florent who first invited me to an observing run in La Palma back in the winter of 2013; that's when I first heard of Binter, Cicar, Castillete, Los Indianos, El Roque; little did I know at the time what these things would become in my life! Talk about a butterfly effect.

Life (shortly and long) after arriving in Sweden would have been much, much harder without the invaluable help of Sandra! It is hard to imagine what I and so many other generations of students would have done without you! Probably spending days and weeks trying to solve something that you often solved with a simple phone call. And a smile. And a cookie. Though the most touching part is your continued help even long after you left the department and I left Sweden. Thank you for always being there! I'm also truly happy that we share so many views on non-scientific topics of actuality. Wink, wink.

Muchas gracias, Rocío, por tu ayuda en todo, desde conseguir cualquier papel que me hiciera falta, o encontrar alojamiento durante mis visitas en Suecia, hasta las preparaciones de mis defensas (del licentiate y también de esta tesis). Y ¡gracias por

siempre tener la puerta abierta y una sonrisa en la cara!

Thank you, Axel, for being a model scientist (and a real dynamo; or was it the other way around?)! It is inspiring to have seen your dedication and total devotion to science first-hand; although we have crossed paths occasionally but not quite (yet) as collaborators, you've still had a big influence of me, and on the way I aspire to do science (I'm sure Illa bears some blame for that, and I thank her for it!)

Thank you, Jesper, for all your work as director of PhD studies: you've always been clear in requirements, helpful in case of need, and funny in a deeply Swedish way that ultimately one cannot help but find charming (although it might take time to understand it)! Many thanks to Dan for translating the abstract of this thesis to Swedish! It was done in the last few days before the final printing, and with all the stress of the test prints and of finishing the main text of the thesis, it was an invaluable help, and one less thing to worry about!

⋆

After my licentiate, in the very beginning of January 2016, I moved to La Palma to start working at the NOT as a student support astronomer. Thank you, Thomas, for inviting me to take up that position (and for the subsequent extension). Many thanks to John, Amanda, Pere and Tapio, for always being helpful, and supportive, and funny. Thank you, Peter, for being so down-to-earth, always full of *joie de vivre*, and for the stellar letter of recommendation you wrote! And many thanks to the entire NOT staff, for almost two years of carefree, happy life. At 2400 m.

I can't talk about the NOT or the ING without mentioning my fellow student astronomers with whom I've crossed paths and often spent inordinate amounts of times in bars, on trips, or on the mountain (not necessarily, but likely, in that order): Tom, always a pleasure to talk to you; even when we don't see eye to eye, I find our discussions very interesting, whether they be about language, or politics, or anything else; I've really come to miss them. Teet and Nissa, always good to see you, I wish you best of luck with your recently-started project for the future. Jussi, we haven't seen each other for a long time, but you always seemed like the coolest of all the students; beers, beard and all; looking forward to your mythical return to La Palma (always spoken of, but never happening)! And to all the other students, it was great to meet you! Though I must single out Grigori for giving me the greatest scare of my life! Don't drive. Ever.

I left the NOT to start a (real) job at the ING (the telescopes, not the bank), almost two years ago. The transition has been easier than I expected, mostly thanks to the people I work with. Thank you, Jure and Don, for hiring me, for guiding me whenever I needed it, for being happy with my work schedule patterns and the results they yield, for always asking about how my PhD is going and giving me the time I needed to work on it, for motivating me to keep at it until I finished. Well – This is it. Gracias, Sergio, por ser un compañero de trabajo tan majo; siempre ha sido un placer

hablar y colaborar contigo, e incluso compartir unos Pictolín; ¡sigamos en busca del próximo "another success"! Thank you, Gary and Frank, for the morning coffees and for the wide range of conversation topics, and the stories and laughs we share. Gracias, Luis y Alegría, por vuestra ayuda con los ordenadores y por los pequeños regalos inesperados como un teclado nuevo, un ratón nuevo, o una chocolatina; siempre se agradece. Thank you, Ian, for always encouraging me to finish the thesis, for being a model of deep astronomical knowledge, and for always being receptive when I had something to complain about; I'll always be there to return the favour!

Y como La Palma no sería La Palma sin su gente y sus tradiciones, agradezco mucho la amistad de unas personas especiales, que me han aceptado como amigo o compañero, mejorándome así la vida mucho (aunque a lo mejor ni siquiera se han dado cuenta del impacto que han tenido sobre mí). Para empezar, gracias, Juancho, por ser mi amigo desde los primeros días después de mi llegada a La Palma; no podría contar las horas que hemos pasado hablando y rehablando, creo que de todo lo que uno se puede imaginar; y aun así, siempre encontramos algo nuevo e interesante; y siempre estás a la distancia de un "¿qué tal, nos vemos?" Gracias por tu apoyo y mucha suerte en todo; acuérdate cuantas veces me has dicho que tenía que acabar esto, y mira que aunque no lo pensábamos, por fin se acabó; ¡ahora te toca a ti! ¡Suerte!

Muchas gracias a Javi y al resto de los "Divinos" de Santo Domingo, que me han aceptado en su grupo casi sin preguntas, ofreciéndome así unos recuerdos muy especiales en las últimas navidades. Para mi ha sido una pasada, y siempre esperaré con ganas la próxima vez. Gracias también a Fran y al resto del grupo de Las Nieves, que también me han aceptado allí con mi timple, sin saber tocarlo muy bien, pero con toda la emoción del mundo. Estas cosas hacen la vida mucho más agradable, y, quiera que no, me han ayudado llegar hasta aquí. Gracias, Shirley: siempre has estado allí para Illa, y aunque uno no se da cuenta del paso del tiempo, resulta que nos conocemos ya desde muchos años, y siempre me has tratado como familia. Gracias también a Juan Arturo: aunque no llevamos mucho tiempo como amigos, desde el principio ha sido un placer compartir un café, un vino, una conversación, una semana ensobrando papeletas y, porqué no, un hígado encebollado. Gracias, Emma, por todas las risas que hemos echado, hablando de Harry Potter, paseando por Madrid, traduciendo de latín, o jugando juegos de mesa.

Mulțumesc Adinei pentru traducerea rezumatului în limba germană, și lui Bogdan pentru corectura traducerii în limba latină; în afara unor schimburi relativ minore de emailuri, nu ne cunoaștem prea bine: sper că asta se va schimba în viitor. Le mulțumesc lui Neluțu, Milică și Sorin (și familiilor!) pentru că de fiecare dată cînd am fost în țară mi-ați fost alături, și întotdeauna am petrecut memorabil – scurt, dar bine; continuăm colaborarea în toate proiectele.

⋆

Llegando ya casi al final, te dije que no te iba a mencionar, Illa. Pero sin darme cuenta ya te he nombrado varias veces, pues hemos compartido tantas cosas que en realidad me resultaría imposible dedicarte sólo un párrafo. Pensándolo bien, casi todo lo que he mencionado hasta ahora son cosas y situaciones donde hemos estado juntos, a veces incluso cosas que yo no quería hacer y tu has insistido hasta conseguirlo, en general teniendo tú razón (te lo admito públicamente en un libro para que quede escrito). Así que, ¡gracias por insistir siempre! No sé dónde estaría ahora sin ti. El título de esta tesis tiene muchos sentidos, como ya sabes, pero al final aquí estamos. Con todo lo que hemos superado, y con todo lo que queda para superar, sé que no hay mejor persona con quien compartirlo todo; lo bueno y lo malo. Gracias, y que se cumplan todos tus deseos; ya nos toca por una vez lo bueno.

În sfîrșit, le mulțumesc părinților mei pentru sprijinul acordat, de fiecare dată cînd am avut nevoie, cerîndu-l sau nu, acceptîndu-l sau nu, fără întrerupere, în ultimii treizeci de ani. Influența familiei e deplină în gene și capitală în mediu – așa că unde am ajuns și ce sînt vi se datorează în mare parte; cum succesul meu e succesul vostru, nu e nevoie de mai multe mulțumiri. Cum zicea cineva drag, "voi știți".